AALBORG
UNIVERSITY

STUDENT REPORT

AALBORG UNIVERSITY
DEPARTMENT OF MATERIALS AND PRODUCTION

MATERIALS AND NANOTECHNOLOGY: MATERIALS TECHNOLOGY

THESIS

Pitting Resistance Study after the Laser Forming of AISI 304 Stainless Steel and its Remediation Methods of Chemical Pickling and Laser Ablation Processes

ANASTASIA GIANNAS

NOVEMBER 14, 2024

DUE DATE: NOVEMBER 14TH, 2024

AALBORG UNIVERSITY

STUDENT REPORT

Department of Materials and Production /
Study Board of Physics and Mechanics
Aalborg University
www.mp.aau.dk

Title:

Pitting Resistance Study after the Laser Forming of AISI 304 Stainless Steel and its Remediation Methods of Chemical Pickling and Laser Ablation Processes

Semester:

4th Semester Materials Technology

Semester theme:

Master's thesis

Project period:

14 August 2024 - 14 November 2024

ECTS:

30

Supervisor:

Mikael Larsen

Participants:

Anastasia Giannas

Page numbers: 82

Abstract:

The current study aimed to evaluate how chemical pickling versus laser ablation remediation treatments affected the removal of the oxide layer on the base and laser-formed AISI 304 stainless steel surfaces with the purpose of mitigating pitting corrosion. This oxide layer is generated when stainless steel is exposed to high-temperature treatments, such as welding and lasers. However, it is frequently essential to remove these oxides and enhance the metal quality, especially while maintaining manufacturing equipment. This study investigated processes to achieve the most pitting-resistant metal behavior. Characterization methods used to evaluate the pitting corrosion resistance were: Ferric chloride pitting test, Cyclic Potentiodynamic Polarization, and SEM with EDX. A newly proposed method of conducting cyclic potentiodynamic polarization measurements was applied to assess the pitting corrosion resistance. The mass loss and surface structures were also evaluated. Due to the dispersion of data, the results were uncertain. Nevertheless, from the correlation relationship between mass loss and pitting resistance, corrosion deterioration of both remediated study groups was greater than the base or laser-formed coupons.

By signing this document, the student confirms participation in the experimentation and documentation of the project. Thus, the student is responsible for all contents of this thesis.

Preface

The following report was authored by Anastasia Giannas, a fourth-semester Materials Technology Master's student at Aalborg University under the guidance of Professor Mikael Larsen. The study presents the findings of Anastasia Giannas's thesis project, which focused on Laser Processing, Metallurgy, and Corrosion Science and was conducted from August 14th to November 14th, 2024.

The report was prepared according to the university's guidelines. It provides an in-depth analysis of the project's findings and presents a comprehensive view of the methodology, data analysis, and results.

Tables, figures and equations are numbered in order of appearance. References to literature are made according to the IEEE citation style. Citations are listed in order of reference with [citation number]. Full references are shown in the bibliography section.

Acknowledgements are given to the supervisor, Mikael Larsen, for his help and guidance in theories, testing and analysis. Thanks are extended to Morten Kristiansen for his assistance with the laser forming and laser ablation process. In addition, my appreciation to LASR® company as they provided me with the laser ablation coupons for testing. Furthermore, thanks to the laboratory team at Fibigerstræde 14, who has assisted with the testing setup.

Anastasia Giannas

Nomenclature

Abbreviations

AES	Auger Electron Spectroscopy
CP	Indicator for Coupons Used for CPP Testing
CPP	Cyclic Potentiodynamic Polarization
DOE	Design of Experiments
EDS/EDX	Energy Dispersive X-ray Spectrometry
EIS	Electrochemical Impedance Spectroscopy
HAZ	Heat Affected Area
HL	HIgher Power Laser-Induced Forming (0,80 [kW])
LA	Indicator for Laser Ablation Remediated Coupons
LL	Lower Power Laser-Induced Forming (0,65 [kW])
LPR	Linear Polarization Resistance
OCP	Open Circuit Potential
P	Indicator for Chemical Pickling Remediated Coupons
PREN	Pitting-Resistance Equivalent Number
PT	Indicator for Coupons Used for Ferric Chloride Pitting Test
SEM	Scanning Electron Microscopy
sol.	Solution
SS	Stainless Steel
XPS	X-ray Photoelectron Spectroscopy
XRD	X-ray Diffraction

Symbols

%	Percent Unit
β_A & β_C	Tafel Constants
®	Registered Trademark
Cr/Fe	Chromium-to-iron Atomic Ratio
d	Density
E	Potential
E_{corr}	Corrosion Potential, or Open Circuit Potential
E_{pit}	Pitting Potential
Fe/O	Iron-to-oxygen Atomic Ratio
I_{corr}	Corrosion Current
i_{corr}	Current Density
R_{pit}	Pitting Corrosion Resistance
SCE	Saturated Calomel Electrode
V	Potential
$wt\%$	Percent by Weight

Summary

This study sought to examine the effectiveness of pitting corrosion mitigation and resistance in AISI 304 stainless steel base metal, both before and after laser forming and following remediation processes such as chemical pickling or laser ablation. The guiding research question derived from this aspiration was whether the remediation process is effective enough to reduce pitting corrosion on laser-formed coupons.

To begin with, two groups of laser forming were analyzed using different laser power levels: 0.65 kW (LL) and 0.80 kW (HL). Following this, the heat-treated laser-formed coupons underwent further processing through either chemical pickling using a mixture of 10-20 [wt%] nitric acid with 1-2% hydrofluoric acid (P) or a laser ablation method (LA). Subsequently, additional characterization was conducted to investigate pitting and uniform corrosion behavior when exposed to an acidic environment using a 0.75 [wt%] ferric chloride immersion test at 20[°C], as well as in 3.5 [wt%] artificial seawater during cyclic potentiodynamic polarization at ambient conditions. A novel developmental procedure for acquiring cyclic polarization experimental data was conceptualized and validated to facilitate unbiased investigations of metastable and stable pitting. Finally, surface scanning was conducted using SEM and EDX.

A summary of the results obtained from the ferric chloride pitting test, CPP and SEM/EDX are presented below :

The average mass loss of the raw material(RM-C) was 10,20±0,3 [mg]. Moreover, the average mass loss for the laser-formed coupons by power 0,65[kW] (LL-C) was 18,00±1,30 [mg], while for the laser-formed coupons by power 0,80[kW] (HL-C) was 18,40±3,60 [mg]. Furthermore, the average mass loss for the laser-formed by power 0,65[kW] (LL-LA) and for 0,80[kW] (HL-LA) initially and laser ablation remediation coupons were 122,10±3,80 [mg] and 140,80±13,90 [mg], respectively. Lastly, the average the average mass loss for the laser-formed by power 0,65[kW] initially and pickling remediation coupons (LL-P) and 0,80[kW] (HL-P) were 164,80±67,00[mg] and 149,10±9,90 [mg], respectively.

The average pitting resistance of the raw material(RM-C) was 198,03±0,3 [mV]. Moreover, the average pitting resistance for the laser-formed coupons by power 0,65[kW] (LL-C) was 84,88±58,58 [mV], while for the laser-formed coupons by power 0,80[kW] (HL-C) was 47,90±12,04 [mV]. Furthermore, the average pitting resistance for the laser-formed by power 0,65[kW] (LL-LA) and for 0,80[kW] (HL-LA) initially and laser ablation remediation coupons were 237,17±136,46 [mV] and 151,83±78,47 [mV], respectively. Lastly, the average the average pitting resistance for the laser-formed by power 0,65[kW] initially and pickling remediation coupons (LL-P) and 0,80[kW] (HL-P) were 152,42±100,87[mV] and 197,69±88,29 [mV], respectively.

SEM scanning analysis found melting and edging at the laser ablation and pickling remediated coupons, respectively. EDX found elevated oxygen concentration in all study groups compared to the base material.

As mentioned above, the results are contradicted since the mass loss and SEM investigation depict more pitting-resistant coupons to the base and laser formed rather than the remediated, as were observed in cyclic polarization testing. Due to significant variability, it is not possible to conclude whether any remediation methods effectively mitigated pitting corrosion following laser formation or to identify the most pitting-resistant study group. The remediated study groups demonstrated higher pitting potential and pitting resistance compared to the laser-formed coupons. Notably, increased surface deterioration was observed on the coupons that underwent either pickling or laser ablation.

Contents

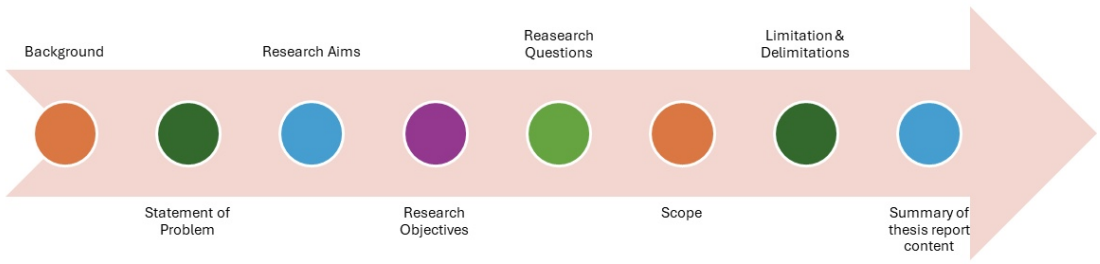

Figure 1: Introduction chapter outline

1 Introduction

Localized corrosion has been a problem that can affect materials in various industries, such as aviation[1], biomaterials[2][3][4], infrastructure[5][6], naval[7][8], mining[9], oil and gas[10] and many more. Pitting is a type of localized corrosion that can appear when a material is exposed to a harsh environment, and it needs to be controlled in order to prevent further material deterioration and damage. It can be challenging to distinguish the effects of pitting from the effects of other types of corrosions, such as uniform. However, it cannot be studied with the same characterization methods as uniform corrosion. Knowledge of laboratory-simulated results can deviate a lot from real-world problems. Pitting can even take place in non-passivating alloys; alas, one alloy material that has pitting corrosion-resistant behavior is austenitic stainless steel [11]. Specifically, AISI 304 has been one of the most compatible material options for its pitting corrosion resistance, with the capability to improve it and enhance it with its passive layer and even with the proper remediation treatment[12].

The methods by which a material can be exposed to corrosion may vary. Interestingly, laser processing can either enhance corrosion resistance or diminish it, depending on the purpose and process. It is very crucial to be able to remediate any exposed stainless steel and, if possible, to prevent further downturn.

The problem would be which pitting corrosion remediation method works the best and whether they are even effective. Therefore, this study aims to investigate the 304 SS corrosion resistance properties after laser processing, specifically laser forming, and later possible remediation methods, such as laser ablation and chemical pickling, as outlined in table 1. To begin with, the study's background will be explored, and then the research statement, problem, aims, objectives, limitations, and scope will be set, as depicted in figure 1.

Table 1: Summary of this Study's Process Steps

Step 1	Laser Forming
Step 2	Remediation Treatment
Step 3	Testing & Characterization

1.1 Thesis Background

Environmental exposure can cause corrosion when in contact with a material, thus deteriorating it and causing failures. Generally, metals become passive(corrosion-resistant) in moderate to strong oxidizing conditions, but under extremely strong oxidizing conditions, the same materials can lose their corrosion-resistant capabilities[13]. Hence, this duality of surface behavior needs to be studied further.

Explicitly, localized pitting is one form of corrosion that can be caused due to the breakdown of the stainless steel (SS) thin passive layer that protects it[14][13]. The rate of localized pitting corrosion is particularly far greater and more aggressive than that of uniform corrosion. Thus, it is detrimental for this type to be explored further[13]. Recent developments have shown that various methods enhance SS behavior against pitting. That was achieved by simulated testing or in-situ studies[13]. Specifically, the Cyclic Potentiodynamic Polarization electrochemical testing method(CPP) can detect the metal's pitting susceptibility[15].

In this study, 304 SS was exposed to laser-induced forming, and afterwards, treatment methods for corrosion resistance reclaiming were conducted and further investigated based on industry standards. The corrosion remediation methods selected to achieve corrosion resistance enhancement were focused on surface treatment, such as pickling and laser ablation.

The first step for our study is to understand better some complex terminology related to this study below:

- *Uniform corrosion*, or general corrosion, is a process that can thin the base metal uniformly but not necessarily achieve localized attack; however, it is common for passive metals such as SS to be subjected to potential localized corrosion[15].
- *Pitting potential(E_{pit})* is the minimum potential at which a material starts to pit at a potential vs. log current density curve, and an indicator of localized pitting corrosion[16]. With the help of corrosion potential(E_{corr}), *pitting corrosion resistance(R_{pit})* can be determined.
- *Laser forming* is the process that uses high-intensity beam lasers to interact with the solid surface with the purpose of bending and forming, causing heat tint staining and phase change at the irradiated heat-affected area (HAZ) [17].
- *Laser Ablation(LA)* is a well-controlled technique of tribological surface topography modifications that has even shown beneficial effects by altering the surface texturing[18].

- *Pickling(P)* is the most common oxide scale removal method that is easily performed by chemical solution(sol.) immersion in an aqueous acid medium[19] [20].

1.2 Statement of the Problem

304 SS pitting corrosion is a significant problem due to its widespread use across various industries, making it a universal concern. Especially when processed via laser medium, causing the metal to corrode more intensely due to the energy power and intensity of the laser heat treatment, deteriorating it by causing surface and phase change. Slowly, studies have started emerging with various methods of correcting that problem. Under some conditions, the corroded material might even be able to recover from those previous intensive processes.

However, various methods exist for removing the scale. We can use existing technologies in the context of this problem. The focus that is missing is removing the oxide layer generated by corrosion due to laser forming and investigating further corrosion properties, resistance behavior, and, if possible, resistance enhancement. A comparison study of comparing two different corrosion remediation methods, such as chemical pickling with a specific formulation against laser forming, and whether these two methods are effective enough to reverse the effects of corrosion resistance behavior based on characterization tests exposing them to chloride(CPP) and acidic environments(Ferric Chloride Pitting Test), will bring additional knowledge to this problem. Two different cases of power parameters via laser-induced forming will be performed to evaluate and validate whether their two trends overlap. In addition, unique process development of experimental procedure was practised for CPP pitting unbiased data acquisition.

1.3 Research Aims, Objectives and Question

Given the lack of specific literature studies on this topic, this research sought to investigate the pitting resistance of an AISI 304 SS metal due to its deterioration via lased-induced forming and later via its remediation methods of pickling and laser ablation. The aim would be to quantify and compare the pitting mitigation quality(resistance) of the base metal before and after laser forming and later after chemical pickling or laser ablation remediation processes.

The research objectives will help with outlining this study's aims and how to tackle them more practically and by action-oriented experimentation. The purpose is to help us make SMART choices for this study. The objectives are mentioned below:

1. To appraise whether remediation will be effective enough to mitigate pitting corrosion on a laser-induced formed coupon.

2. To assess the material's deterioration via mass loss, which is an indication of corrosion resistance from the Ferric Chloride Test.

3. To analyze pitting potential (E_{pit}) and to quantify pitting corrosion resistance (R_{pit}) from CPP curves. The purpose is to mitigate pitting and uniform corrosion, thus investigating resistance.

4. To assess the surface structure of each coupon control from every step of the lased forming remediation process in this study via SEM and EDX.

The study's overall combined results can answer research objective 1. Objective 2 will be determined by the use of the Ferric Chloride immersion test (ASTM G 48). Furthermore, question 3 can be determined by CPP (ASTM G 5,61), and to achieve further surface investigation for objective 4, SEM and EDX will be used.

With the help of the study's research question, we underpin the decisions made during our study, hence the design of the experimental methodology. This study's research question would be:

Is remediation effective enough to mitigate pitting corrosion on laser-formed coupons?

1.4 Thesis Project Scope

To narrow down the focus of this study, the scope will involve:

- The determination and quantification of pitting corrosion resistance(R_{pit}).
- In addition, the mass loss before and after treatment via the Ferric Chloride Test.

After collecting all the data from the characterization methods, a comparison between the base material, laser-formed (in lower and higher laser powers), and remediated methods(pickling and laser ablation) can be performed. The intention is to determine which step and under which treatment exposed to this study process has the best pitting corrosion-resistant behavior.

1.5 Research Limitations and Delimitations

For structural purposes of this study, it is understandable for possible limitations to exist. Limitations in a small population of literature and data results limited the academic access observation and results. Hence, the literature study needed to be extended from adjacent literature from other industries. For instance, there was a limited amount of articles that discussed laser formed and remediation methods, plus their characterization methods of CPP and/or Ferric Chloride Pitting Test.

In addition, limited access was allowed by third-party companies that use laser ablation remediation technology for this goal; thus, no knowledge from their side was obtained. So, the process development was able to be obtained from academic articles.

Moreover, limitations to sample sizes allowed us to have only a small data pool for analysis. Plus, a number of coupons had to be rejected due to crevice corrosion, which is outside the scope of this study. Hence, due to the sampling size, the generalisability of these results is not certain; however, we were able to have at least three(3) coupons worth of results for statistical purposes for cases for characterization tests such as CPP and Ferric Chloride Test.

Furthermore, this study's research design methodology did not allow for all coupons to have only pitting corrosion. Apart from crevice-localized corrosion, uniform corrosion was observed on their surfaces.

Lastly, the study's limitations could be due to human impact experience and bias. For example, the preparation of the 304 SS coupons for CPP involved waxing the coupons in a certain way to avoid crack propagation from their "naked" edges. Because the waxing of the coupons that took place was manual, the waxing dimensions that covered the coupon's surface could deviate, even if the purpose of sealing the edges was successfully met.

The research delimitations set determines what was excluded from the study, narrowing down the focus. They are influenced by the research aims, question, and scope mentioned above.

- Even though this report is investigating localized corrosion, only pitting was studied, and any crevice corrosion observations and research were omitted.
- During CPP characterization, only E_{corr} and E_{pit} were the focus of this study. Details of the CPP curve hysteresis and repassivation potential will be excluded due to the lack of cycle times of CPP runs and uncertainty.

1.6 Summary of Thesis Content

In chapter one(1), the context of this study is introduced, along with the thesis aims, objectives, question, scope, limitations, and delimitations. Chapter two(2) outlines the literature review conducted for this study. Chapter three(3) includes theory and background knowledge of the topic discussed here, such as corrosion and laser processing, and details on characterization methods used, such as CPP and SEM/EDX. Chapter four(4) explains in detail the methodology used, and chapter five(5) presents the results with a discussion on the topic studied. Lastly, chapter six(6) summarizes the results determined and observed.

2 Literature Study

In this chapter, we will elaborate on the existing knowledge gained from experimentation to identify potential research gaps by reviewing and synthesising existing literature based on this study's aim.

As a reminder of this study's research aim, we will investigate the pitting resistance of AISI 304 SS properties via laser-induced forming, followed by an examination of remediation methods such as pickling and laser ablation.

The foundation for this study's theory framework is recorded in Chapter 3, "*Theory and Background Knowledge*", including topics such as laser processing and ablation, pickling, corrosion theory and an explanation of the characterization method theory used. Here, the empirical research summaries of research publications will be summarized in a methodological order and discussed, and lastly, the research gap will be identified.

Firstly, articles related to welding and heat treatment are mentioned below:

- Bautista and others[21] examined the impact of welding on the corrosion behavior of corrugated bars made from two austenitic SSs of (low-nickel AISI 204Cu and traditional 304) and a duplex SS. Welds were created using shielded metal arc welding. It was found that oxides formed during welding are capable of decreasing (restoring/remediating) the corrosion resistance of the SS. Two cleaning methods, pickling and sand-blasting, were tested for effectiveness in removing these oxides. While pickling did not entirely fully eliminate oxides, sand-blasting rather effectively removed them but introduced aeration cells and surface deformation.

- Terasaki's[22] study investigated the effects of welding-induced factors on corrosion pit growth in specimens immersed in artificial seawater for 1 to 5 months. The deepest pit occurred in specimens submerged for 3 months, and the deepest pit was observed in the region where the strain energy was larger than 0,01$[MJ/m^3]$.

- Vazquez-Santoyo and colleagues[23] showed the reflectance spectra show that the samples have high-purity colour primarily in the yellow region (560-590 [nm]) and orange spectra (590-630 [nm]) on SS surface, which are attributed to interference oscillations in the visible range. Reduced iron content and significant oxygen presence in the near-surface region suggest the formation of a mixed oxide layer. Atomic-force microscopy reveals that the sample surface has an island structure.

Moreover, articles relevant to laser processing are depicted below:

- Svantner and others[24] presented the key characteristics of laser technology for marking SS, which can be used for modification of material surface visible properties, focusing

on its effects on surface roughness, phase composition, and corrosion resistance. The results showed a relationship between the ferritic phase content and the new oxide layer content on the marked material surface, which affected the corrosion resistance of the laser-affected surface. The possibility of an additional acid picking of laser-treated SS surfaces was also tried. The corrosion resistance relied on a protective oxide layer that was damaged during laser marking. Methods like pickling and passivation could not restore this layer without affecting the marking's quality. The results showed that laser marking processing parameters variation can lead to very different results from the point of view of corrosion resistance of the marked surfaces.

- A Q-switched Nd:YAG laser was used for marking SS, examining how pulse frequency affects mark depth, width, and contrast. Results showed that higher pulse frequencies lead to less material evaporation and increased oxidation, improving mark contrast. The optimal mark contrast was achieved at a pulse frequency of around 8 [kHz][25].

- The impact of laser treatments on 420 SS at ambient conditions was studied to observe surface changes. The treatments were conducted at various scanning speeds. High-speed scanning resulted in surface cleaning, micro-striping, and solid oxidation, while lower scanning speeds caused element redistribution and material transfer. Additionally, variations in surface oxides were observed along the individual laser scanning tracks[26]. Therefore, laser speeds can affect the surface oxides generated, thus their corrosion deterioration.

- The marking was performed with a nanosecond pulsed fibre laser, varying in pulse duration (9 to 200 [ns]), repetition frequency, and pulse energy. Despite similar visual results, different laser parameters led to variations in phase composition and corrosion resistance. It was concluded that longer pulse durations combined with higher repetition rates best preserve the corrosion resistance of SS after laser marking[27].

- In this study, Psyllaki and Oltra [28] used a pulsed laser for the surface cleaning of three SS samples for the removal of the oxide layer generated by exposure to high-temperature oxidation(see figure 2), thus mitigating localized corrosion. The laser irradiation effectively removed the oxide layer without causing any material removal from the underlying metal.

Furthermore, more scientific articles involving pitting corrosion and characterization methods are briefly mentioned below:

- In this study, microscopy was used by Ghods and more[20] to investigate the properties of mill scale and its effect on the chloride thresholds of carbon steel rebar. From the Fe/O ratios observed in the backscattered, the observations regarding the chemical stoichiometry of the iron oxides in the mill scale were not certain; however, the light layer consistently had a higher Fe/O ratio when compared with the dark layer. Also, in electrochemical testing, the rate of metal loss was directly proportional to the passive current density. The

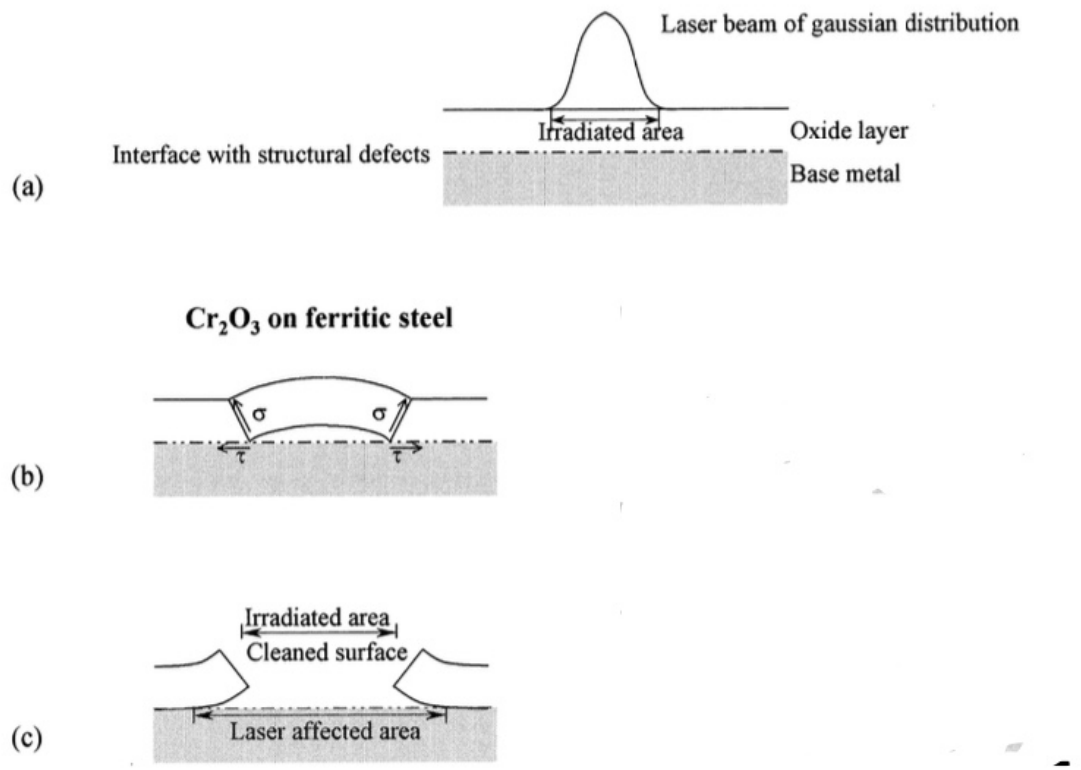

Figure 2: Oxide layer removal mechanisms during laser cleaning on SSsurfaces with weak interface (for example, Cr_2O_3 on ferritic steel): (a) Initial situation, just before the interaction between laser and material. (b) Development of stress field leading to material removal. (c) The final situation of the surface, after the interaction between laser and material[28]

present study claimed that could be used to explain why as-received rebar was more susceptible to chloride-induced depassivation than rebar without mill scale. The suggested mechanism was similar to that of typical crevice corrosion: oxygen depletion in the crevice results in reduced hydroxide.

- A mixture of ammonium fluoride (NH_4F) and HNO_3 was evaluated as an alternative to HF/HNO_3 for the pickling of weldments in certain SSs, including UNS S31600, UNS S32205, and UNS S32750. Both the HF/HNO_3 and the NH_4F/HNO_3 solutions effectively eliminated the heat tint created during welding, and these two pickling solutions demonstrated comparable passivation properties after 24 hours of pickling as assessed by CPP. This study indicated that the NH_4F/HNO_3 solution could be a viable substitute for the HF/HNO_3 solution in the pickling of SSweldments, according to Xiong and others [29].

- The degree of sensitization and corrosion resistance of AISI304 SSs was evaluated by double-loop electrochemical potentiodynamic reactivation and EIS. It was found that the as-received specimens had higher pitting corrosion potential and corrosion resistance than the sensitized ones. The Mott-Schottky results showed that sensitized SS had more defects in the passive film than as-received one. The compositions of the passive films were mainly Cr and Fe oxides via XPS, according to Zhang and others[30]. However, the

duration of the heat treatment was 5 [hr] at 675 [°C], while laser forming in this study uses an amount of minutes, instead.

- The risk of SS corrosion in brines is influenced by chloride content, temperature, pH, and oxygen levels. This paper examined the corrosion resistance of various SSs in highly concentrated sodium chloride solutions at 90°C, specifically in 20,000, 100,000, and 200,000 ppm Cl^- concentrations. The study assessed the effects of chloride and oxygen content, as well as solution pH, on test coupons with and without welds and on U-bend specimens. The corrosion resistance ranking for the SS grades was: UNS S31603 < UNS N08904, UNS S32205 < UNS S31254, UNS S32750 < UNS S34565 < UNS S32654. Aerated conditions were found to be the most corrosive, with higher chloride content and lower pH resulting in increased corrosion, based on findings in [31].

- Zatkalikova and Markovicova [32] examined how elevated temperature (50 [°C]) impacted the pitting corrosion resistance of AISI 304 electropolished SS in a 1 M chloride solution. They found that all AISI 304 surfaces decreased pitting corrosion resistance at this temperature, with the most significant decline in the "as-received surface." The ground and electropolished (G+EP) surface showed the best passive film quality and corrosion resistance, but a notable decrease in effectiveness at 50 [°C] indicated inadequate protection against pitting corrosion in aggressive chloride environments. Therefore, electropolishing 304 SS material can withstand pitting corrosion only at ambient and not at elevated temperatures.

- The samples heated to 1000[°C] exhibited a uniform reddish-brown color, which led to lower pitting potential and diminished corrosion resistance, impacting both uniform and crevice corrosion. A precise estimate of the corrosion rate could not be determined due to the significant asymmetry in the anodic and cathodic current curves, according to Pradeep [33].

- AISI 316L SS specimens were tested for pitting corrosion after forming oxide films through heating in air at various temperatures (200–1000[°C]). It was found that thermal oxides promote the nucleation of corrosion pits due to stresses and lattice defects but do not affect their growth. The peak susceptibility to pitting occurs after heating at 600[°C]. Although pickling removes thermal oxides formed at 200–800[°C] and improves pitting resistance, it does not restore initial stability due to residual stresses and lattice defects. Pitting tendencies increase after pickling when specimens are heated at 1000[°C] [34].

- The tests showed that pitting is a stochastic process, resulting in varied E_{pit} values. However, as the potential sweep rate decreased in CPP tests, the E_{pit} also decreased. In constant potential tests, E_{pit} decreased with longer exposure times. The researchers identified a specific pitting potential, called Eu, where pit formation begins[35]. In the end, the sweep rate parameter can affect the E_{pit} value.

- Burstein and Ilevbare [36] findings were that the size of the test specimen influenced the pitting potential of SS in acidic chloride solutions. Specifically, as the surface area of the specimen increases, the pitting potential decreases.

- Pistorius and Burstein[37] discussed the evolution of corrosion pits on SS in chloride solutions, highlighting three stages: nucleation, metastable growth, and stable growth. They focused on the metastable growth phase, noting that all pits initially grow under metastable conditions with a pit stability product that increases linearly over time but remains below the critical value of 0.3 $[Am^{-1}]$. During this phase, pits grow at a constant mean current density, maintained by periodic partial rupture of the protective cover. Thus giving us an idea of the metastable pit's character.

- The study by Tian and colleagues [38] focused on metastable pitting corrosion of 304 SS. Key findings include: the dissolution rate of metastable pits increased over time, peaking before repassivation; the average lifetime of these pits decreased with potential; however, the maximum pit lifetime, peak current transients, and pitting nucleation numbers increased with potential. Additionally, metastable pits changed from cone-shaped to dish-shaped during growth, with metal cations diffusion identified as the primary factor controlling growth despite an ohmic potential drop occurring between the pit interior and the bulk solution. To sum up, metastable pitting is affected by time(in the passive area of the curve), therefore scanning rate parameters.

- Von Moltke and colleagues[39] discussed the relationship between low pitting potentials and the behavior of metastable pits, noting that lower potentials lead to a higher density of smaller pits before repassivation. They highlighted that the iron-rich oxide film dissolves in acidic solutions, causing adverse effects mainly when the potential increases rapidly into the pitting range. Additionally, the colour of the heat-tinted surface did not indicate the composition of the oxide or its pitting resistance.

- A study was conducted by Elshawesh and Elhoudto[40] to investigate the effects of simulated heat tint from air oxidation on the pitting potential of 304 austenitic SS at temperatures of 200, 400, 600, 800, and 1050 [^{o}C] in various chloride concentrations. It was found that the heat tint effect increased with higher temperatures, particularly at 1050 [^{o}C], resulting in lower pitting potential and corrosion resistance. To enhance pitting corrosion resistance, hydrochloric acid pickling was performed, with improved pitting potential noted as pickling time and temperature increased, likely due to the removal of depleted chromium oxide film formed during the heat tint process.

As researched, a lot of laser procedures use the CPP method to study further any potential pitting problems on SSs. Also, AISI 304 has been mentioned several times to be one of the most resistant materials against localized pitting corrosion. Pickling has proven, in a few cases, to reverse the effects of corrosion deterioration, as well as laser processing methods by removing the generated in-situ oxide layer on the surface from various origin methods.

A recap on the key points of the literature foundation mentioned that would build up this study are:

1. Even if similar laser processing visual results are presented, different laser parameters can lead to variations in phase composition and corrosion resistance[27].
2. The laser irradiation method could remove the oxide layer without causing any material removal from the underlying metal[28].
3. Pickling of heat-tinted samples improved corrosion resistance [40]. But in some other cases, methods like pickling and passivation could not restore the SS layer without affecting the surface quality[24].

The absence of methodological diversity creates a research gap that needs to be filled in order to advance our understanding of this field. Thus, the intention is to be able to determine the pitting-resistant behavior of austenitic AISI 304 SS due to synergistic procedural effects of laser processing, such as laser forming with the purpose of altering the physical appearance, such as bending; laser remediation(pickling and laser ablation), and lastly, exposure to corrosive environments. Based on the research gap and knowledge provided in this study, the gap needs to be filled with various experimental SS coupon testing results, recording and interpretation for an overall view of the loss of corrosion resistance due to the process steps mentioned, and if possible enhancement is feasible.

Based on the theory collected and studied, this knowledge will be used to build up the methodology with the help of this study's context research articles (at chapter 4, *"Materials and Methods"*), on the basis of the hypotheses assumed to be applied here as well due to scientific reproducibility.

3 Theory and Background Knowledge

The goal of the in-depth investigation into the areas specified in this chapter below is to uncover any potential deficiencies in the existing literature that may give rise to uncertainty and interest. In this chapter, the theory of the topics will be studied with the purpose of better comprehension, thus beginning our research study.

3.1 Laser Material Processing

Lasers are commonly utilized in industrial applications as thermal processing instruments because of their operational accuracy, targeted treatment, rapid processing capabilities, and affordability[17]. High-energy lasers serve as a crucial source of energy for cutting-edge material processing and sophisticated, intelligent manufacturing. Also, utilizing the thermal effects of lasers to create advanced material shaping techniques like additive manufacturing[4][41].

Researchers are exploring the shock waves generated by pulsed lasers as force application methods; therefore, investigating material processing technologies that leverage these laser-induced force effects[42]. The required high power levels of the laser process initiate a phase transition and generate significant temperature variations in the treated area. This is inevitable because the laser beam must penetrate deeply into the substrate material to enhance the thickness during the procedure. Moreover, high-power laser heating encompasses heating in the solid phase, melting, and eventual evaporation at the surface.

Unfortunately, the rapid nature of the laser heating process leads to the inevitable creation of steep temperature gradients near the heated area, which is critical for high-power laser applications. The defect areas created in the laser-induced workpiece, as a result of excessive heating, restrict the practical use of laser processing because they lead to lower quality in the final product. Those areas are referenced as "Heat-Affected Zones" (HAZ).

Lasers with outputs of power 0,5-10[kW] can be used for metallurgical processing and be able to modify the properties of metal without affecting the bulk material[43]. As the laser power increases, the energy absorbed by the material's surface acts like a heat source, causing a notable increase in surface temperature. In some cases, this rise in temperature exceeds the evaporation threshold of the substrate material, leading to the evaporation of the surface. As the surface undergoes evaporation, the melted material at the surface pulls back towards the solid bulk. The surface evaporation undergone is inevitable when performing deep penetration laser processing or welding on metals. As a result, due to the quick nature of laser heating and the phase change process, there are high cooling rates during the solidification of the molten area[17][44].

Due to the development of significant temperature gradients in the regions where phase changes occur, which raises the thermal strain in these areas, the formation of thermal stress in the welded section is inevitable. Based on the intensity and type of residual stress(compressive or tensile) produced in the irradiated area, bending(see 8) induced by thermal effects can occur in

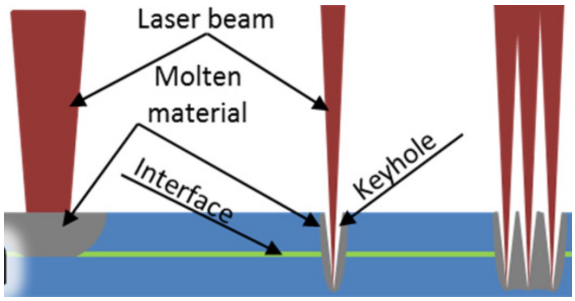

Figure 3: Laser surface conductive welding for overlap passes[46]

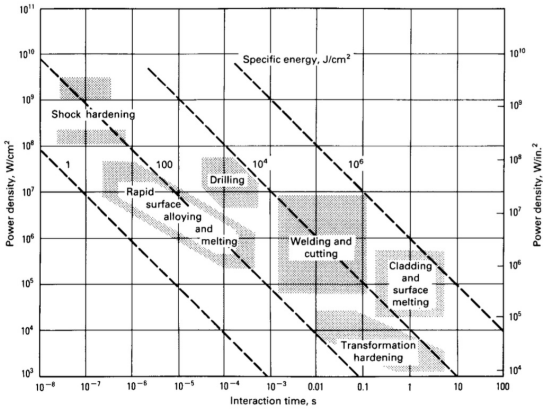

Figure 4: Interaction times and power densities necessary for various laser surface processes[43]

the substrate metal [17][44].

In the end, laser processing can be used to create corrosion-resistant surface layers. The longer a laser beam interacts with a material, the deeper it processes the layer[43](see figure 4). However, corrosion-resistant materials are expected to have very low general corrosion rates due to the presence of a protective surface oxide film[45].

3.2 Laser Forming

Laser-induced forming is a technique that modifies metallic components without direct contact. This method of applied laser energy is selected to create bends, spatial shapes, and alignments in both metallic and nonmetallic materials. Similar to welding techniques[47], laser forming can fulfill industry requirements due to its benefits, such as operational precision, cost-effectiveness, and localized treatment.

The laser forming process depends on temperature distribution to control the plate's deformation without any mechanical external loading. It can generate thermal stresses on a metal by irradiating it with a laser beam. This results in rapid localized heating (see figure 6) and subsequent cooling when the laser is turned off. During heating, if the thermal strains in the irradiated area exceed the material's elastic limits, affected by temperature and shape, these strains will become plastic compressive strains. Therefore, because of cooling, the irradiated material contracts, resulting in bending or alteration in the shape of the workpiece in the irradiated area. The bending of the metal sheet occurs due to both thermal strains and strains induced by stress. Specifically, as the metal sheet is heated, it tends to bend away from the laser beam because of the significant thermal expansion on the upper surface during laser scanning. The uneven distribution of the thermal strain gradient results in a complex stress distribution, causing the sheet to curve in the opposite direction.

It is crucial to understand how different processing parameters can influence the heat transfer

medium from the laser beam. Laser-induced forming involves complex interactions among various process parameters, including those related to laser beam irradiation (like power density and motion speed) and the thermal and mechanical properties of the material (such as absorption coefficient and thermal conductivity)[17][48].

Heat-inducing a specimen via a laser beam can increase surface oxidation, resulting in interference metal colour tint hues on the surface depending on the thickness of the oxide layer[23]. Laser parameters can affect the degree of this laser staining or tinting on the HAZ[49]. Lasers, like weldments, can undergo all traditional types of corrosion; however, they are especially vulnerable to those influenced by changes on surfaces, in microstructure and composition. At the HAZ (see figure 7), each location undergoes a distinct thermal experience during the laser thermal process, involving variations in both peak temperature and cooling rate. Consequently, every location exhibits its unique microstructural characteristics and vulnerability to corrosion.

During the laser processing of SS, there often arise locally sensitized areas (i.e., zones prone to corrosion)[50]. Sensitization occurs due to the formation of chromium carbide at the grain boundaries, leading to a reduction of chromium in the surrounding areas. This reduction in chromium creates highly localized galvanic cells. If the chromium content of the SS alloy falls below the critical 12 wt% essential for sustaining a protective passive film, the area will become susceptible to corrosion, leading to intergranular attack. This form of corrosion typically happens within the HAZ. This corrosion phenomenon is referred to as weld decay, also seen during the laser forming of SSs[14]. The higher the carbon content, the more carbide precipitation occurs, which means that alloys with lower carbon levels are less prone to sensitization compared to those with higher carbon levels. Specifically, quick cooling minimizes the occurrence of carbide precipitation and sensitization. Welds in thicker materials remain within the sensitization temperature range longer, making them more vulnerable to this issue. The minimum duration needed for sensitization, depending on the carbon content in a typical stainless steel alloy, is shown in figure 5. The structure's corrosion resistance needs to be regained by removing the high-temperature oxide that forms during heat treatment. In practice, post-weld heat treatment is seldom implemented[14][51]. SS sensitization control could be achieved by using either a postweld high-temperature anneal and quench to redissolve the chromium at grain boundaries and hinder chromium carbide formation during cooling and/or selecting a low-carbon grade of stainless steel to avoid carbide formation all together[14].

When performing laser processing, like laser forming, particularly in the absence of gas shielding, the thickness of the passivating chromium-rich oxide can vary. This inconsistency in oxidation leads to a gradient in the amount of chromium depletion near a stainless steel weld. Such behavior can result in a higher likelihood of localized corrosion. Evidence of this issue can be observed through the formation of heat-tint oxide. Defects such as insufficient penetration and microfissures can cause crevices that lead to crevice corrosion. Proper selection of welding consumables, correct techniques, and complete slag removal are crucial.

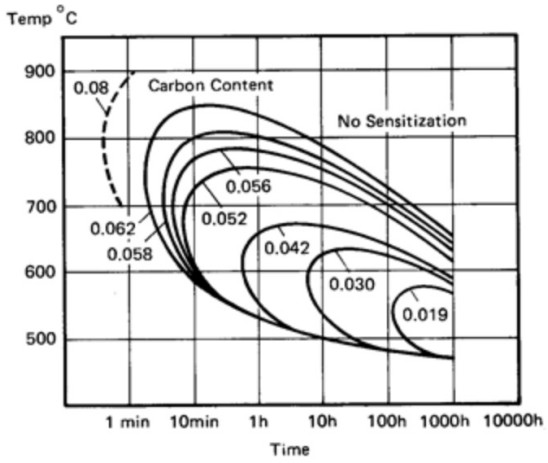

Figure 5: Time – Temperature – Sensitization Curve for 304 SS Grade[14][52]

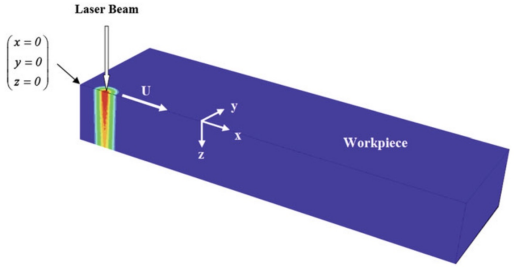

Figure 6: Diagram of laser heating process, indicating localized heating, and its coordinate system [17].

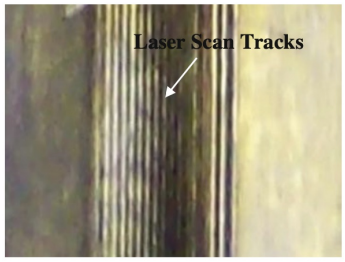

Figure 7: Laser generated scanning marking/tint at the HAZ [17].

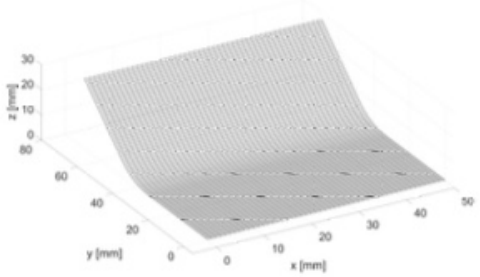

Figure 8: Laser forming v-bend configuration[53].

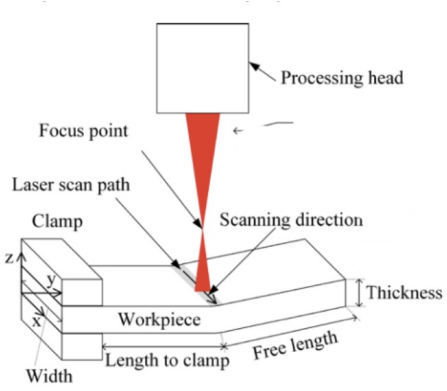

Figure 9: Laser setup diagram[54].

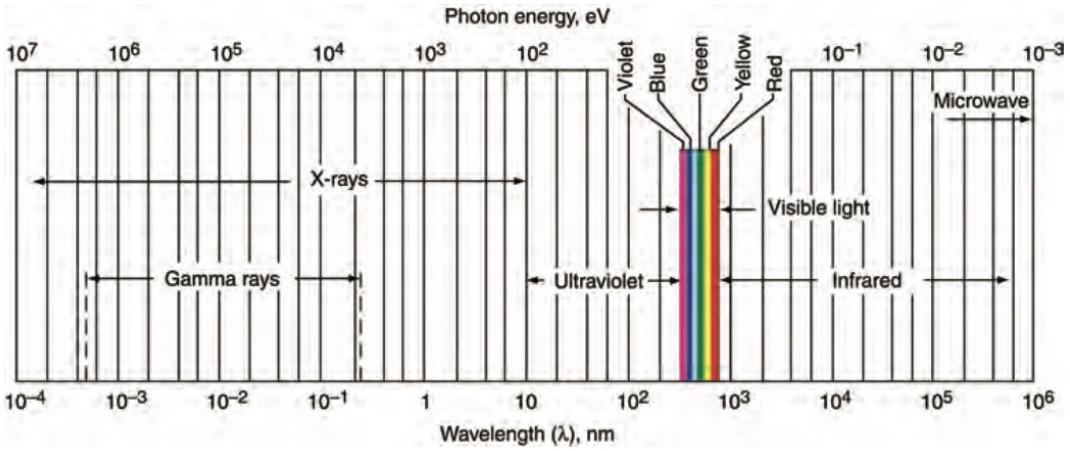

Figure 10: Electromagnetic spectrum of radiation types[57]

3.3 Laser Ablation

Laser-ablation processing [18][55][56] is able to create topographical features on nearly any material via tribological surface micro texturing. This method of laser texturing is clean, versatile, and fast, allowing for precise control over surface characteristics. Laser ablation is even able to change hydrophilic surfaces to superhydrophobic due to the increased roughness modification it can create. Nonetheless, it can lead to the formation of undesirable localized burrs or bulges made of melted and redeposited material, which could require further surface polishing. Due to the high power density of the laser beam pulse, the surface undergoes melting and rapid resolidification. Those small burrs or channels can eliminate the effect of wear particles by entrapping them. Therefore, deterioration of the surface is unavoidable.

The absorption coefficient of various materials during laser ablation varies greatly with wavelength, so by choosing a laser wavelength that spans from deep ultraviolet to infrared, it's possible to manage how materials are processed accurately[18].

3.4 Chemical Pickling

After the heat treatment of steel and surface texturing, proper cleaning operations are recommended, such as the method of pickling. Pickling is the most popular method of removing the scale from steel surfaces[58].

To begin with, the bulk material consists of four distinct layers(see figure11): the deformed boundary layer, the reaction layer, the sorption layer, and the contamination layer. The binding energy for every layer decreases as it approaches the surface. The deformed boundary layer is created through mechanical processing, while the reaction layer comprises metal oxides, sulfides, or compounds of phosphorus. In the sorption layer, the grease compounds adhere through chemisorption or physisorption. The outermost layer is the contamination layer, which

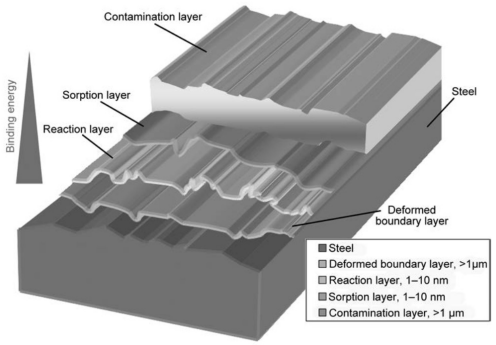

Figure 11: Bulk Metal layers[58]

Table 5 Sequence of procedures for pickling 300-series stainless steels

Cycle	Solution composition(a), vol %	Operating temperature °C	Operating temperature °F	Immersion time(b), min
Sulfuric acid dip	15-25 H_2SO_4(c)	71-82	160-180	30-60
Water rinse(d)	...	Ambient	Ambient	...
Nitric-hydrofluoric acid dip	5-12 HNO_3, 2-4 HF	49 max	120 max	2-20
Water rinse(d)	...	Ambient	Ambient	...
Caustic permanganate dip(e)	18-20 NaOH, 4-6 $KMnO_4$(f)	71-93	160-200	15-60
Water rinse(d)	...	Ambient	Ambient	...
Sulfuric acid dip	15-25 H_2SO_4(c)	71-82	160-180	2-5
Water rinse(d)	...	Ambient	Ambient	...
Nitric acid dip	10-30 HNO_3	60-82	140-180	5-15
Water rinse (dip)	...	Ambient(g)	Ambient(g)	...

(a) Acid solutions are not inhibited. (b) Shorter times are for lower-alloy steels; longer times are for more highly alloyed types, such as 309, 310, 316, 317, and 318. (c) Sodium chloride (up to 5 wt%) may be added. (d) Dip or pressure spray. (e) Sometimes used to loosen scale. (f) Percent by weight. (g) Boiling water may be used to facilitate drying.

Figure 12: Pickling procedure guidelines for 300-series SS[19]

plays a crucial role in the cleaning procedure. This layer keeps remnants from earlier processing stages, such as oil, grease, shavings, cleaner residues, or water components. Specifically, rust and scale that form on surfaces are generally removed via physical techniques due to the varying adhesion mechanisms involved[58].

The pickling process can perform the removal of oxide scale from mill products and fabricated parts. Scale that originates from hot work must be removed/remediated before subsequent processing is initiated. This oxide scale originates during the hot working or hot rolling of steel when the surface of the metal reacts with oxygen in the air to form oxides of iron or mill scale. The pickling process is identified as the chemical removal of scale by immersion with an aqueous acid solution. The required time to remove the scale is inversely proportional to acid concentration and temperature. Pickling of two alloys of the same material concurrently is not advised in the same immersion solution(sol.), and a trial prior is recommended for validation purposes.

Hydrochloric acid(HCl) is a common agent to use for pickling. For example, the reaction of HCI with scale(i.e. FeO) that is substantially Iron(II,III) oxide(Fe_30_4) mixed with iron(Fe) will form ferrous chloride precipitate and water:

$$FeO + 2HC1 \Rightarrow FeC1_2 + H_20 \tag{1}$$

$$Fe_30_4 + Fe + 8HC1 \Rightarrow 4FeC1_2 + 4H_20 \tag{2}$$

While the reaction of HCl with base metal forms ferrous chloride and hydrogen gas:

$$Fe + 2HC1 \Rightarrow FeC1_2 + H2(g) \uparrow \tag{3}$$

Underpickling is when the steel has not been sufficiently pickled. Whereas overpickling pickling leads to the porosity of the transverse surfaces, resulting in a rough texture throughout the entire surface, along with discolouration and a reduction in size and weight. To prevent overpickling, it is essential to take the material out of the bath promptly after the scale has been fully removed. Pitting can be caused by overpickling. In addition, rusting or uniform corrosion

can be accelerated if pickling sol. residue remains on the surface due to improper or inadequate after-cleaning[19].

3.5 Corrosion Properties

Corrosion is a damaging natural electrochemical phenomenon that leads to the deterioration of materials through their attack reaction with their environment. This reaction involves two half-reactions that occur simultaneously at the same rate on a material's surface:

- An oxidation or anodic reaction is indicated by an increase in valence or a release of electrons.
- A cathodic or reduction reaction decreases in valence charge or the consumption of electrons.

Specifically for metals, always in corrosion reactions, the anodic reaction is the oxidation of a metal to its ion. The electrons produced must equal the valence of the ion. This can be generally written as:

$$M \Rightarrow M^n + ne^- \tag{4}$$

where n is the quantity of electrons released.

Moreover, there are a number of different cathodic reactions that are frequently involved in metallic corrosion. The most common cathodic reactions are:

- Hydrogen evolution:

$$2H^+ + 2e^- \Rightarrow H_2 \tag{5}$$

-Oxygen reduction in an acidic sol.:

$$O_2 + 4H^+ + 4e^- \Rightarrow 2H_2O \tag{6}$$

-Oxygen reduction in a neutral and basic sol.:

$$O_2 + 2H_2O + 4e^- \Rightarrow 4OH^- \tag{7}$$

-Metal-ion reduction:

$$M^{3+} + e^- \Rightarrow M^{2+} \tag{8}$$

-Metal deposition:

$$M^+ + e^- \Rightarrow M \tag{9}$$

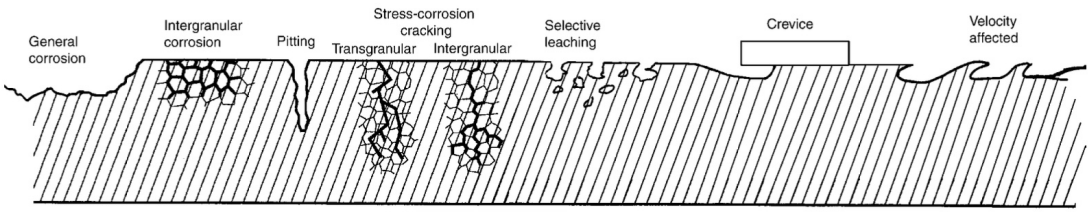

Figure 13: Forms of corrosion [60]

For example, when the iron(Fe) is immersed in water or seawater, the specimen rusts; thus, corrosion occurs[59]. Hence, the anodic reaction is based on equation 4:

$$Fe \Rightarrow Fe^{2+} + 2e^{-} \tag{10}$$

Because water and seawater are close to neutral pH and are exposed to a dissolved oxygenated environment, the cathodic reaction is equation 7. However, sodium and chloride ions do not participate in the reaction.

The overall reaction can be obtained by adding equations 12 and 7, and can be seen below:

$$2Fe + 2H_2O + O_2 \Rightarrow 2Fe^{2+} + 4OH^{-} + \Rightarrow 2Fe(OH)_2 \tag{11}$$

In the end, Ferrous (Fe^{2+}) hydroxide precipitates from the sol. leaving it unstable in its oxygenated environment, and gets oxidized to ferric (Fe^{3+}) salt; thus, the final product is rust [13]:

$$2Fe(OH)_2 + H_2O + 1/2O_2 \Rightarrow 2Fe(OH)_3 \tag{12}$$

Moreover, passivation significantly enhances the corrosion resistance of 304 stainless steel and restores its natural passive layer. The process of passivation enhances the natural formation of the chromium oxide (Cr_2O_3) passive film on clean surfaces, providing effective protection against corrosion[61]. The aim of a passivation treatment is to remove any residual iron particles or contaminants from the metal's surface. Plus, a properly conducted passivation can improve the Cr/Fe ratio[62]. According to ASM Handbook, Vol.5, passivation immersion of 300 series SS should be with 20-50% nitric acid at elevated temperatures for 30-60$[min]$[61][63]. The passive layer generation reaction is below[64]:

$$3Cr + 3O_2 \Rightarrow 2Cr_2O_3 \tag{13}$$

Degradation happens when a more strongly adsorbing harmful anion, such as a chloride anion (Cl^{-}), replaces the oxygen that constitutes the passive film. Once the Cl^{-} attaches to the surface, the breakdown process begins as the connection between the metal ions and the metal lattice becomes weakened, hence, corrosion initiates[61].

Uniform, or else general corrosion, is the attack on an exposed metal surface, resulting in a homogeneous thickness loss(thinning). This means the metal loss is spread evenly over the

surface instead of localized, such as pitting localized corrosion(see figure 13 to compare)[11]. Uniform corrosion thinning can be caused by various conditions, for instance[15]:

- Atmospheric corrosion
- Aqueous corrosion
- Galvanic corrosion
- Stray-current corrosion (which is similar to galvanic corrosion, but does not rely on electrochemically induced driving forces to cause rapid attack)
- Biological corrosion (which is a microbial-assisted form of attack that can manifest itself as uniform corrosion by forming weak or cathodic oxides, or it can also generate localized attacks)
- Molten salt corrosion and liquid-metal corrosion (which have become more of a concern as the demand for higher-temperature heat-transfer fluids increases)
- High-temperature (gaseous) corrosion

The materials selection, coatings, inhibitors, cathodic protection, and, in some cases, anodic protection could mitigate it.

This mass loss is the difference between the initial mass of the metal tested and the mass afterwards a known exposure duration. For engineering purposes, uniform corrosion rates are stated as loss of metal thickness per unit of time, for instance, micrometres per year, while these corrosion rates can be obtained via electrochemical testing. Alas, a low uniform corrosion rate would provide a bias and uncertain sense of confidence in the corrosion performance that would be contradicted by unexpected failure during the metal's lifetime. Also, general corrosion thinning is not as severe a problem as the formation of pitting attacks[11].

The concentration of Cl^- ions required to initiate corrosion can be as low as a few mg/L (ppm) for certain stainless steels in high-purity water conditions. The greater the susceptibility based on an alloy to uniform corrosion, the lesser the influence of Cl^- ions. In chloride-containing aqueous sol., low-carbon steel typically experiences uniform corrosion instead of localized attack[11][65].

3.6 Localized Corrosion: Pitting and Crevice

PITTING CORROSION

Passive films can experience a localized breakdown, which leads to an increased rate of degradation of the metal. When the corrosion starts on an exposed surface, it is known as pitting corrosion, whereas when it occurs in an enclosed space, it is referred to as crevice corrosion.

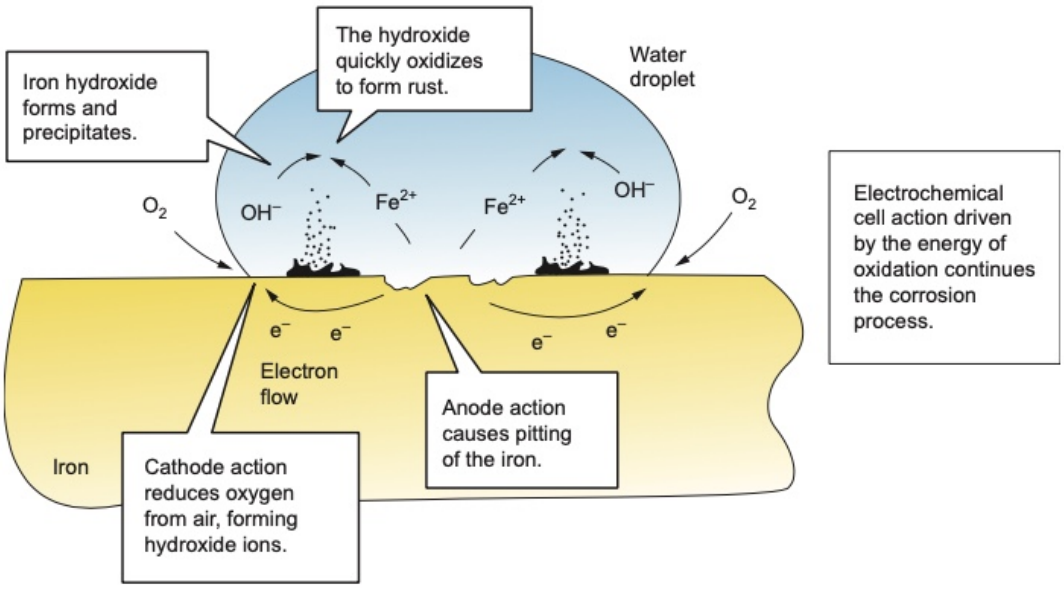

Figure 14: Positive ferrous ions react with negative hydroxide ions, creating rust, resulting in pits on the surface[57]

Classical pitting corrosion, resulting from the failure of the passive film, can only happen when aggressive anionic species are present and chloride ions are typically involved. Chloride is a small anion with a high diffusivity, and it can interfere with passivation. In general, most oxidizing agents increase the risk of pitting corrosion by supplying additional cathodic reactants. Commonly, dissolved oxygen is the most prevalent oxidizing agent. By eliminating oxidizing agents, like removing dissolved oxygen through deaeration, is an effective method for eliminating the likelihood of localized corrosion. It is important to highlight that chromate acts as an oxidizing agent and generally prevents corrosion by reducing it into a chromium passive film. The level of an anionic species, such as chloride, must increase within the pit to balance the charge associated with the concentration of cations and maintain charge neutrality[16][66]. When a sample has not been passivated properly, pits might appear.More causes of pitting corrosion include[15]:

- Local inhomogeneity on the metal surface
- Local loss of passivity
- Mechanical or chemical rupture of a protective oxide coating
- Discontinuity of organic coating
- Galvanic corrosion from a relatively distant cathode
- Formation of a metal ion or oxygen concentration cell under a solid deposit (crevice corrosion)

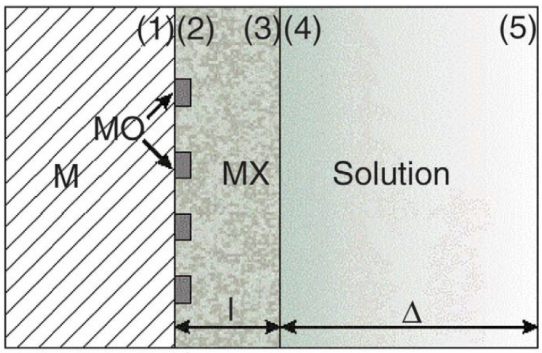

Figure 15: Diagram of the phases and interfaces on a metal surface immersed in a halide sol. (M, metal; MX, metal halide; MO, metal oxide; the numbers indicate the interfaces between the phases[70][73].

Pits[16][67][68][69] typically begin at some form of chemical or physical heterogeneity present on the surface, which can include inclusions, second-phase particles, solute-segregated grain boundaries, defects, mechanical damage, or dislocations. The oxide grain boundary regions have lower ionic transport resistance, hence are open sites for oxide breakdown, while Cl^- and OH^- adsorption compete with each other and accelerate ion transport at the defected site[70]. Also, theories regarding the breakdown of passive films and, later, the initiation of pits have been divided into three primary mechanisms: passive film penetration, film rupture, or adsorption[71][72]. Pitting is regarded as an autocatalytic reaction; once a pit begins to develop, the surrounding conditions change to encourage further pit advancement. The anodic and cathodic electrochemical processes involved in corrosion occur separately during pitting. The environment within the pit becomes depleted in cathodic reactants (like oxygen), which causes most of the cathodic reaction to shift outside the pit cavity, where this reactant is more abundant. The dissolution process within the pit increases the concentration of metal cations in the pit, as seen in equation 4.

An extra factor of the local metal pit environment that needs to be taken into account is the pH, which lowers due to metal cation hydrolysis and Cl^- migration[70], as seen in the equation below:

$$M^{2+} + 2H_2O \Rightarrow H_2O + H^+ + M(OH)^+ \Rightarrow M(OH)_2 + 2H^+ [16] \tag{14}$$

The common cathodic reactions that accompany the dissolution occurring in the pit, such as the oxygen reduction reaction (Eq 1), contribute to a localized increase in pH at the cathodic sites. Acidity is generated inside the pit, while the cathodic reaction does not neutralize it. This segregation between the anodic and cathodic processes states the need for more effective mitigation strategies.

As mentioned above, the local pit environment is characterized by a reduced concentration of the cathodic reactant, like dissolved oxygen, and an increased presence of metal cations and anionic species, such as chloride, leading to an acidified condition. This acidic chloride could inhibit repassivation. Also, it can encourage the ongoing growth of the pit. Therefore, it is crucial

to mitigate corrosion and enhance metal durability in such conditions. The environment in local pits is characterized by a lower concentration of cathodic reactants, such as dissolved oxygen, along with an increased presence of metal cations and anionic species like chloride, which results in an acidic condition. Acidic chloride conditions significantly affect the durability of metals by hindering the repassivation process[74], which allows for ongoing pit development. Investigating these factors is essential for creating strategies to mitigate corrosion and enhance the longevity of metals in such environments.

A significant collection of pitting potential values exhibits a normal distribution, indicating random variation. The likelihood of pitting (P) can be calculated by:

$$P(E) = n/(1+N)[16] \tag{15}$$

where N is the total quantity of samples studied, and n is the sample quantity that had pitted at a potential(E) or lower. The potential at specific P is a representative value for a given material and surface preparation.

Metastable pits are small pits that begin to form and expand for a limited time before becoming repassivated. While larger pits may cease growing for various reasons, metastable pits are generally regarded as those measuring no more than a micron and having a lifespan of seconds or shorter. Understanding metastable pits is crucial because, under specific circumstances, they can continue to expand and develop into larger pits, becoming stable pits. Stable pits endure beyond the metastable phase and keep growing, in contrast to metastable pits, which repressivate and stop their growth for some reason[16].

For SS, processes like heat treatment, grinding, and more have been shown a negative affect pitting resistance[75][76]. Pickling in nitric acid hydrofluoric acid mixtures or passivation in nitric acid can be beneficial. Heat treatment in air produces a chromium oxide layer and creates a chromium-depleted zone beneath it. Typically, the oxide layer is removed mechanically, and the chromium-depleted zone is eliminated through pickling[16].

Pitting is not easily evaluated by testing methods, such as metal mass loss caused by uniform corrosion. However, pitting properties can be determined for characterization purposes using standardized ASTM tests[11][77]:

- Test *ASTM G 48* [78] details a procedure for immersing stainless steel coupons in an oxidizing chloride environment, such as ferric chloride, either at ambient temperature or at an elevated temperature during a specific duration. Metal mass loss evaluates corrosion performance. Mass loss is a poor indicator of pitting unless uniform corrosion exists slightly while pitting is severe. Nevertheless, if there is significant mass loss from uniform corrosion, the pitting influence is small.
- *ASTM G 61* [79][80] is a method involving electrochemical testing by performing cyclic potentiodynamic polarization(CPP) to determine the susceptibility to localized corrosion.

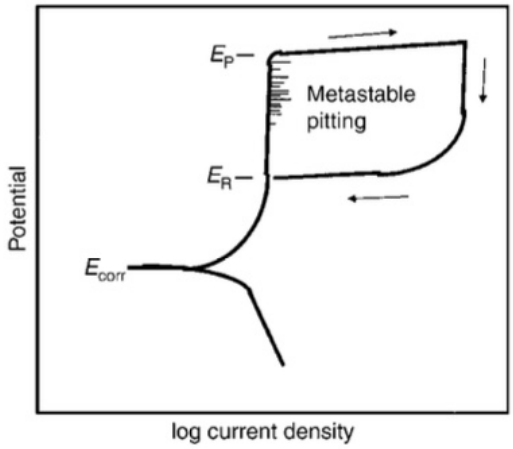

Figure 16: Plot of a polarization curve[16]

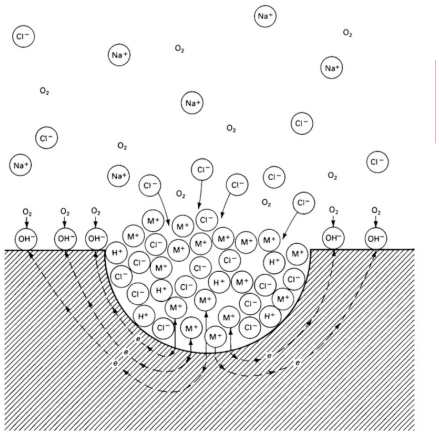

Figure 17: Autocatalytic process occurring inside a pit in NaCl[16]

In this method, pits initiate and proliferate at a more noble(higher) potential than the breakdown pitting potential(E_{pit}) of the passive film.

CREVICE CORROSION

Crevice corrosion, which occurs in occluded areas, is among the most harmful types of material deterioration, and its attack appears as uniform corrosion or pitting. It occurs when a wetted metallic surface is close to another surface, and it can have a highly distributed geometry.

Crevice corrosion consists of three processes, such as electrochemical reactions, homogeneous chemical reactions, and mass transport. However, the most intense corrosion reaction takes place outside the crevice instead of inside it. It is commonly believed that the buildup of metal ions in the electrolyte within the crevice makes this area act as a cathode compared to the region just outside the crevice's opening. Corrosion occurring outside the crevice (anode) continued to develop because the surrounding environment had a significantly lower concentration of metal ions. Pits and crevice locations often involve acidic solutions, as the metal cations produced by the dissolution of the alloy interact with water to generate metal hydroxides and hydrogen ions. While for pit initiation, surface flow effectively delays or prevents aggressive solution development. In contrast, the large length-to-gap ratio in a crevice makes initiation control much less effective than in pits.

In the case of electrochemical testing, maintaining the open-circuit potential for a material beneath the repassivation potential can significantly reduce the occurrence of localized corrosion. Typically, anodic polarization increases the speed at which crevice corrosion occurs. When eliminating electrolytes from these areas, crevice corrosion cannot occur since one of the necessary conditions for its form of corrosion has been eliminated [70][81][82].

3.7 Electrochemical Corrosion Testing Theory: Cyclic Potentiodynamic Polarization(CPP)

OPEN CIRCUIT POTENTIAL (OCP)

The Open Circuit Potential (OCP)[83][84] is a crucial initial voltage measurement taken before performing other electrochemical corrosion tests. It helps determine whether the following tests will demonstrate linear, causal, or stable behavior in the Gamry software, thereby verifying the validity of the raw test data.

- A system is linear when it obeys Ohm's law. If not, no harmonics were generated during the testing run.
- A system is stable when it does not change with time and returns to its original state after the perturbation.
- A system is causal when the response of the system is due only to the applied perturbation.

Therefore, it can measure the voltage in an open circuit without the presence of an external load, similar to DC current. When two metallic materials are immersed in an electrolytic solution, they create a potential difference referred to as open circuit potential. This potential difference can be measured using an electrode. The electrochemical reaction takes place within a device called an electrochemical cell. In this setup, chemical reactions in a medium are transformed into electrical signals. In this process, electrons are oxidized as they travel from the metal with a lower potential (anode) to the metal with a higher potential (cathode). Consequently, OCP can indicate the metallic characteristics of a material when it is subjected to electrochemical analysis.

A three-electrode configuration is frequently utilized in electrochemical analysis and consists of a reference electrode, a working (test) electrode, and a counter (auxiliary) electrode. In this arrangement, electrons move solely between the working and counter electrodes, thereby maintaining a stable reference potential[85].

CYCLIC POLARIZATION (CPP)

Techniques for testing electrochemical corrosion that rely on redox reaction principles can assess the electrochemical characteristics of a metal or alloy when placed in a corrosive environment. The Cyclic Potentiodynamic Polarization(CPP) technique is normally used to qualitatively evaluate a metal's tendency to pit in a corrosive environment while the destruction of the passive film occurs[86]. Therefore, it can be used to characterize localized corrosion[87].

An open circuit or corrosion potential (E_{corr}) can determine the kinetics of the reaction via the corrosion rate. In the anodic polarization scan, the process begins at the corrosion potential once the steady state has been achieved[83]. By CPP, quantitative details that can be obtained

are pitting or breakdown potential (E_{pit} or Eb), and passive current (ip). The corrosion current density (i_{corr})[88] can be determined through the evaluation of anodic and cathodic polarization curves, a process commonly known as Tafel extrapolation(β_A & β_C)[89][90].

The CPP testing setup parameters are detailed below:

- **Initial E:** The initial sweep for data acquisition begins at this step.
- **Forward Scan:** The forward scan rate is the speed of the potential sweep during the initial scan and is measured in [mV/s]. The recommended maximum scan rate is 1 [mV/s], as higher rates may produce unreliable results due to the potentiostat's settings for long-time constants.
- **Apex E:** One of the two prerequisites for reversing the potential sweep is that the sweep will reverse upon reaching the Apex E, provided that the Apex I (current) is not encountered beforehand.
- **Reverse Scan:** The reverse scan rate refers to the speed at which the potential changes after a scan reversal. Scan Rate is in mV/s, and the maximum recommended is 1 [mV/s]. While also here higher scan rates can be used, they may produce unreliable data because the instrumentation is set up for slower changes.
- **Final E:** Ending point for the potential sweep following scan reversal. The allowed range is ±10 V with a resolution of 1/8 [mV]. Its accuracy depends on the setting. The Scan Range, defined as the most anodic voltage in the scan minus the most cathodic voltage, must be less than 8 [V].
- **Apex I:** Establishes one of the parameters that trigger a reversal of the initial ramp. The scan will reverse immediately when the absolute value of the current surpasses the Apex I. The unit for Apex I is milliamperes [mA]. The permissible range for Apex I extends from zero to the maximum current specified for the potentiostat. Negative values for Apex I are prohibited due to the use of absolute value in the assessment.
- **Sample Period:** Spacing between data points.

The experiment involves a gradual linear increase in the potential of a metal. The first sweep is directed towards anodic potentials. When the detected current attains a certain threshold, the direction of the sweep reverses or changes, resulting in a cathodic-going sweep. The raw data extracted consists of a graph depicting the logarithm of current(I_{corr})(or current density(i_{corr}), if selected) against potential(E or V). A notable hysteresis observed between the sweeps suggests the occurrence of pit formation depicted in figure 16 [2][79][91]. The lack of a hysteresis loop during the reverse scan may indicate uniform corrosion[83].

E_{pit} is the minimum potential at which the material tends to initiate pitting corrosion. When above the E_{pit}, new pits will initiate and develop[92][93].When a CPP scan is conducted at

electrode potentials that are lower than the pitting potential, the resulting curve often exhibits some variations. This transient behavior is caused by the formation of metastable pits, which can initiate and expand pitting but are rapidly stopped and undergo repassivation. While both stable and metastable pits contribute to an increase in anodic current density, the rise occurs for metastable pits only for a short duration due to the inadequate development of concentrated acidic chloride solution within these pits[83].

In a CPP *E vs logi* plot, the increase in anodic current density at potentials lower than the E_{corr} potential is due to the onset of pitting and the formation of localized corrosion (E_{pit}). The other factor contributing to the rise in current density prior to oxygen evolution may be the deterioration of the oxide layer and the onset of pitting corrosion in the presence of aggressive ions. When aggressive ions are not present, the passive layer remains stable above the electrode potential for O_2 evolution. A significant increase in anodic current at potentials surpassing E_{corr} suggests that the surface is exhibiting active corrosion behavior. Scanning to elevated positive potentials increases the susceptibility of the surface to damage [83][94].

The conditions under which a specimen is examined significantly influence its behavior in the CPP test. The dissolution of different gases such as H_2, O_2, and CO_2 influences the overall corrosion behavior, formation of the passive film, and, eventually, its pitting corrosion. Due to the damaging effects of hydrogen on high-alloy stainless steel[69], the stability of the protective passive film is observed to cause a decrease in E_{corr} and E_{pit}. When the solution with chloride ions is less concentrated, the pitting potential will be observed at higher (more noble) potentials[83].

Pitting corrosion resistance (R_{pit}) is a way to characterize the pitting resistance of a material when exposed to corrosive-induced conditions, and can be determined from the equation:

$$R_{pit} = |E_{corr} - E_{pit}| \text{[83]} \tag{16}$$

Values to be extracted from *E vs logi* plot.

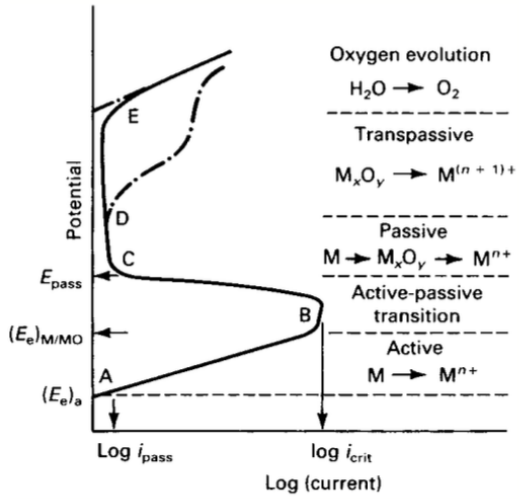

Figure 18: Potential vs. log current density plot chemical reactions occurring per step[95]

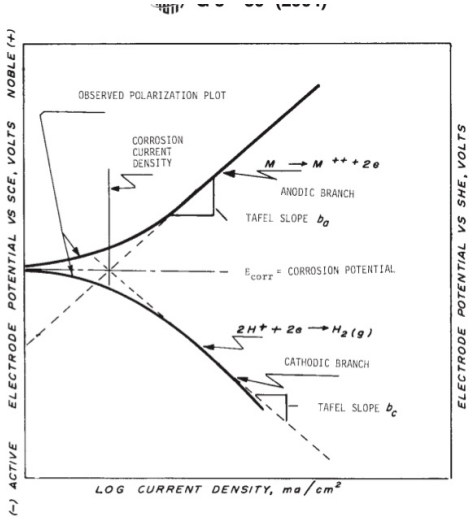

Figure 19: Cathodic and anodic polarization diagram[96]

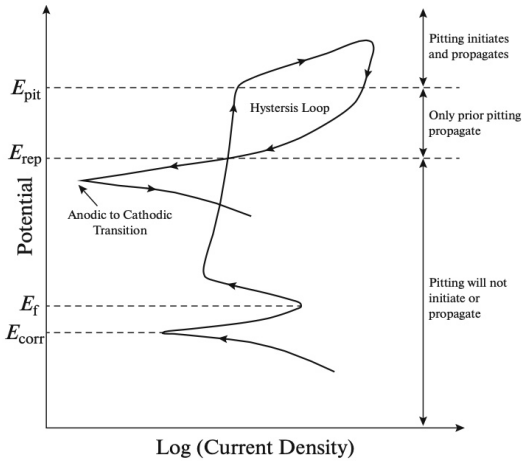

Figure 20: CPP curve and corrosion parameters. The arrows show the direction of polarization[83].

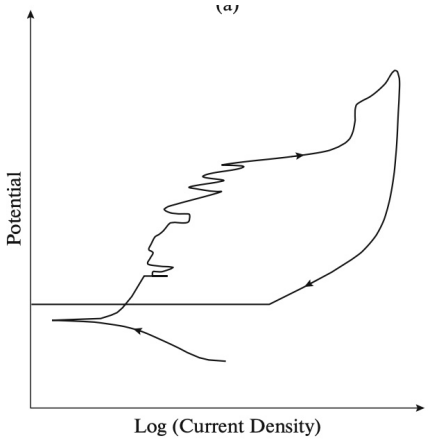

Figure 21: CPP scan of 304 SS in 3.5 [wt%] NaCl sol.[83].

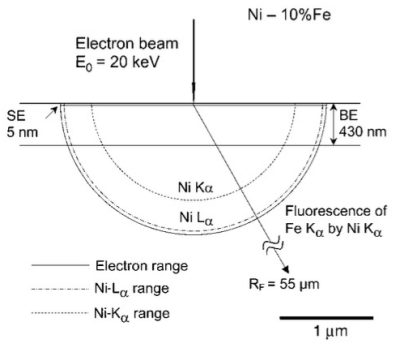

Figure 22: Diagram of the interactions between the electron beam and a sample (Ni- 10%Fe alloy). Displayed are the electron range, the sampling depths of backscattered electrons (BE) and secondary electrons (SE), the x-ray generation ranges for Ni-Ka and Ni-La, and the range of fluorescence radiation, R_F, for Fe-Ka excited by Ni-Ka[97].

3.8 Scanning Electron Microscopy (SEM) with Energy Dispersive X-ray Spectrometry (EDS/EDX) Theory

Scanning Electron Microscopy (SEM)[97] can be used as a localized corrosion characterization method. It is a method of visualizing microstructural features in greater depth. Moreover, SEM serves as a non-destructive characterization method, and it can detect a variety of signals, including backscattered electrons, which allow for the differentiation of variations in atomic number and the production of corresponding images (elastic impact). In addition, secondary electrons are effective in delivering topographic details of the examined sample (inelastic impact)[98].

To carry out elemental analysis, Scanning Electron Microscopy (SEM) can be enhanced with Energy-dispersive X-ray spectroscopy (EDS/EDX), which employs X-ray signals to generate chemical data. Each element has a unique number of electrons situated at its energy levels. When an electron beam displaces one of these electrons, it creates a positively charged electron-hole. An electron from an outer shell subsequently fills this vacancy, prompting a transition from a higher to a lower energy level. The energy released during this transition is emitted as an X-ray. These emitted X-rays are then detected by a silicon drift detector connected to a personal computer. Consequently, achieving accurate elemental quantitative analysis requires careful calculations of peak intensities to ascertain the atomic concentrations of the present elements[99]. The ratio method can illustrate the X-ray intensities of two elements irrespective of their thickness in relation to their atomic ratios or weight fractions using the equation:

$$\frac{C_A}{C_B} = k_{(AB)} \frac{I_A}{I_B} (17)$$

where k_{AB} is the factor for the relative efficiency of the generation and detection of X-ray waves [100]. The compounds with the greatest thermodynamic stability are found with a higher Cr/Fe ratio. The Cr/Fe ratio influences atomic bonding, which in turn affects the characteristics of the carbide [101].

4 Materials and Methods

This chapter will provide a detailed explanation of the methodology employed in this study, which was based on the literature reviewed and the experimental design according to the research aim, objectives, question, and scope of this investigation.

The study examines several cases to compare the pitting resistance and corrosion behavior at each step of this laser-forming sourced oxide layer remediation process (see table 2), according to the Design of Experiments (DOE) method, which will determine the relationship and effects between multiple factors. Each coupon was a combination of factors to examine and characterize afterwards, and the labelling nomenclature used is detailed in table 3. Hence, this study will focus on the remediation process, meaning every step of the process will be examined for observation, thus trying to interpret the observations and answer the research question set above in chapter 1. The research strategy that was followed was experimental, meaning for every step of the process, a control was reserved for a comparison study against the experimental group of coupons. The sampling strategy will not be random; coupons will be subjected to individual processing pattern for an overall examination of mainly quantitative data collection for further descriptive and inferential statistical analysis.

4.1 Laser Forming

The materials and apparatus used are listed below:

- 304 SS coupons
- Acetone, pure

AISI 304 SS coupons were precisely cut to the same dimensions outlined in the accompanying table 5. They were prepared for laser processing, specifically laser forming, on-site at the AAU campus. All coupons came from the same batch and same sheet. Unfortunately, the exact chemical composition of the metal could not be obtained, so a reference AISI 304 SS composition is depicted in the table 4. The laser forming aimed to bend the coupons, causing an angle and also creating a distinct interference colour difference that facilitates the examination of the oxide layers generated on the surface, in line with the objectives of the study case. The detailed parameters for the laser forming process are provided in the table 6.

To ensure the accuracy of the location lasered, each sample was carefully secured in a fixture within the laser chamber at ambient temperature, with a capacity to accommodate four coupons per laser cycle. For this project, half the sampling population was effectively laser-formed at a power of 0.65 [kW](coupons labelled for this study as LL), resulting in a yellow heat-tint hue only on the HAZ. Meanwhile, the other half of the samples were laser-formed at 0.80 [kW](labelling of HL used), producing a vibrant orange to reddish hue. This systematic approach will allow us to

Table 2: Coupon Preparation Plan Summary

Step 1	AISI 304 SS Obtain, Clean and Degrease
Step 2	Laser Forming (Low and High Power)
Step 3	Remediation Treatment (Laser Ablation and Chemical Pickling)
Step 4	Testing & Characterization (Ferric Chloride Immersion Test, CPP, and SEM/EDX

Table 3: Study Coupon Labeling and Nomenclature

RM-	AISI 304 SS raw/base material
LL-	Lower laser power parameter during laser forming (0,65 [kW])
HL-	Higher laser power parameter during laser forming (0,80 [kW])
-C	Control (not processed)
-LA	Laser Ablation Remediation Method
-P	Chemical Pickling Remediation Method

Table 4: Chemical Composition of AISI 304 SS [12]

C	**Mn**	**P**	**S**	**Si**	**Cr**	**Ni**	**Fe**
0,08	2,00	0,045	0,030	1,00	18,00	8,00	bal.

continue with our research study of either mitigating or enhancing corrosion resistance via their heat-tint scale surface characteristics. At least one of each different laser power coupon was reserved as a control for further testing of CPP and SEM/EDX. Lastly, each coupon laser formed was cleaned in a pure acetone sonicator bath for 2 [min], rinsed with pure acetone, wiped any potential residuals from the laser-heat treatment, risen once more with pure acetone and left to air dry.

The hypothesis would be to have two distinguishable heat tints generated that would indicate the variance in the thickness of the oxide layer on the surface and different colour intensities. Based on the literature study, even if coupons obtain the same visual heat tint, it does not mean they would have the same corrosion resistance. The laser-formed coupons are expected to have some surface deterioration, thus being less pitting-resistant than the 304 SS raw/base/as-received material.

The methodological limitation of laser forming in this study was the fluctuation of laser power, which could generate deviated oxide layer thicknesses for each coupon. Also, each coupon was secured manually on the laser fixture, so deviated HAZ locations on the coupons' surface may exist.

Table 5: Characteristics of Study Coupons Tested

Material:	304 SS
Dimensions:	80x50x1 [mm]
Laser Generated Bending Angle:	$10^o(0,65[kW]laserpower(LL))$ $20^o(0,80[kW]laserpower(HL))$
Laser Generated HAZ Dimensions:	50x15 [mm]

Table 6: Laser Forming Process of 304 SS Coupons at AAU facility

Laser Travel Speed:	100 [mm/s]
Cooling Time between Pathes:	15 [s]
Beam Diameter at the Plate:	3 [mm]
Laser Power (Low):	0,65 [kW]
Laser power (High):	0,80 [kW]

4.2 Remediation Methods: Chemical Pickling and Laser Ablation

The materials and apparatus used are listed below:

- 304 SS coupons of LL and HL laser processed
- 10[wt%] HNO_3 + 1% HF sol. and 20[wt%] HNO_3 + 2% HF (for Pickling)
- Analytical beakers and lab equipment
- Balance ± 0,1 [mg] tolerance (AND Instruments)

After laser forming, acetone degreasing and cleaning, the coupons were labelled based on their experimental purpose and process to be followed.

CHEMICAL PICKLING

Then, to prepare the laser-formed coupons for their pickling remediation treatment, the initial mass was collected to determine the mass loss after the pickling was completed. Pickling took place at ambient temperature inside a laboratory fume hood for 60 [min] per study case. The pickling immersion sol. was a mixture of 1[wt%] hydrofluoric acid with 10[wt%] nitric acid (HNO_3/HF sol.) After conducting two pickling cycles with the mixture mentioned above for the LL coupons and three cycles for the HL coupons, the converted mass loss based on the double-sided surface volume could not achieve a value close to 1μm. Therefore, one extra pickling cycle was conducted with a modified mixture of 2[wt%] hydrofluoric acid with 20[wt%] nitric acid sol. that was capable of reaching an as-close-as predictable mass loss in order to have significant overall results for further characterization.

LASER ABLATION

Laser ablation of the indicated laser-formed coupons was outsourced to a company. The laser ablation performed parameters used are detailed in table 7. LL and HL laser-formed coupons were laser ablased with the laser ablation parameters. The entire surface of each coupon was laser ablased, while during laser forming, only the HAZ area was scanned. Afterwards, the laser-formed ablased coupons were returned to AAU for further characterization, while at least one coupon per case (LL-LA and HL-LA labelled coupons) was reserved as controls.

At the end of every remediation treatment, a visual record was kept, and controls were reserved (LL-P, HL-P and LL-LA, HL-LA).

Table 7: Laser Ablation Remediation Method of 304 SS Coupons

Machine:	200W pulse laser water-cooled
Power:	80%
Frequency:	30 [kHz]
Speed:	8000 [mm/s]
Width:	50 [mm]
No. Overflows:	2
Overflow Angle:	30 °

The hypothesis of both remediation methods, based on the literature review, is to remove the entire oxide layer from the surface of the SS coupons and remediate their pitting and corrosion resistance, hence being less susceptible to pitting during further characterization tests.

4.3 Ferric Chloride Pitting Testing

The materials and apparatus used are listed below:

- 304 SS coupons (LL/HL-LA/P-PT[#])
- 0,75 [wt%] Ferric Chloride, $FeCl_3$(aq) sol. (VWR Chemicals) (pH: 1-2)
- Temperature Control Cooler/Heater
- Balance ± 0,1 [mg] tolerance (AND Instruments)
- Waterproof SiC Sandpaper, FEPA P no. 320, US no.280, Grain size 46μm (Struers) (QTY: 2)
- Rotary Grinding Machine (see figure 23)

Continuing with the ferric chloride pitting test influenced by the ASTM G 48 [78] standard, all coupons' mass was weighed prior to and after the testing ended to determine the mass loss. The goal of this test was to evaluate the corrosion behavior via average mass loss of each study group after exposed to laser forming and remediation treatment.

All coupons reserved for the chloride immersion test were ground and polished by a rotary grinding machine(figure 23) with no.280 sandpaper only at their four edges to avoid any crack or pitting propagation from the exposed sides. The acidic immersion sol. was ferric chloride($FeCl_3$) with 0,75[wt%] concentration. The duration of the test was 24 [hr] at 20[^{o}C] for three identical samples per study case. Each coupon was submerged under the immersion sol. individually located inside a larger water bath that maintained the desired temperature, as depicted in figure 24. A mixer was helping to maintain the temperature, and a cooler/heating source was stabilizing the water bath temperature. Lastly, visual examination and mass loss statistical analysis took place. Under a 20x magnification of a microscope, the observations for potential deterioration were checked.

Figure 23: Rotary Grinding Machine

Figure 24: Ferric Chloride Pitting Testing Apparatus

A trial of one raw 304 SS coupon(unprocessed) was tested initially for validation purposes. It was observed that because it was immersed with a plastic ABS holder, at the location surface where they came in contact, pitting was observed. Hence, individual beakers were used in the actual experimental setup.

The hypothesis is to observe mass loss due to the synergistic effect of laser processing, reme-

diation treatments and acidic immersion exposure for all study groups. Uniform corrosion, suggested by the literature study, may be present, apart from potential pitting.

Methodological limitations may exist on the immersion testing conditions due to possible temperature fluctuation during the entire duration of the immersion and for each overnight cycle.

4.4 CPP

The materials and apparatus used are listed below:

- 304 SS coupons (LL/HL-LA/P-CP[#])

- For Passivation Process Step:

- 20 [wt%] Nitric acid (VMR Chemicals)
- 3M Vinyl Tape (dimensions: 25x30 [mm])
- Glassware, hot plate, thermometer

- For Electrochemical Testing:

- Wax (Organic)
- Gamry Instruments Potentiostat, Gamry Electrochemical Cell accessories(Ag/AgCl calomel and its KCl storing sol., electrode, air compressor, 1000[ml] jacketed beaker cell, etc.) and Software (Instrument, Echem Analyst)
- 3,5 [wt%] Sodium chloride, NaCl(aq) sol. (VWR Chemicals) (pH: 6-7)
- Waterproof SiC Sandpaper, FEPA no. 320, US no.280, Grain size 46[μm] (Struers)(if needed)

The CPP experimentation was based on ASTM G 61 Standard[79][80], with the testing conditions at ambient temperature, aerated with compressed air and using sodium chloride, 3,5[wt%] NaCl(aq). An Ag/AgCl calomel was used in the experimental testing. One hour of OCP was performed prior to all CPP runs with the same parameters, with a total time 3600[s], sample period of 1[s] and stability 0[mV/s]. CPP testing parameters used are indicated in table 8.

Development of Experimental Procedure

Preliminary development of the experimental procedure took place to validate a unique method of sample preparation for better data acquisition. Afterwards CPP of actual 304 SS coupons were tested for their pitting potential and resistance recognition. Initially, a raw material(nonprocessed) that was passivated with a 25x30 [cm] tape, was tested on different Gamry parameters, such as

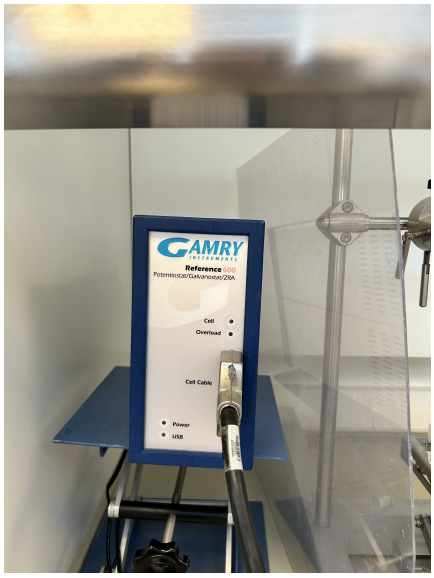

Figure 25: Gamry Potentiostat

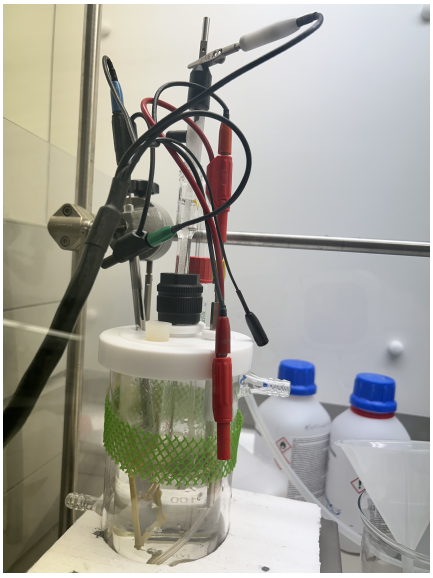

Figure 26: Jacketed Corrosion Cell Used for Testing 304 SS Coupons

with Apex I:5$[mA/cm^2]$ and sample period:2[s]. Also combinations of sample periods of 1[s] with Apex I:0, 1$[mA/cm^2]$ and 1$[mA/cm^2]$ where tested. In addition, trials of coupon passivation method deviation took place. Three different coupon passivation ways for sample preparation were suggested:

1. Coupon was not passivated at all
2. Coupon had their whole surface passivated(no tape was needed)
3. Coupon had their whole surface passivated while a tape sealed a squared area(where the HAZ was located for heat-treated coupons)

Lastly, after deciding on the best Gamry CPP setup parameters and passivation ways, a welded(and bent) coupon was tested on the conditions mentioned above.

Actual Experimentation

To begin with and verify the validation of the development of the experimental procedure performed above, the steps of preparing 304 SS coupons for the CPP characterization test were performed:

1. Applied a waterproof tape cover in the location indicated in figure 27. The tape was located on top of the HAZ when heat-tinted. The dimensions of every tape used on coupons were 25x30[cm]. The purpose was for the covered area not to get passivated by the nitric acid, thus later being more susceptible to pitting corrosion when tested in the NaCl medium.
2. 20[wt%] nitric acid passivation for 30[min] at 60[°C] with the tape cover.

Figure 27: Example of a 304 SS Coupon that was passivated with the taped area sealed from the nitric acid passivation sol., and later waxed.

3. The edges and back surface were seal-waxed as in figure 27. At the 3/4 length from the bottom, sealant was applied horizontally, and wax stopped at the same location at the back side too, where the NaCl liquid of approximately 300[ml] reached its height when inside the jacketed electrochemical beaker cell of 600[ml] capacity.
4. Ground the area where the working electrode would be attached during testing for better contact during data acquisition.
5. Left to dry wax overnight and let to repassivate surface after removing the tape.
6. Set up into the electrochemical cell the coupon tested and started CPP data acquisition.

All study groups had a sample population of at least three coupons of the same treatments tested to verify the reproducibility of their behavior and to be used for statistical analysis.

The hypothesis for CPP was that localized corrosion was predicted conservatively to occur at potentials above the repassivation potential. Thus, it should not take place if the pitting potential remains below the repassivation potential [70]. However, due to a lack of time, the curve hysteresis was not set to be completed, thus we cannot determine the repassivation potential. The results are expected to show E_{pit} for the remediated coupons approximately as close as the raw material in order to prove that remediation was effective in retrieving pitting resistance.

The methodological limitations were the deviated manual waxed dimensions covering each coupon's surface. Therefore, the possibility of crevice corrosion rejects was higher.

Table 8: CPP Settings for the Characterization of 304 SS Coupons

Initial E:	-0,1 [V vs. SCE]
Forward Scan:	0,1667 [mV/s]
Apex E:	1,5 [V vs. SCE]
Reverse Scan:	0,01667 - 10 [mV/s]
Final E:	-0,1 [V vs. SCE]
Apex I:	0,1 [mA/cm^2]
Sample Period	2 [s]
Sample A:	7,5 [cm^2]

4.5 SEM with EDS/EDX

The materials and apparatus used are listed below:

- 304 SS coupons per study group(controls/not processed))
- Zeiss EVO LS15 SEM-EDS/EDX
- SmartSEM Software
- INCA EDS X-ray Microanalysis System Software

SEM with EDX was performed on all controls, apart from high power laser formed control due to lack of materials. Also, all were scanned for their material character, to reverse engineer their elemental composition of oxygen, iron, and chromium percentages. Deep cleaning with acetone was performed prior. Note that all coupons were controls, meaning that after their indicated treatment, they were reserved and no further processing was performed on them and no testing(CPP or Ferric Chloride Testing). For example, the RM-C coupon was the base material, the LL-C and HL-C were the low and high laser power formed controls, respectively, and the same trend for LL and HL-LA for the laser ablation, and lastly LL and HL-P for the pickling. All SEM coupons were scanned only on their HAZ, and only one coupon from each study group was scanned. The oxygen concentration of each coupon generated is relative to every coupon compared to their bulk composition. Their elemental ratios of iron and chromium with oxygen were calculated and compared.

The hypothesis is to have increased oxygen concentration on the HAZ for study group coupons of LL-C and HL-C caused by laser forming and then reduced after both remediation methods. The raw material oxygen concentration can function as a baseline to estimate approximately the degree of oxidation on the surface due to processing. Also, via SEM, the laser-formed and ablazed surface structures are expected to have melting on their grain boundaries, while for pickling, more etching is to be observed, based on literature observations.

The limitation of SEM and EDX is that the elemental results of the scanning could be biased since the scanning can penetrate deeper than an oxide layer and detect elements from the bulk material and still count them in their elemental composition extracted data list obtained.

Figure 28: SEM/EDX System at Aalborg University

5 Results and Discussion

The following section will present and analyze the quantitative findings from the study conducted in chapter 4. Here, we will elaborate on the answers to the research question posed in section 1.3. To begin by discussing the results of the ferric chloride pitting test, including the associated mass loss. Next, we will present the values obtained from the CPP characterization method, such as E_{pit}, E_{corr}, R_{pit}. Finally, we will examine the surface structure and elemental analysis results from the SEM and EDX tests.

5.1 Ferric Chloride Pitting Testing

The ferric chloride pitting test was able to help answer the research question by testing for objective 2. The coupons tested are presented in figure 32. The statistical analysis can be found in the Appendix in the figures 67,68 and 69.

Regarding the development of the experimental procedure, as mentioned in section 4.3, a trial 304 SS coupon was immersed for 24 [hr] in a 0,75[wt%] ferric chloride sol. The results from this trial, as seen in figure 30, indicated pitting on the surface where the coupon came in contact with the plastic holder. By doing this preliminary trial, it was found how susceptible to pitting the material was; the pitting would have been generated from bias and not from the actual pitting corrosion generated when not affected by other components.

Continuing with the actual experimental results, no pitting was observed on any coupons tested, even under a microscope. Therefore, the pitting density over the double sides area of the coupon's surface was zero. However, due to uniform corrosion, mass loss was seen. The higher the mass loss, the lower the pitting corrosion resistance.

For each study group, an average value of mass loss was determined via statistical analysis.

- The average mass loss of the raw material(RM-C) was 10,20±0,3 [mg] with 95% confidence that the true value lies between 9,50 to 11,00 [mg]. The relative standard deviation (RSD) was 3%, while the relative average deviation (RAD) was 67%.
- The average mass loss for the laser-formed coupons by power 0,65[kW] (LL-C) was 18,00±1,30 [mg], with 95% confidence that the true value lies between 14,70 and 21,30 [mg]. The RSD% was 7% and RAD% was 67%.
- The average mass loss for the laser-formed coupons by power 0,80[kW] (HL-C) was 18,40±3,60 [mg], with 95% confidence that the true value lies between 9,50 and 27,40 [mg]. The RSD% was 20% and RAD% was 74%.
- The average mass loss for the laser-formed by power 0,65[kW] (LL-LA) initially and laser ablation remediation coupons was 122,10±3,80 [mg], with 95% confidence that the true value lies between 112,80 and 131,40 [mg]. The RSD% was 3% and RAD% was 69%.

- The average mass loss for the laser-formed by power 0,80[kW] (HL-LA) initially and laser ablation remediation coupons was 140,80±13,90 [mg], with 95% confidence that the true value lies between 106,62 and 175,40 [mg]. The RSD% was 10% and RAD% was 67%.
- The average mass loss for the laser-formed by power 0,65[kW] initially and pickling remediation coupons (LL-P) was 164,80±67,00[mg], with 95% confidence that the true value lies between 1,60 and 331,20 [mg]. The RSD% was 41% and RAD% was 67%.
- The average mass loss for the laser-formed by power 0,80[kW] initially and pickling remediation coupons (HL-P) was 149,10±9,90 [mg], with 95% confidence that the true value lies between 124,50 and 173,70 [mg]. The RSD% was 7% and RAD% was 67%.

The lower the Relative Standard Deviation (RSD), the narrower the spread of the data results, indicating a higher level of precision. The Relative Average Deviation (RAD) can be utilized to evaluate the accuracy, stability, and variability of a data set. A lower RAD percentage indicates whether an instrumentation is acceptably accurate; thus, the smaller the percentage, the more accurate the results are. Due to the relatively high percentage of precision and accuracy results, it is hard to be certain that the actual results are representative of the true average mass loss. Hence, the error bars in the comparison chart in figure 31 indicated a large deviation of the results and uncertainty, especially in the LL-P study group.

The comparison bar chart in figure 31 showed that the mass loss of the laser-formed coupons was similar to that of the raw material, in contrast to the remediated coupons, where the mass loss was extremely high with deviated error bars magnitudes. Understandably, the laser formed would lose more mass than the raw since it gained due to the oxide layer formed because of the laser processing. Deterioration in the remediation study groups could be due to the series of processes performed on the surface of the coupons; thus, deterioration via uniform corrosion was accelerated. Better pitting and corrosion resistance was observed from the raw material and the laser-formed materials since they behaved similarly in a ferric chloride environment.

The results agreed with the hypothesis of the uniform corrosion, but not with the pitting existence. That could be due to the modified ferric chloride concentration being more diluted than the concentration of the ASTM G 48 standard of 6[wt%].

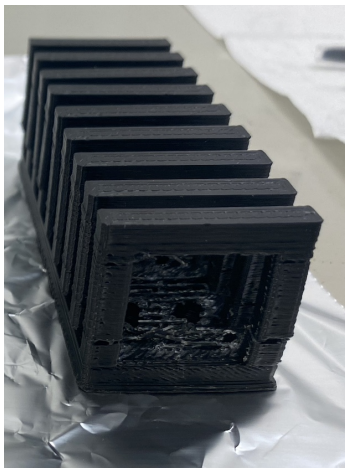

Figure 29: Plastic Holder for SS Coupon Used for Immersions

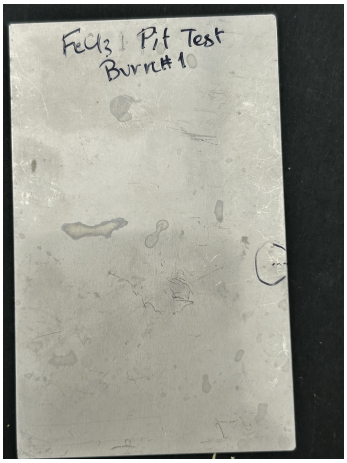

Figure 30: Ferric Chloride Pitting Test Coupon Used for Process Development

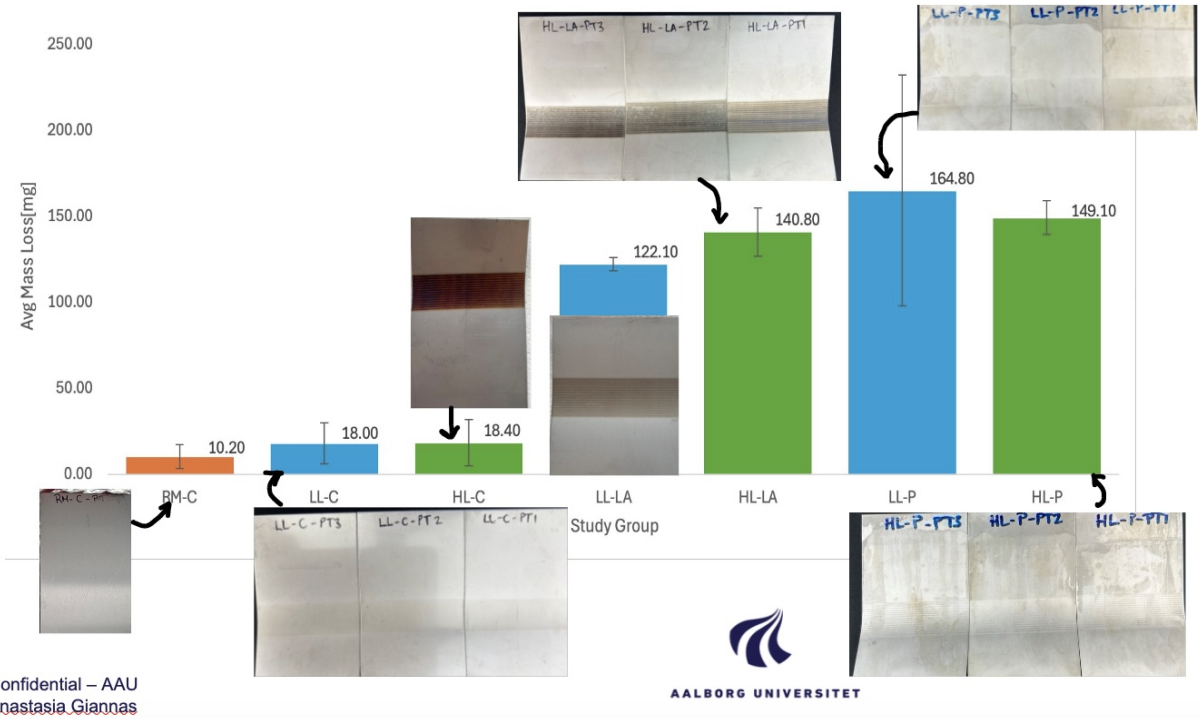

Figure 31: Mass Loss Comparison Bar-chart per Study Group

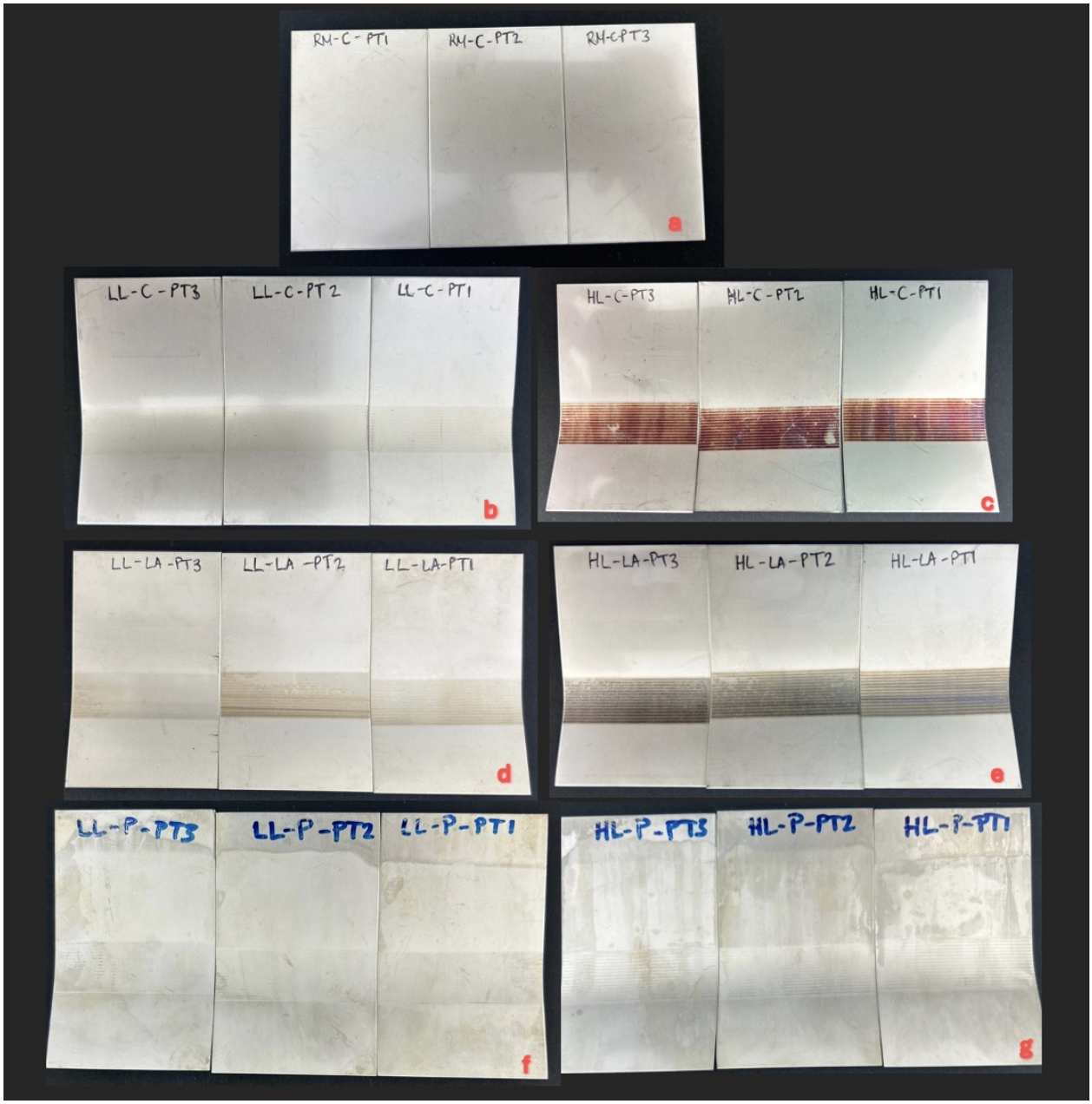

Figure 32: Depiction coupon results after Ferric Chloride testing, where a) is RM-C study group,b) LL-C,c) HL-C, d) LL-LA,e) HL-LA,f) LL-P and g) HL-P

5.2 CPP

The CPP test was able to answer the research question by testing for objective 3. Detailed raw data obtained with their statistical analysis for CPP can be found in the Appendix , in the figures 71 to 78.

As mentioned in section 4.4, the goal of the experimental procedure development was to establish a method that would allow us to obtain pitting potential and resistance from a smaller, non-passivated area. At the same time, the surroundings were passivated and more corrosion-resistant. The series of coupon preparations was passivation, waxing, grinding the working electrode contact area, and left overnight prior to testing. For the method development, various tests were performed to evaluate the Gamry software testing parameters, such as Apex I and sample period (see figure 70 in the Appendix), in order for our test coupons to have pitting mostly inside the non-passivated area and limited to no pitting in the surroundings by avoiding crevice corrosion.

Development of Experimental Procedure

As mentioned in the methodology, the first test prior to a CPP run was the OCP. The most important evaluation of the preliminary data was the comparison study of the runs evaluating the passivation to be used.

In figure 35, the OCP plot includes a sample that was passivated at the whole surface without any tape to seal an area, another coupon that was not passivated at all and another with the use of the tape. For coupon 4, we can see that the coupon has the most pitting inside a square area, while the passivate and nonpassivated have pitting spread out over the entire exposed surface. Most importantly, in figure 36, the results of their CPP curves(potential vs. log current density), a comparison depiction, indicated that the whole passivated surface was the most corrosion resistant; however, we had no metastable pitting to study, only stable pitting. Afterwards, a nonpassivated coupon was tested, and not only was there metastable and stable pitting but also uniform corrosion. The best method was the passivated coupon with a nonpassivated seal square area because the metastable and stable pitting exists without uniform corrosion. So, as we can see, this curve is between the whole and nonpassivated curves. Hence, the pitting corrosion resistant series from the most resistant to the least was: all surface passivation>tape method passivation>nonpassivation, based on their E_{pit} indication on the plots.

Lastly, a welded coupon was tested to validate our selected method of passivation for the coupon preparation. The tape was sealing partially HAZ. The picture of the coupon in figure 36 shows a welded coupon with a thin HAZ that was welded several times on the same area and had an intense black surface colour, thus being heavily heat-tinted/stained(see figure 33 and 34). However, the visual results indicated no pitting on the surface. Anyway, it would have been hard to see pitting due to the dark staining. Nevertheless, from the welded coupon CPP curve, there was no pitting, only uniform corrosion at a lower potential(thus lower corrosion resistance) than the other non-heat-treated coupons in this method development study. Also, the welded coupon

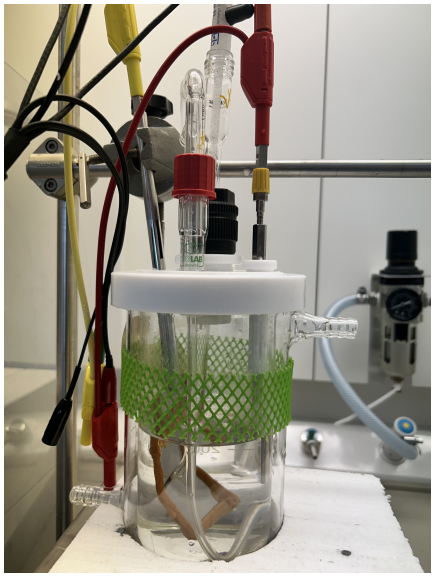

Figure 33: Three-electrode setup with bent and welded coupon setup for CPP with the purpose of experimental process development testing

Figure 34: 304SS welded used for process development connected to the working electrode

showed no passivation area from the curve.

The results of this development process gave us a first impression of the behavior of the base material (RM-C) to be tested as an actual study coupon for the 304 SS laser forming and remediation pitting resistance study.

Actual Experimentation

In relation to the OCP run for all study groups, as shown in figure 38, we observe the stability of the potential during the sodium hydroxide passivation process over the course of an hour of aeration. A more stable passivation indicates greater corrosion resistance, which is attributed to the stability of the passive layer formed on the metal's surface.

After validating the method to be used for preparing the CPP coupons, below are the results related to the study inspired by the research aim, question per objective 3.

For the base material investigation study group (see a depiction of coupons in figure 39), the Gamry software parameters that had been validated were Apex I: 1 $[mA/cm^2]$ and sample period 2[s]. Nine(9) coupons were CPP ran, with three(3) having crevice corrosion, thus rejected. The pitting probability was 0,6 based on equation 15. The CPP potential vs log current density curves of all RM-C coupons are depicted at figure 40, where we can see that almost all curves have metastable and stable pitting and a large passivation area. This is an example of a well pitting resistant behavior.

For the LL-C coupons(figure 41), the parameters were changed after crevice corrosion was found; therefore, it was decided to reduce the current density to avoid rejects since one of the study's limitations was the quantity of coupons processed. The Apex I was changed to 0,1$[mA/cm^2]$

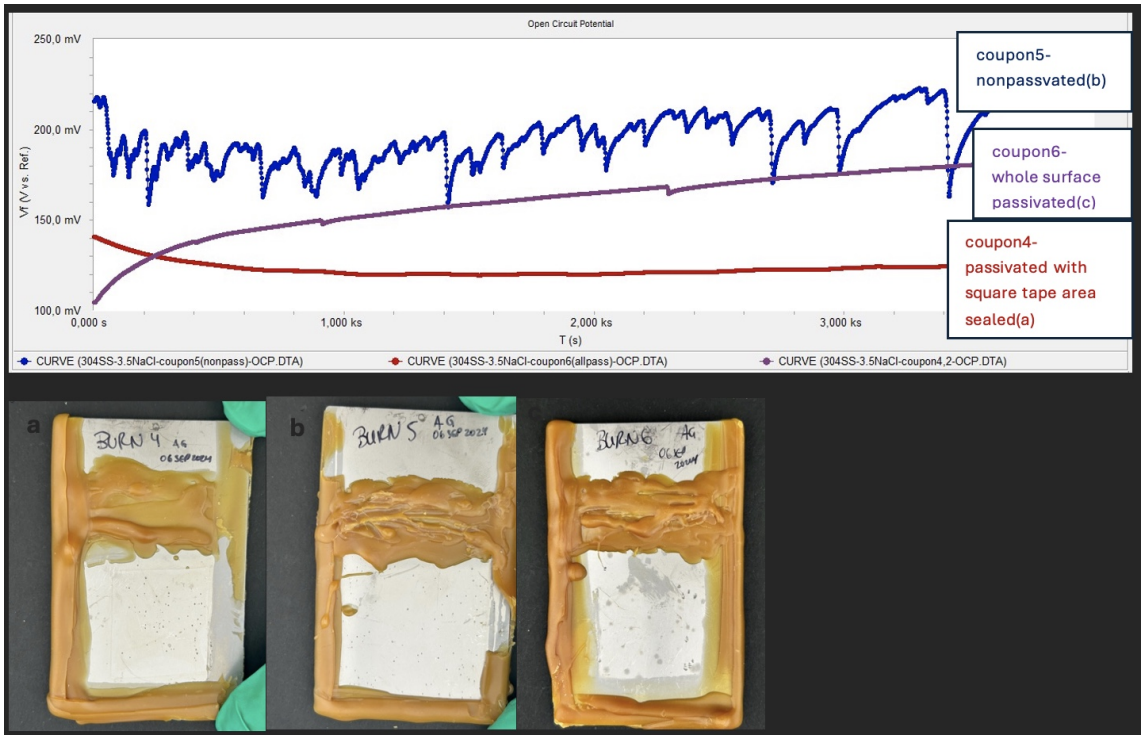

Figure 35: OCP Gamry Plot for Coupons during Process Development for Experimental Procedure and their Indicated Coupons

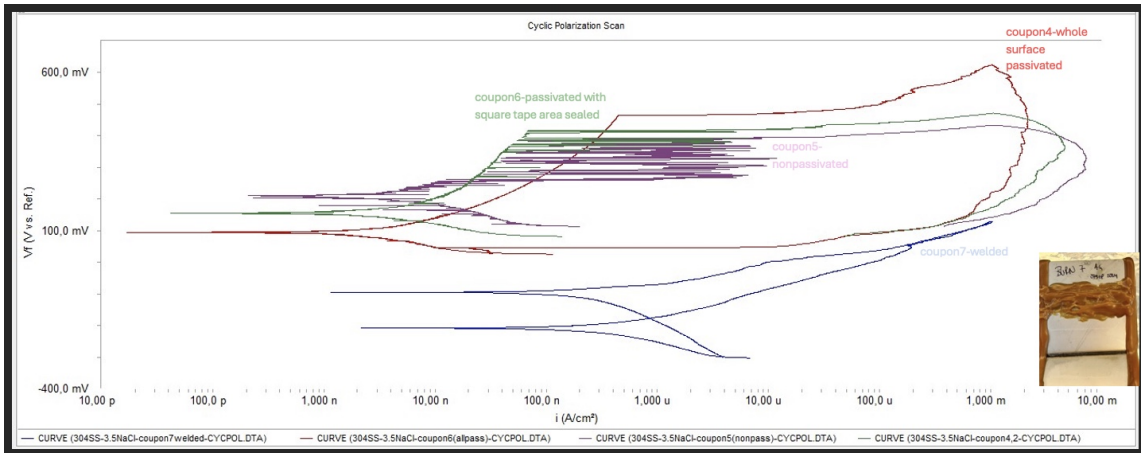

Figure 36: Potential vs Log of Current Density Gamry Plot for Process Development for Experimental Procedure Coupons.

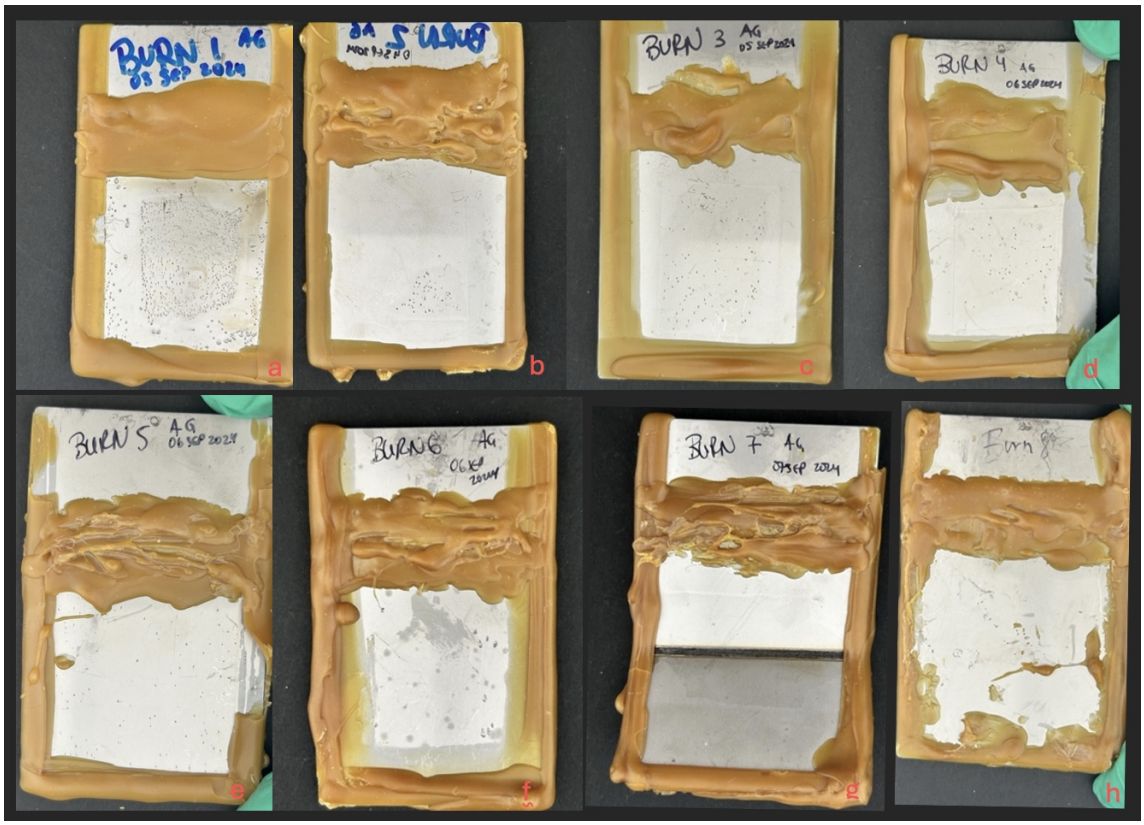

Figure 37: 304 SS(base material) depiction of coupon results after CPP, where a) is Burn coupon 1,b) Burn 2,c) Burn 3, d) Burn 4,e) Burn 5,f) Burn 6, g)Burn 7 and h) Burn 8. For further details per burn test, see figure 70 used for the development of the experimental procedure.

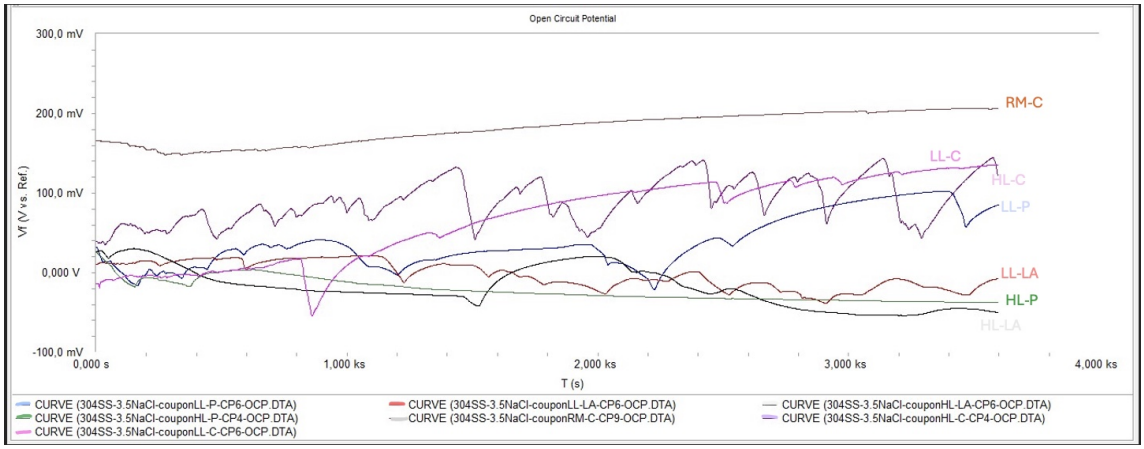

Figure 38: OCP Gamry Plot Comparison per Study Group

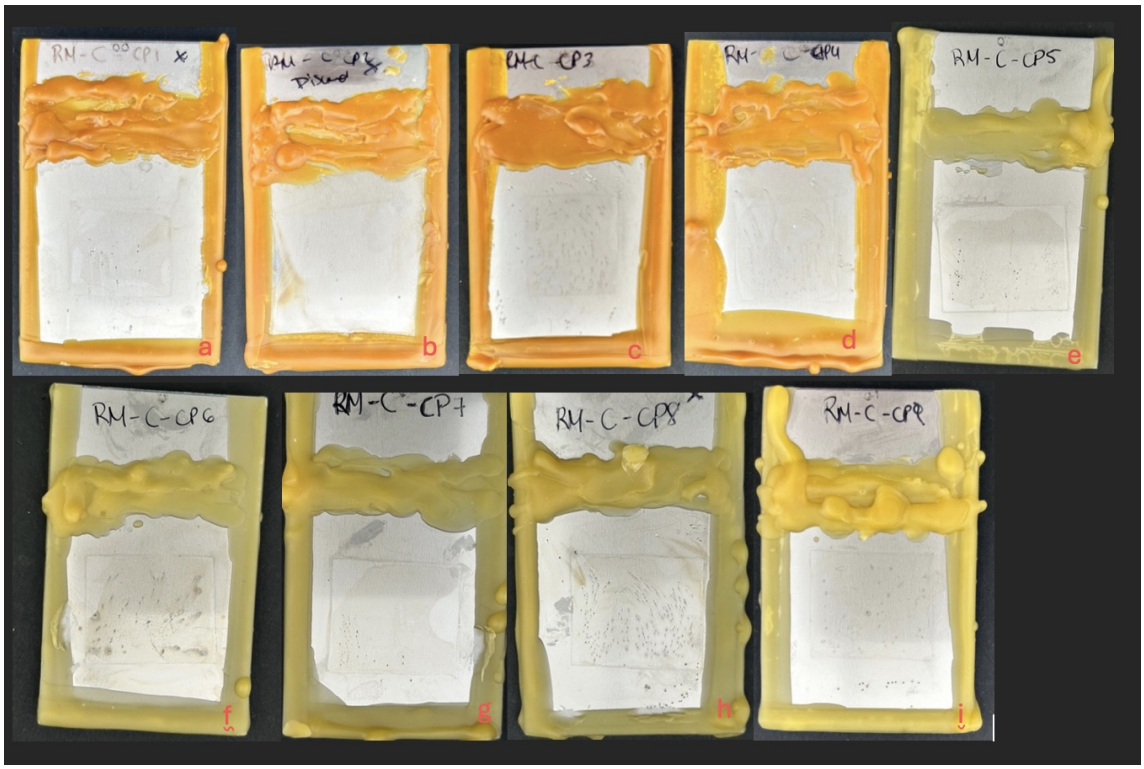

Figure 39: Depiction of coupon results after CPP, where a) is RM-C-CP1,b) RM-C-CP2,c) RM-C-CP3, d) RM-C-CP4,e) RM-C-CP5,f) RM-C-CP6 and g) RM-C-CP7, g) RM-C-CP8 and i)RM-C-CP9.

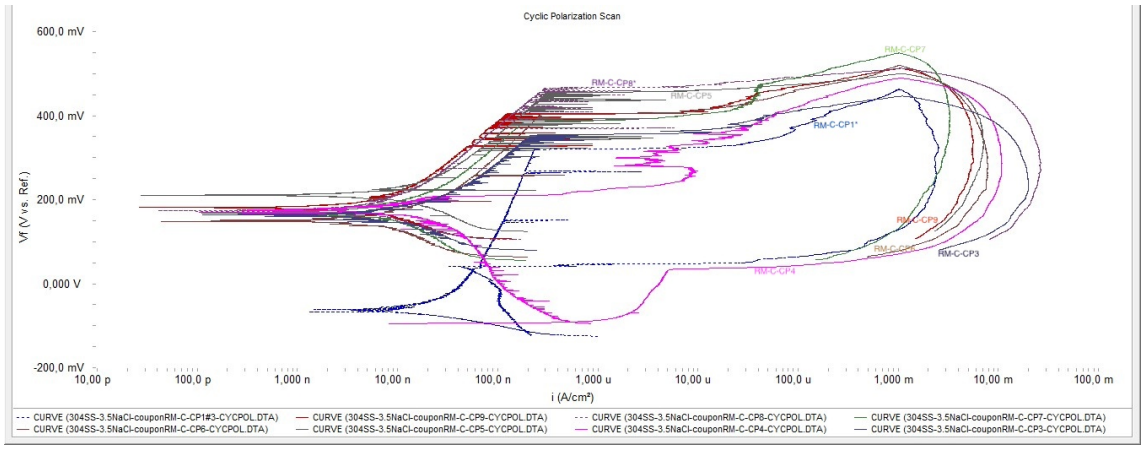

Figure 40: All CPP Potential vs. Log of Current Density Runs of RM-C

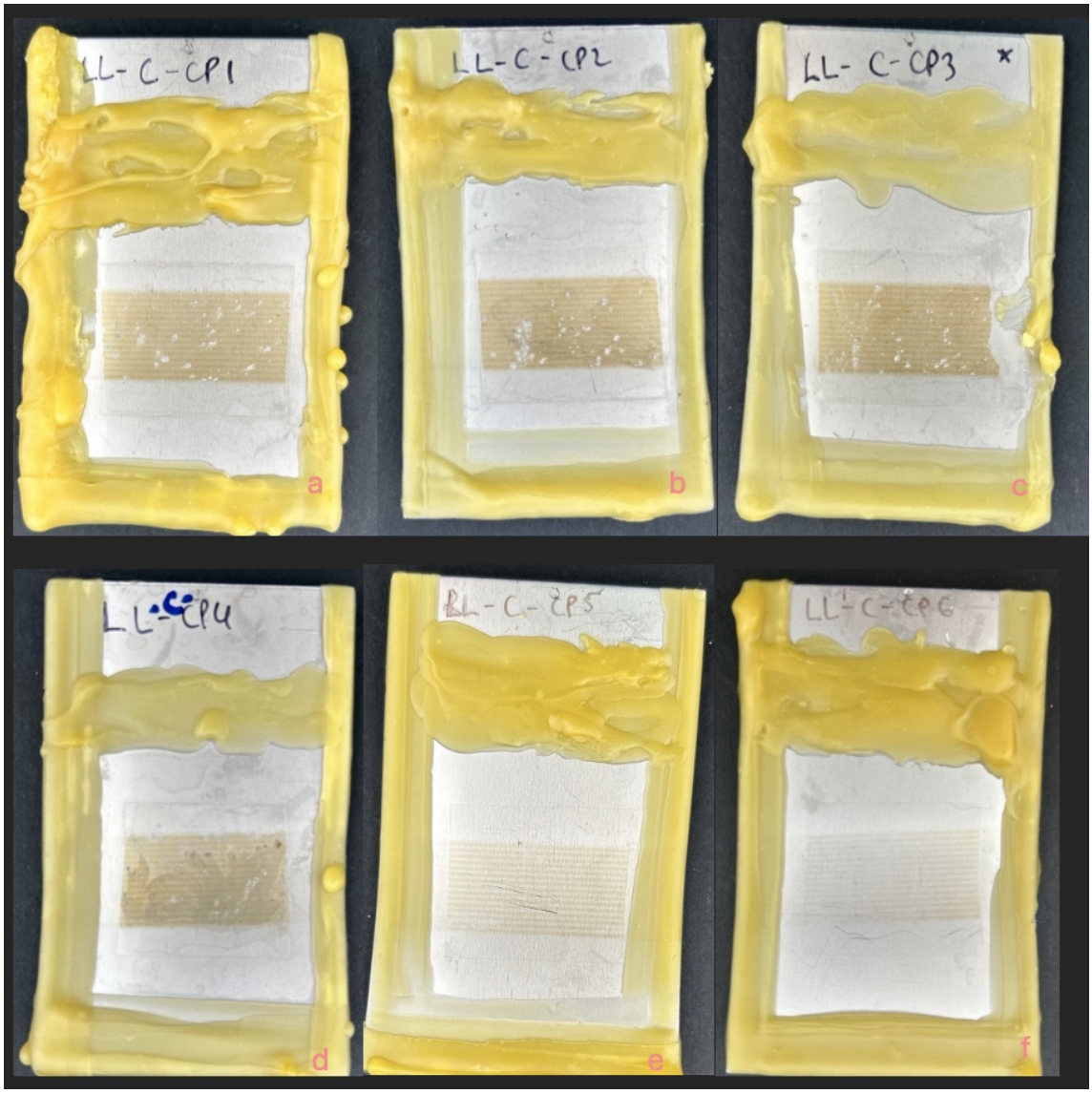

Figure 41: Depiction of coupon results after CPP, where a) is LL-C-CP1,b) LL-C-CP2,c) LL-C-CP3, d) LL-C-CP4,e) LL-C-CP5, and f) LL-C-CP6.

since there was no need for data acquisition obtained from the hysteresis loop, which is out of scope. The pitting probability was 0,7. The CPP potential vs. log current density curves of all LL-C coupons are depicted at 42, where we can see metastable and stable pitting and slight uniform corrosion towards the end of the run.

For the HL-C coupons (in figure 43), the parameters were the same as those for LL-C, with a pitting probability of 0.6. The CPP potential vs. log current density curves of all HL-C coupons are depicted at 44.

For the LL-LA coupons in figure 45, the parameters for the reverse scan changed to 0,1667 [mV/s] due to the many crevice rejects. The pitting probability was 0,4. The CPP potential vs. log current density curves of all LL-LA coupons are depicted at 46, where we see a smaller than the LL and

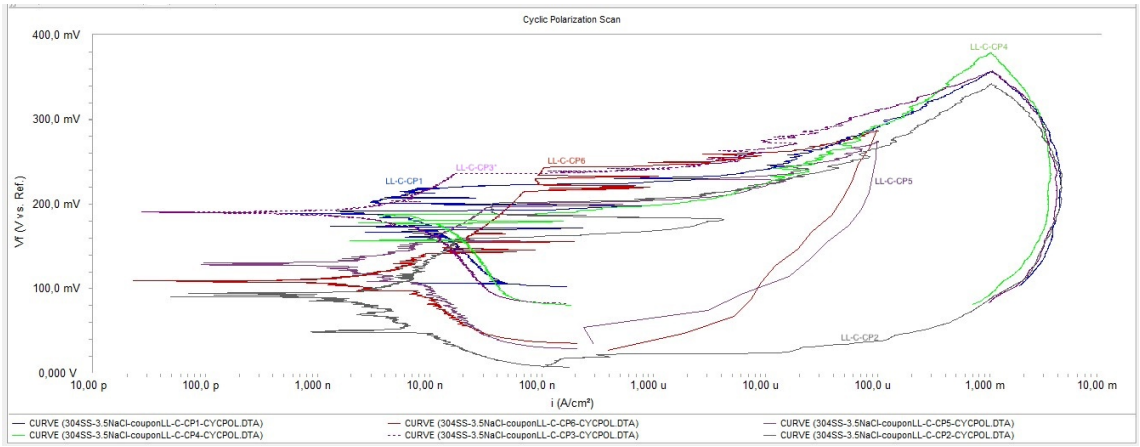

Figure 42: All CPP Potential vs. Log of Current Density Runs of LL-C

, where we see a slightly even more uniform corrosion, compared to LL-C, and still metastable and stable pitting. The passive area has started to get smaller, compare the results above.

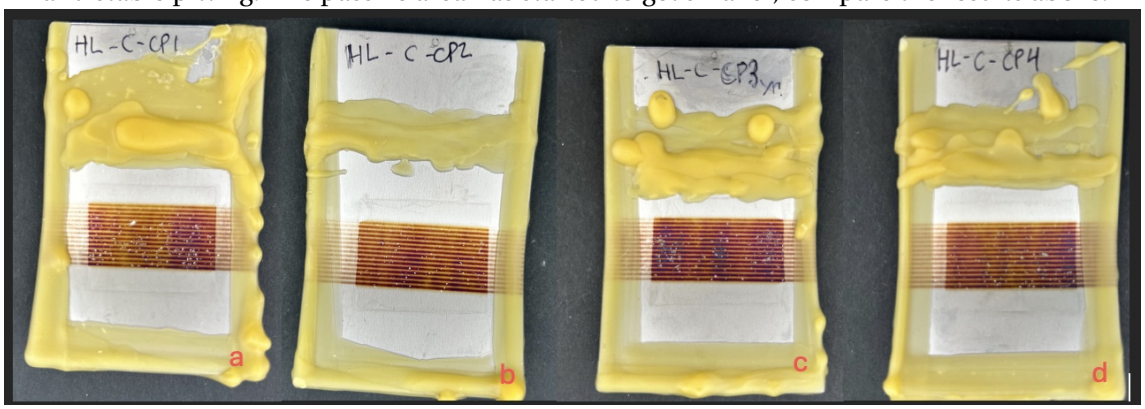

Figure 43: Depiction of coupon results after CPP, where a) is HL-C-CP1,b) HL-C-CP2,c) HL-C-CP3, and d) HL-C-CP4.

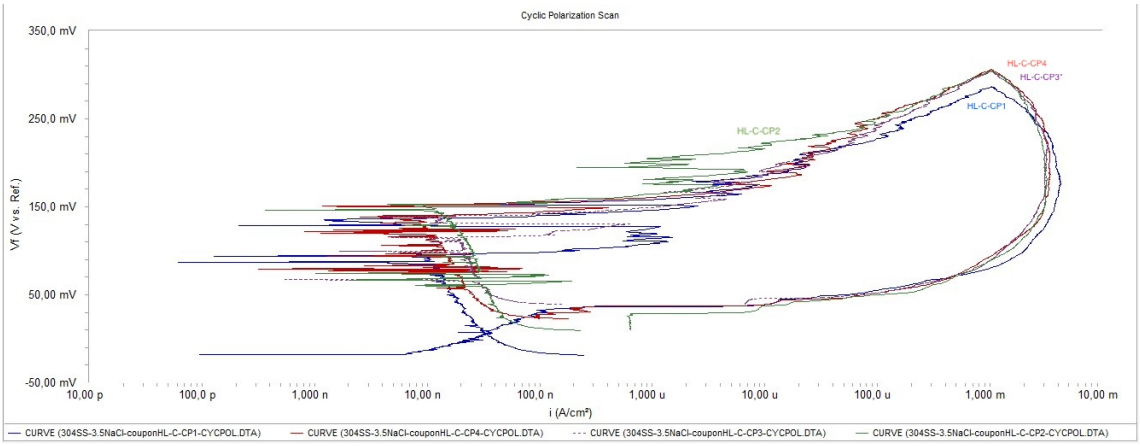

Figure 44: All CPP Potential vs. Log of Current Density Runs of HL-C

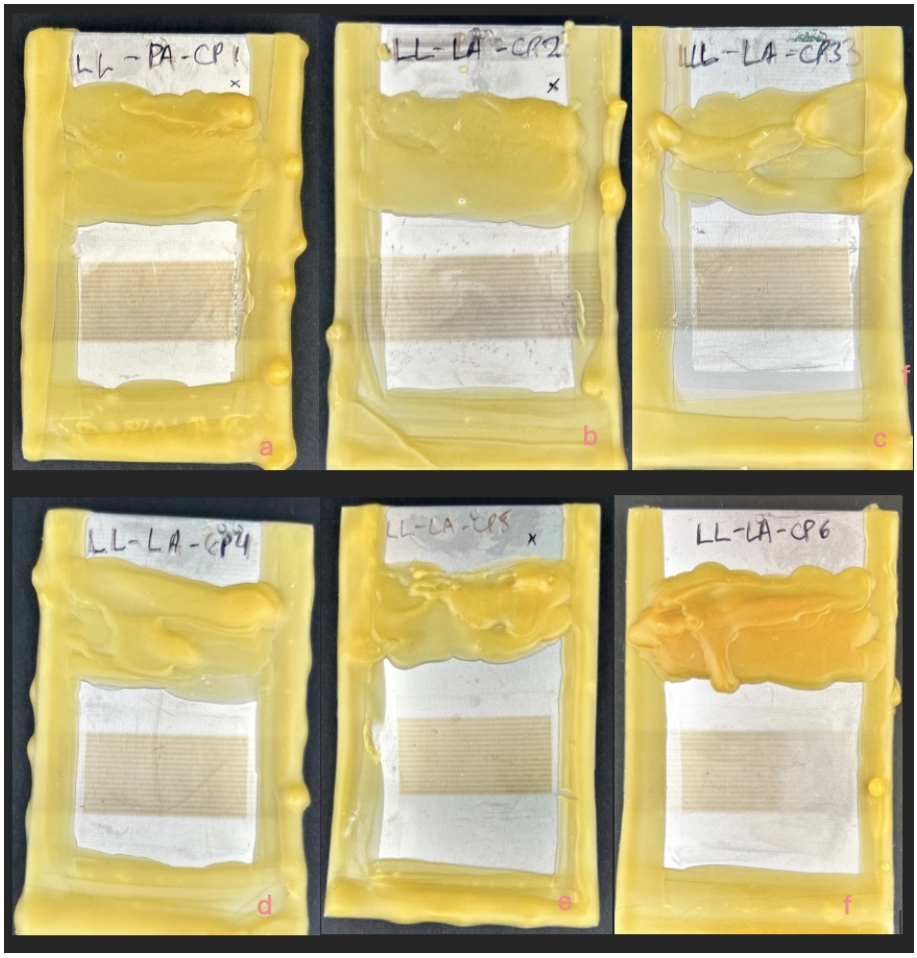

Figure 45: Depiction of coupon results after CPP, where a) is LL-LA-CP1,b) LL-LA-CP2,c) LL-LA-CP3, d) LL-LA-CP4,e) LL-LA-CP5, and f) LL-LA-CP6.

HL-C passive area, plus metastable and stable pitting.

For the HL-LA coupon in figure 47, the parameters for the non-creviced coupons were the same as those for LL-LA, with a pitting probability of 0.4. The CPP potential vs. log current density curves of all HL-LA coupons are depicted at 48, where we see at most of them metastable and stable pitting,except of the coupon trial of HL-LA-CP6 which has no passive area, no pitting and uniform corrosion.

The parameters remained the same for the LL-P coupons in figure 49, and the pitting probability was 0.9, with zero crevice rejects. The CPP potential vs. log current density curves of all HL-LA coupons are depicted at 50, where we observe better passive area, compared to the LL and HL-LA coupons, with a few having only metastable and stable pitting, and a few also uniform corrosion.

The parameters remained the same for the HL-P coupons in figure 51, and the pitting probability was 0.8, with zero crevice rejects. The CPP potential vs. log current density curves of all HL-P coupons are depicted at 52, where there is a small passive area, but no metastable pitting, so just

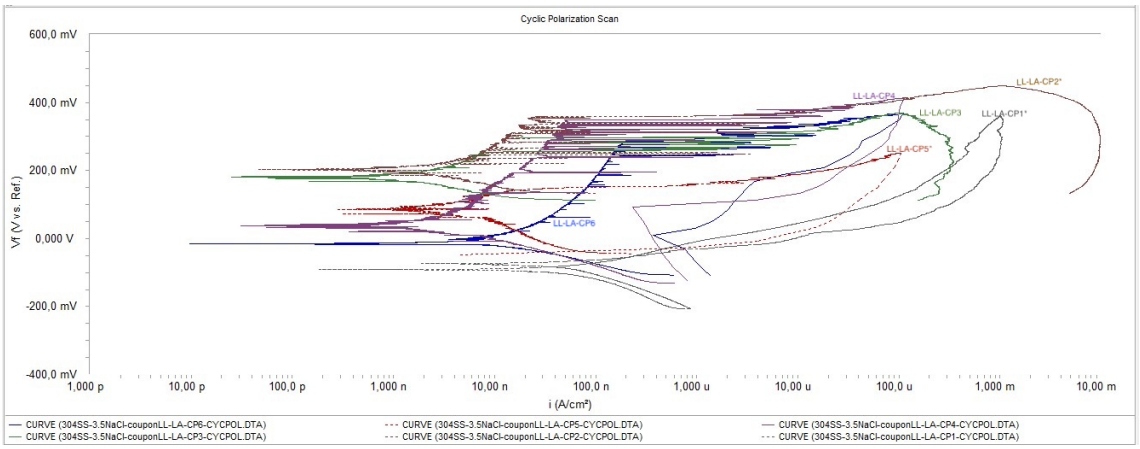

Figure 46: All CPP Potential vs. Log of Current Density Runs of LL-LA

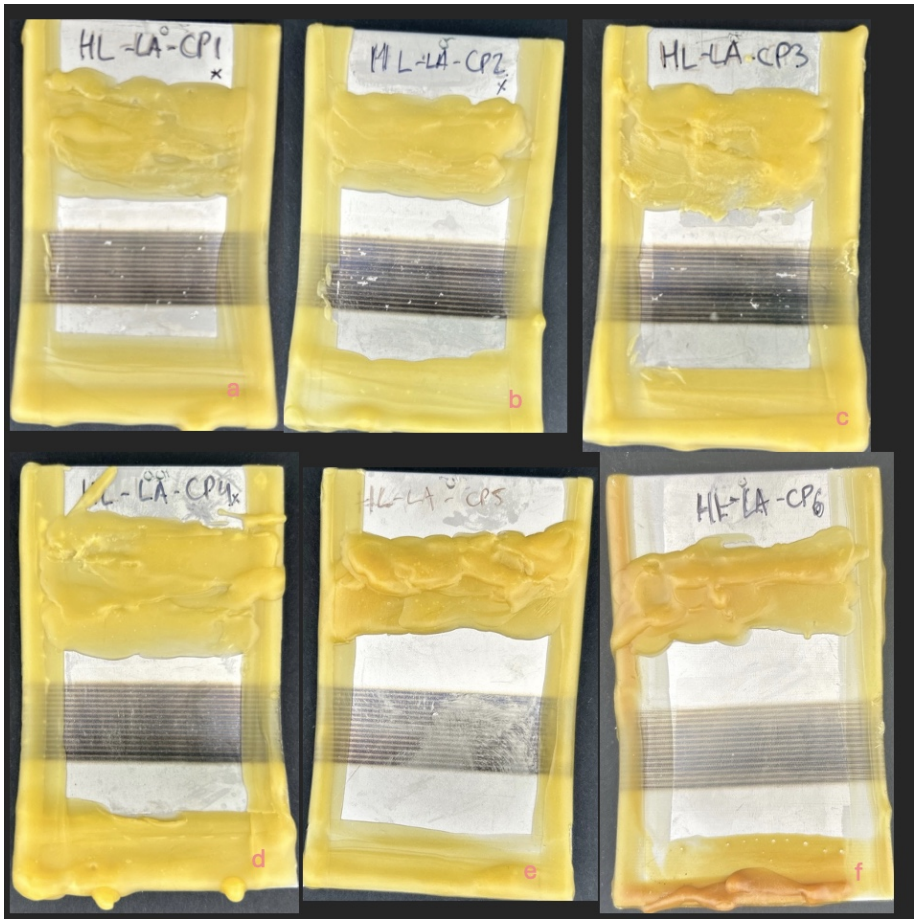

Figure 47: Depiction of coupon results after CPP, where a) is HL-LA-CP1,b) HL-LA-CP2,c) HL-LA-CP3, d) HL-LA-CP4,e) HL-LA-CP5, and f) HL-LA-CP6.

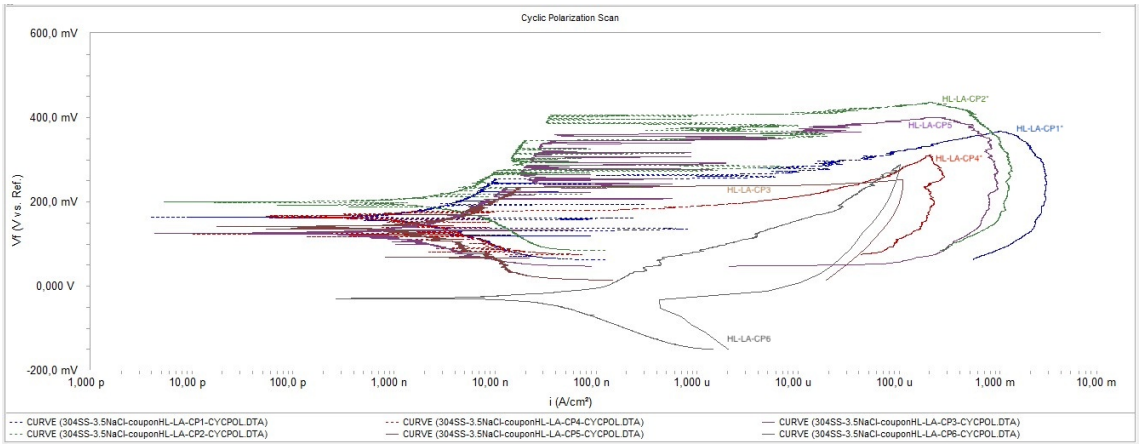

Figure 48: All CPP Potential vs. Log of Current Density Runs of HL-LA

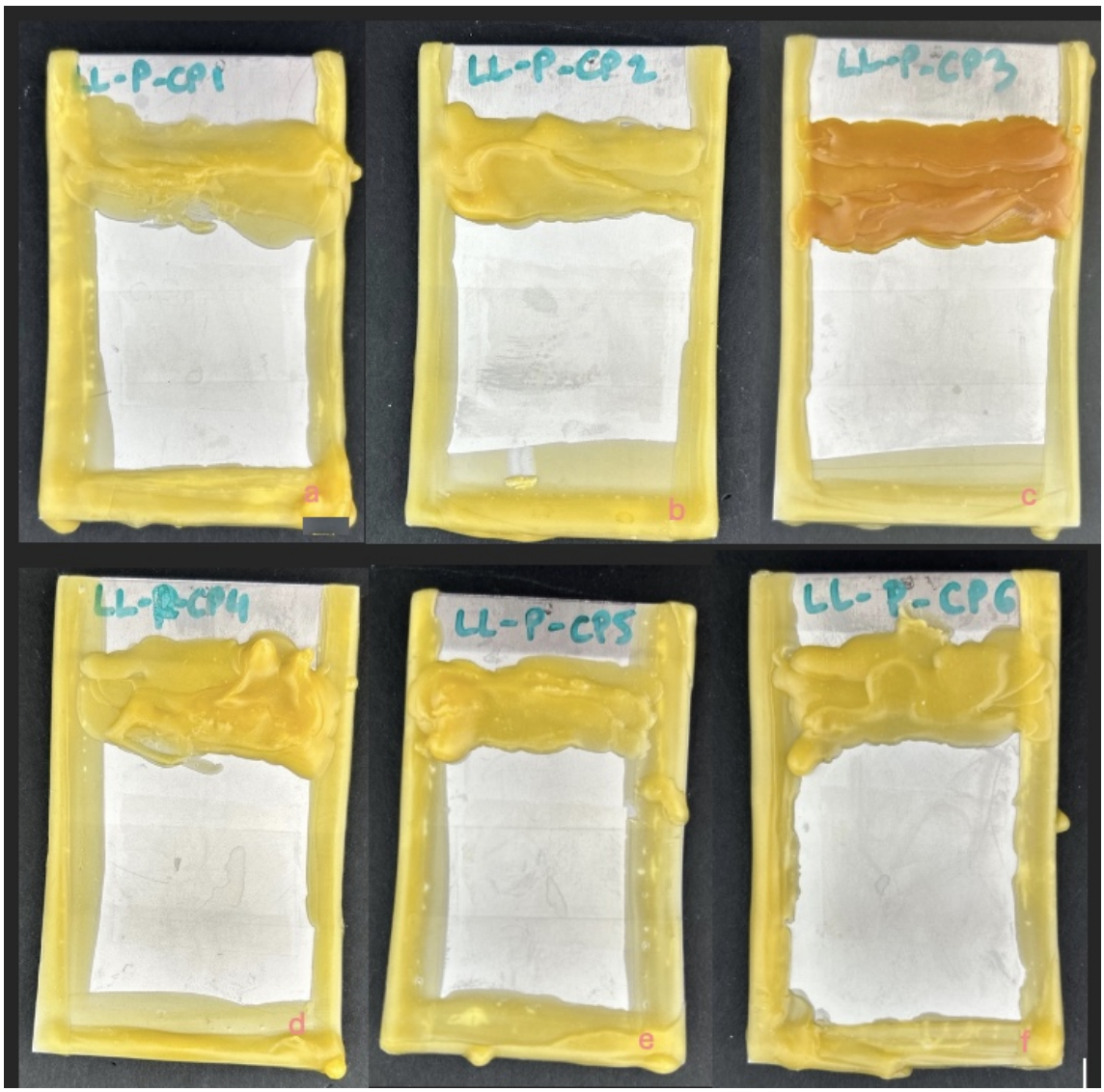

Figure 49: Depiction of coupon results after CPP, where a) is LL-P-CP1,b) LL-P-CP2,c) LL-P-CP3, d) LL-P-CP4,e) LL-P-CP5, and f) LL-P-CP6.

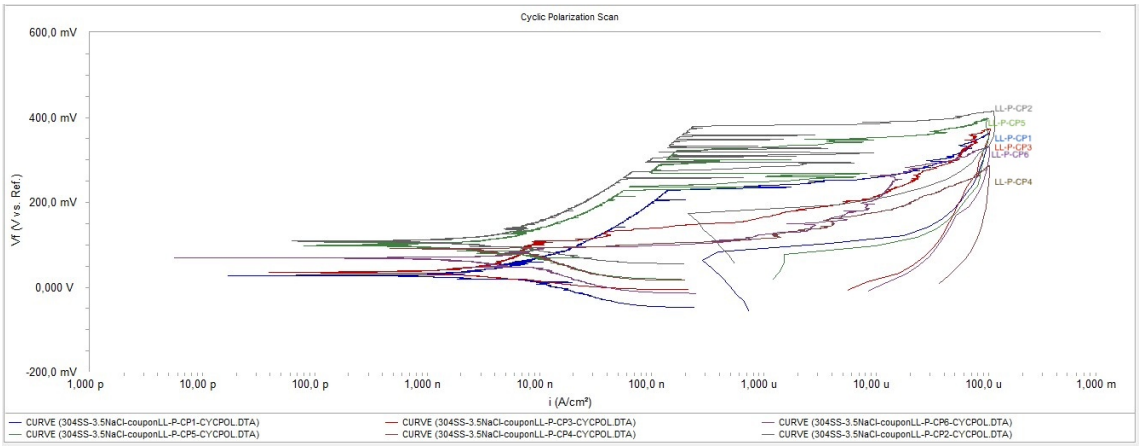

Figure 50: All CPP Potential vs. Log of Current Density Runs of LL-P

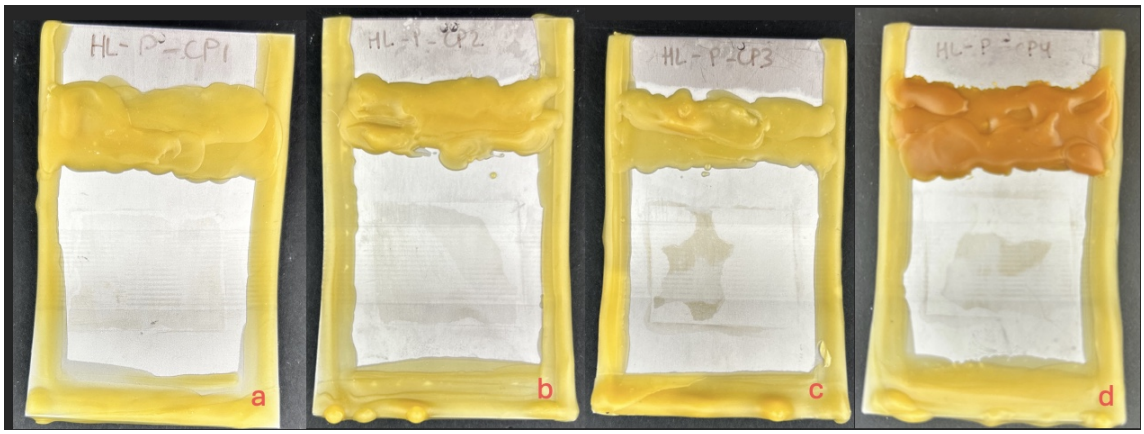

Figure 51: Depiction of coupon results after CPP, where a) is HL-P-CP1,b) HL-P-CP2,c) HL-P-CP3,and d) HL-P-CP4.

stable pitting with uniform corrosion.

Continuing with the electrochemical values extracted from CPP runs. The corrosion values needed to determine the pitting corrosion resistance(R_{pit}), E_{corr} vs SCE and E_{pit} vs SCE (equation 16) were extracted from the curves and their average values are summarized and compared per study group in figures 53 and 54, respectively.

A rise in E_{corr} may be linked to a reduction in the anodic reaction due to the generation of a passive film, or it may be due to an enhancement in the cathodic reaction connected to higher levels of dissolved oxygen. Conversely, a decline in E_{corr} can be associated with an escalation in the anodic reaction or a reduction in the cathodic reaction [102]. In figure 53, the error bars indicate large uncertainty. Therefore, it is hard to conclude which study group is the most corrosion-resistant.

The fact, that in a few cases, we saw metastable, stable and uniform corrosion, E_{pit} was extracted at 1 $\mu A/cm^2$, instead of the minimum potential where pitting was initiated, so this was a systematic and consistent way of obtaining E_{pit} and be able to compare it per study group, as

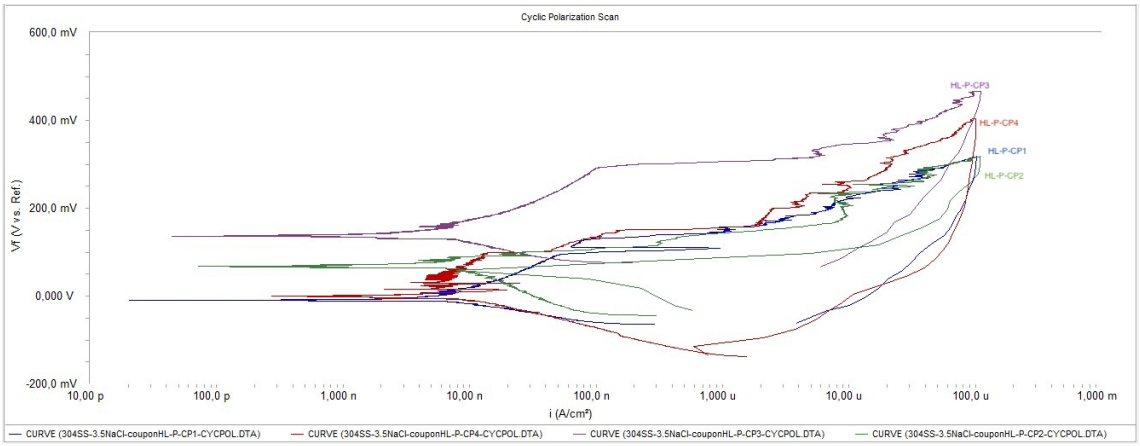

Figure 52: All CPP Potential vs. Log of Current Density Runs of HL-C

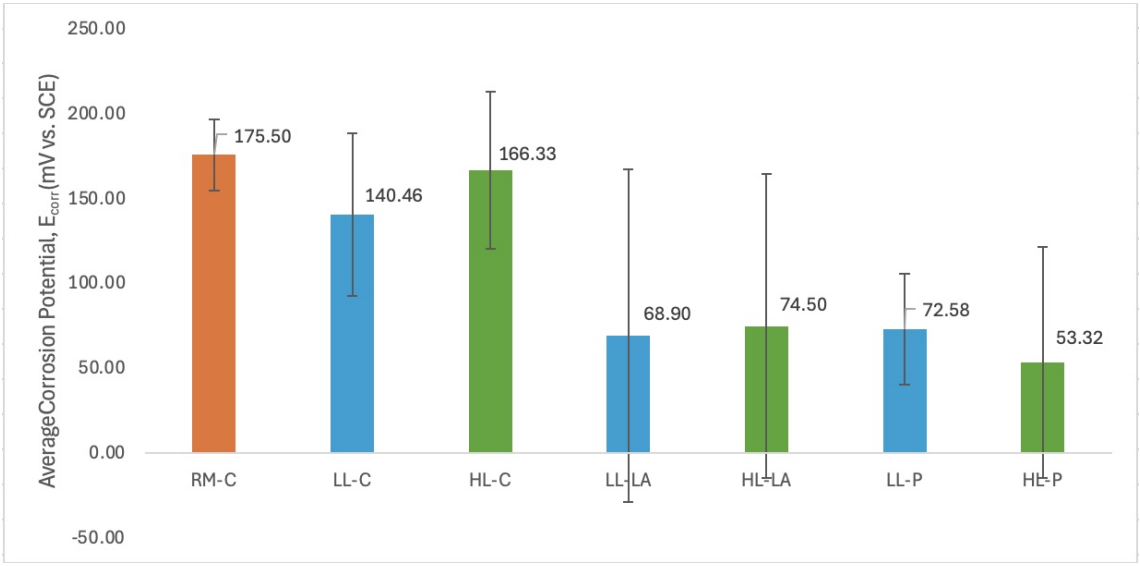

Figure 53: Average Corrosion Potential per Study Group

was also conducted at project [103]. Therefore, with this method, we can determine the pitting corrosion resistance at each step for each method. The more noble (higher potential) the E_{pit} is, the more pitting resistant it is due to the stability of its passive behavior, also indicated by the large passive area on the curve. What we can observe in figure 54 is that the base material has higher E_{pit}, making it the most corrosion resistant, but due to the remediation method error bars again, it is uncertain whether remediation treatment was effective enough to mitigate pitting. The base material has the highest E_{pit} until it gets laser-formed and becomes more susceptible to pitting.

In figures 54 and 55, we can see that both laser ablation and pickling remediation methods showed improvement in their corrosion resistance, but there is a large dispersion in the results, so again, it is hard to compare them and cannot conclude much.

A summary of the average values of E_{corr}, E_{pit} and R_{pit} are summarized in figure 56, along with

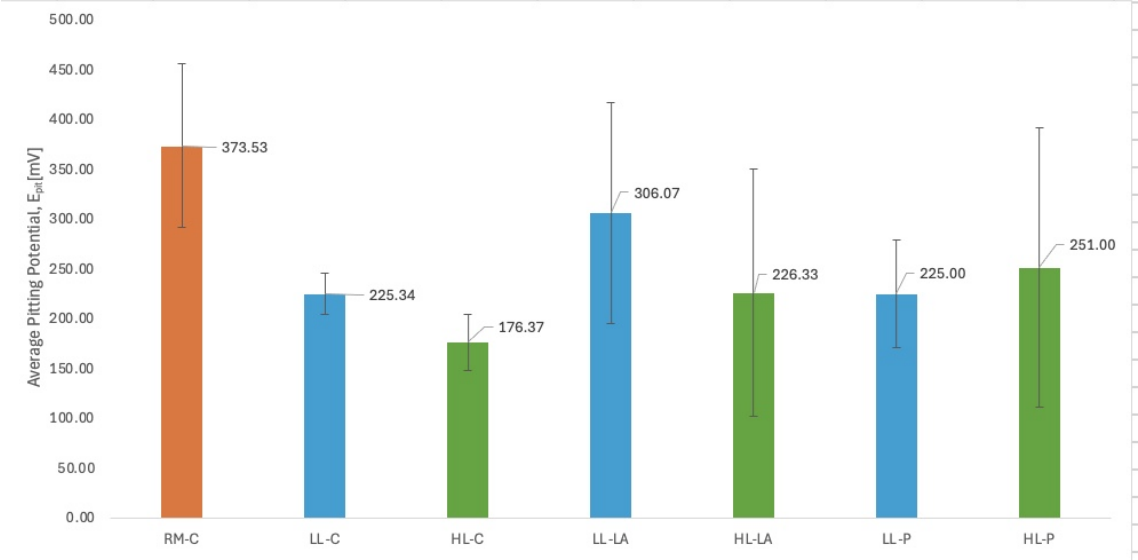

Figure 54: Average Pitting Corrosion Potential per Study Group

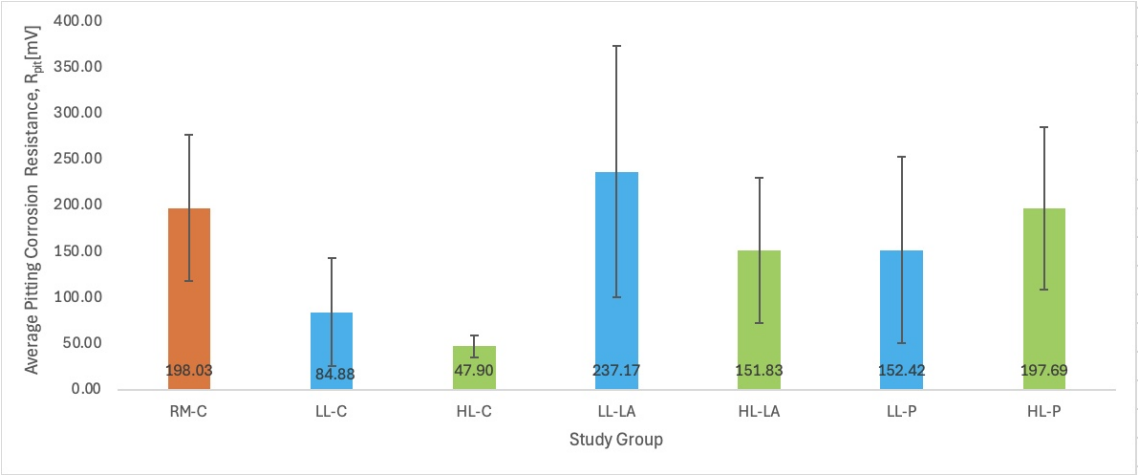

Figure 55: Average Pitting Corrosion Resistance Potential per Study Group

their deviation and limits of true value with 95% confidence.

The RAD% is accuracy between experimental and accepted values, and for R_{pit} there is a range between 33-55%, which shows how much the experimental data deviate from the true value. The same for RSD% for R_{pit}, where the values are 45-58%. So, the data were not accurate, nor precise due to the large variability seen.

The hypothesis mentioned in the section 4.4, assumed that results were expected to show E_{pit} for the remediated coupons approximately as close as the raw material in order to prove that remediation was effective enough in retrieving pitting resistance. Definitely, both graphs of E_{pit} and R_{pit} showed that the base material deteriorated due to the laser forming, and at the next step, remediation, the values were increased, making them again more corrosion resistant. However, due to the data dispersion and deviation, the overall CPP results were too ambiguous to retrieve a straight answer to the research question.

Process Step:	CPP Summary Table												
	Study Group:	Ecorr (mV)				Epit (mV)				Rpit (mV)			
		Average	Standard Deviation	Lower Limit (95%Conf)	High Limit (95%Conf.)	Average	Standard Deviation	Lower Limit (95%Conf)	High Limit (95%Conf.)	Average	Standard Deviation	Lower Limit (95%Conf)	High Limit (95%Conf.)
1.Base Material	RM-C	175.50	20.98	153.48	197.52	373.53	82.12	287.34	459.72	198.03	79.04	115.07	281.00
2.Laser Forming	LL-C	140.46	47.96	80.92	200.00	225.34	20.68	199.67	251.01	84.88	58.58	12.16	157.60
	HL-C	166.33	46.37	51.13	281.54	176.37	28.00	106.80	245.93	47.90	12.04	17.99	77.81
3-4.Remediation Method: Laser Ablation	LL-LA	68.90	97.80	-174.07	311.87	306.07	111.04	108.45	341.55	237.17	136.46	*-101.84*	*576.18*
	HL-LA	74.50	89.56	-147.99	296.99	226.33	124.22	53.36	448.64	151.83	78.47	*-43.13*	*346.79*
3-4.Remediation Method: Pickling	LL-P	72.58	32.71	38.25	106.92	225.00	54.39	170.95	441.18	152.42	100.87	*46.54*	*258.29*
	HL-P	53.32	68.07	-54.98	161.61	251.00	140.33	-122.29	574.95	197.69	88.29	*57.21*	*338.16*

Figure 56: CPP Data Summary Table

5.3 SEM with EDS/EDX

Using SEM and EDX, we observed the surface structure and presented the elemental composition on the HAZ surface of the study coupons. The SEM/EDX analysis helped us to answer the research question by testing for objective 4.

The corrosion morphologies of the base, laser-formed and remediated specimens are shown in figures 57 to 62, along with their surface picture attached to each SEM figure to observe and value the intensity of the HAZ colours and their removal. The coupons were scanned by SEM on-site prior to any testing and characterization.

The visual observation of the coupons that got laser formed showed a heat-tint on their HAZ of yellow and orange-reddish hue for LL-C and HL-C coupons, respectively. For the study group that got remediated with the method of laser ablation, the colouring hues changed to darker yellow and brownish-black colours for LL-C and HL-C coupons, respectively. On the contrary, pickling was successfully capable of removing the oxide layer generated from the laser forming step for both LL and HL laser power cases. However, since the qualitative results of the visual removal of the oxide layer are out of the scope of this study and focus only on the quantitative results for pitting resistance, we can not claim with certainty that pickling was the best remediation method. Regardless, as mentioned in the literature study, the amount of oxide layer thickness generated visually could not be a good estimate of corrosion resistance to determine metal quality.

Moreover, SEM results indicated deterioration mostly in the laser ablation study coupons, with more melting on the grain boundaries at the HL(figure 61) and only slightly on the LL(figure 59), as was expected. Furthermore, etching was observed mostly on the pickled coupons (figures 60 and 62).

To confirm with the SEM observation, the surfaces' of coupons were viewed under an optical microscope where the laser pulses were visible, but the HAZ areas were not uniform, especially after laser ablation, but rather rough and with peaks("mountains"), even at the flatter centre location of the HAZ area. Also, due to the 3D structure of the bent coupon, the equipment might do have been so accurate in obtaining data from curved surfaces, making this instrumentation problem a systematic limitation for the study.

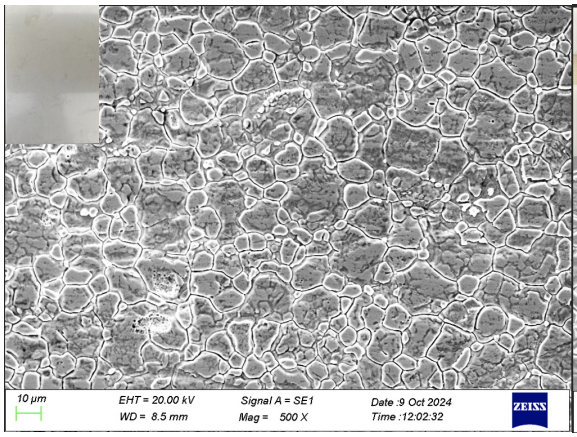

Figure 57: SEM of RM-C Control

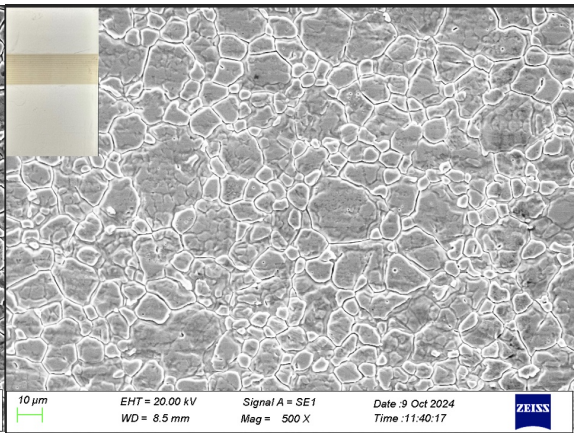

Figure 58: SEM of LL-C Control

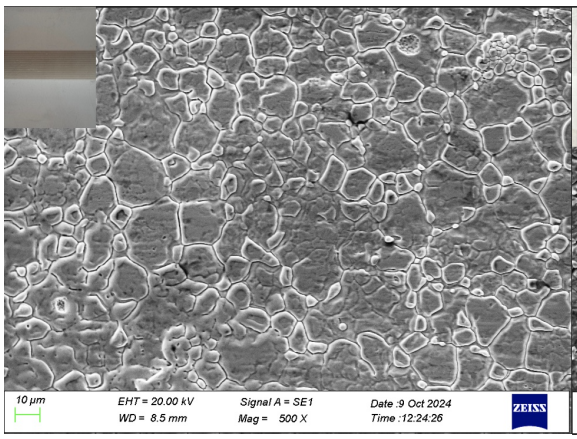

Figure 59: SEM of LL-LA Control

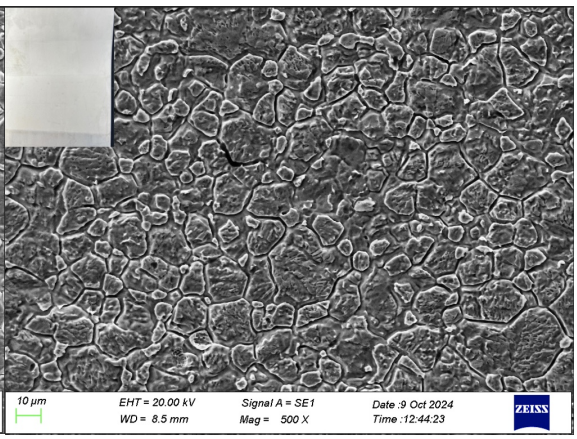

Figure 60: SEM of LL-P Control

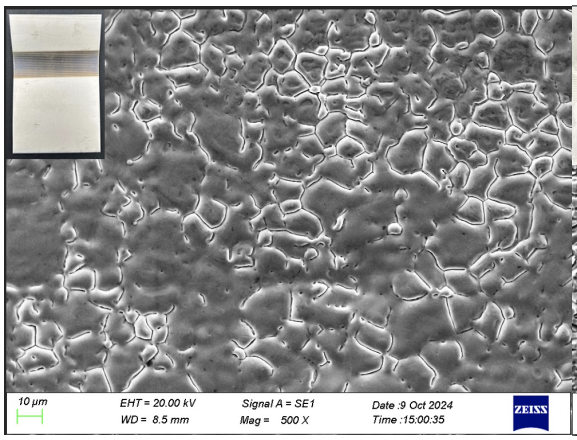

Figure 61: SEM of HL-LA Control

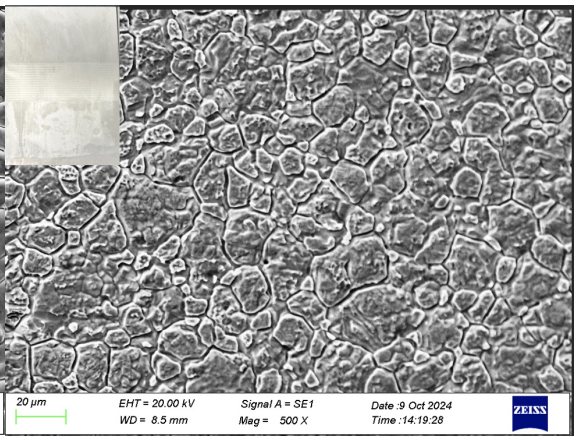

Figure 62: SEM of HL-P Control

Table 9: Elemental Concentration Percentage of Oxygen via EDX Characterization

Coupons Tested	[O]%
RM-C	0,83
LL-C	1,86
LL-LA	1,75
HL-LA	3,18
LL-P	1,53
HL-P	1,57

The EDX elemental composition and ratios can be found in the Appendix in the figure 80. Due to the instrumentational limitations, results are uncertain of the amount of oxygen present on the surface of the coupons ranged from 1,57 to 3,18%. The only observation that was made was that the most corrosion-resistant coupon with the least amount of oxygen present was the raw material with 0,83%. Further comparison of the elemental concentration can be seen in figures 81 and 82 in the Appendix.

Lastly, we were not able to help answer the research question in conjunction with the limitations mentioned in the Methods section. In theory, a thicker oxide layer induces a decrease in corrosion resistance, while a higher chromium enrichment would make it more corrosion-resistant, thus stabilizing the chromium oxide passive film for SS surface protection. It was certain, though, that no remediation treatment reduced the thickness of the oxide layer. For example, this specific pickling method did not prove to be successful, since there was still an elevated concentration of oxygen on the coupon's surface when scanned. A potential explanation for the increased oxygen concentration due to laser processing and laser ablation(HL-LA) was due to the dark colouring of the HAZ, making it more susceptible to the absorption of energy and heat.

Lastly, the EDX hypothesis was assumed to have an increased oxygen concentration on the HAZ for study group coupons of LL-C and HL-C caused by laser forming, and then reduced after both remediation methods, but that was not observed. On the contrary, we saw increased oxygen for all processed coupons. Alas, the SEM hypothesis agreed that seeing melting and edging on the surface was also observed.

5.4 Overall Results Discussion

By completing all 304 SS processing and following their characterization methods, objectives 2,3 and 4 were achieved successfully. The only objective remaining is objective 1, to appraise whether remediation would have been effective enough to mitigate pitting corrosion on a laser-induced formed coupon. In order to be able to make that appraisal, the overall results must agree on which, or if any, remediation methods were successful enough to mitigate pitting corrosion when exposed to tests with an acidic and artificial seawater sol. The present study has evaluated the pitting resistance, mass loss, and surface structure. Note that this study was focused only on the 304 SS coupon surface interactions.

To briefly summarize the results:

- At the ferric chloride pitting test, no pitting was observed for all study groups, and almost identical average mass loss was determined for groups RM-C, LL-C, and HL-C, which was much lower than the remediated coupons, LL-LA, HL-LA, LL-P, HL-P. Therefore, the base and laser-formed coupons were the most pitting corrosion resistant, with a surprising observation that the material, after laser forming at both powers cases, still behaved similarly to the base metal, so laser forming deterioration was not intensive. Unfortunately, a large dispersion of data was seen.
- At the CPP test, it was observed how different each study group was behaving in the sodium chloride electrochemical testing. Each study group behaved differently, as detailed in section X, with varying the existence of metastable, stable and pitting on their surface. From the data acquired and plotted in bar charts for comparison, both remediation methods were able to improve their pitting behavior after laser forming; however, due to statistical error, still the results were ambiguous and widely deviated.
- At SEM/EDX analysis, a greater degree of surface deterioration was noted on the remediation coupons. For example, the laser ablation coupon exhibited melting at both laser-formed power levels. Additionally, both laser-formed pickling coupons displayed signs of edging. Consequently, the SEM observations suggest that the remediation coupons could end up being less corrosion-resistant compared to both the base material and the laser-formed. Regarding EDX, the only notable observation was that the oxygen concentration was definitely smaller on the base material. At the same time, for all other study groups, their compositional percentages and ratios were similar to each other.

After reviewing the overall results, surprisingly, the results from the ferric chloride with SEM and EDX contradict the results of CPP, wanting to state that the most pitting resistant study groups were the remediated groups of laser ablation and pickling, while mass loss and surface structure scanned indicated the opposite.

So, in order to be able to answer the research question: "Is remediation effective enough to mitigate pitting corrosion on laser-formed coupons?" maybe we have to consider the sample pool of the coupons tested, the process and equipment limitations, and determine which characterization method was the most valid. Unfortunately, based on the statistical analysis, all data were very dispersed and deviated; therefore, it is uncertain which remediation method was the best from the individual characterization tests.

With correlating the results, as seen in figure 63, we came up with the observation that the best decision to make when dealing with laser formation and remediation of 304 SS, according to the conditions in this report, is to not proceed to any remediation method since the pitting corrosion behavior of the base and laser formed coupons behave similarly. Therefore, when dealing with such small laser beam powers between the range of 0,65 to 0,80[kW], the 304

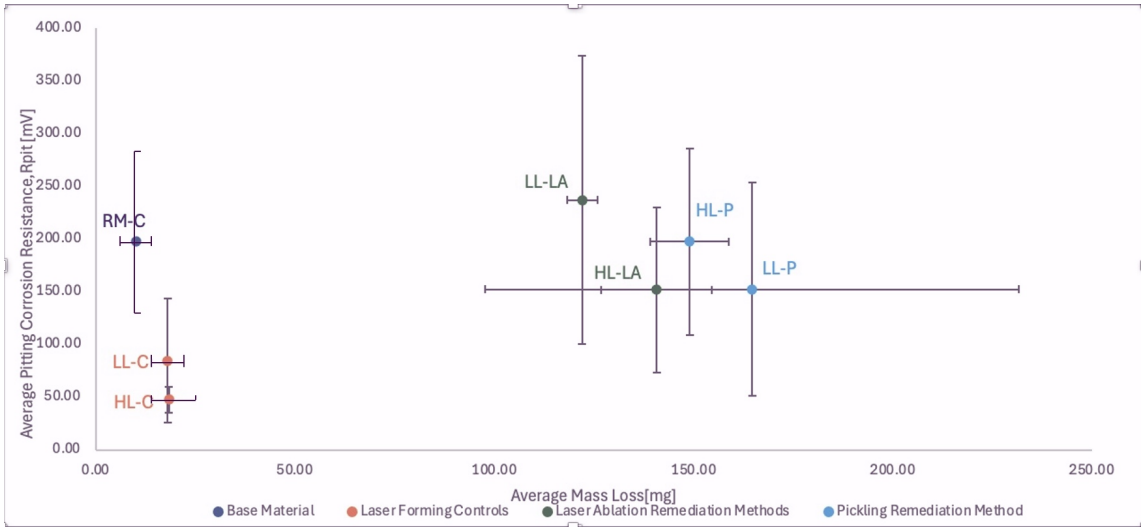

Figure 63: Correlation Plot of Mass Loss from Ferric Chloride Pitting Test vs. Average Pitting Resistance from CPP.

SS material deterioration is slight to almost negligible. Sensitization could play a role in the intergranular corrosion of an SS sample due to laser heat treatment, and the stability of the protective passive film. Also, the E_{corr} can be higher when exposed to higher laser temperatures, thus sensitization[30].

If the results had been precise, accurate, and thus certain, our results would agree with Bautista and others[21] of the removal of the oxide layer from their 304 SS via pickling. Vazquez-Santoyo and colleagues[23] had similar visual results of the heat-tint colouration of their coupon. Therefore, we can extract our samples that might have high-purity colour primarily in the yellow region (560-590 [nm]) for the lower laser power laser forming(LL-C) and orange spectra (590-630 [nm]) for the high power laser forming due to oxygen layer thickness increase.

However, Svantner and others[24], saw corrosion deterioration during laser marking(which is similar to laser forming), contradicting our observation that the laser formed and base material behave similarly, thus being both corrosion resistant. Hence, we must think about what role played the laser power in our results. If the laser forming cycles were conducted at a higher power than 0,65-0,80[kW], more surface deterioration would have affected the coupon, thus requiring a remediation process. Due to the low power utilized in our study, we did not experience melting of the surface, nor did we observe the same level of oxidation. Hence, trying to remediate our coupons, more deterioration occurred during that step and not during the laser-formed step. So, if a 304 SS coupon that had experience welding, heat treatment or laser processing, in conjunction with a dark heat-tint, indicated a thicker oxide layer, remediation would have been successful in removing the oxide layer and improving pitting resistance.

Of course, the observation mentioned above would have been nice to be backed up with deeper microstructural investigation methods, apart from EDX, to analyze the phase composition and oxygen layer properties. Also, roughness could have been attributed more to the observations

of this study, in conjunction with the remediation methods used, but that was out of the scope for our study. A larger sample pool for statistical evaluation could have made it clearer which process treatment series was the most pitting resistant. In this study, having a sample pool of a minimum of three 304 SS coupons(plus crevice rejects), it is difficult to conclude which remediation method relating to surface interaction is the best. Given the intricate nature of this process, it is essential to recognize that each stage influences the outcomes. Factors such as utilizing the same base material and consistent laser settings in the remediation treatment may play a significant role in shaping and validating the final results.

6 Conclusions

This chapter summarises the main findings that address the research study's question and aim and discusses potential opportunities for future research endeavours.

This study aimed to investigate the pitting mitigation quality(resistance) of the AISI 304 stainless steel base metal before and after laser forming and later after chemical pickling or laser ablation remediation processes. The research question inspired by the aim was:

Is remediation effective enough to mitigate pitting corrosion on laser-formed coupons?

In order to be able to answer the research question, the objectives for this study were set to be:

1. To appraise whether remediation will be effective enough to mitigate pitting corrosion on a laser-induced formed coupon.
2. To assess the material's deterioration via mass loss, which is an indication of corrosion resistance from the Ferric Chloride Test.
3. To analyze pitting potential (E_{pit}) and to quantify pitting corrosion resistance (R_{pit}) from CPP curves. The purpose is to mitigate pitting and uniform corrosion, thus investigating resistance.
4. To assess the surface structure of each coupon control from every step of the lased forming remediation process in this study via SEM and EDX.

Initially, two groups of laser forming were studied with different laser powers, 0,65[kW](LL) and 0,80[kW](HL). Afterwards, those heat-treated laser-formed coupons were processed further with either a chemical pickling(10-20[wt%] nitric acid with 1-2% hydrofluoric acid mixture at ambient)(P) or a laser ablation method(LA). Lastly, further characterization took place to be able to investigate pitting and uniform corrosion behavior when exposed to an acidic environment via a 0,75[wt%] ferric chloride immersion test at 20[^oC] and when exposed to 3,5[wt%] artificial seawater during cyclic potentiodynamic polarization at ambient. A unique developmental procedure for cyclic polarization experimental data acquisition was conceptualized and validated in order to make it easier to investigate metastable and stable pitting unbiasedly. Lastly, surface scanning was performed via SEM and EDX.

The results indicated a contradiction between the characterization methods of the ferric chloride test mass loss against the cyclic polarization pitting resistance. The average mass loss in groups RM-C, LL-C, and HL-C was similar and significantly lower than that of the remediated coupons LL-LA, HL-LA, LL-P, and HL-P. The base and laser-formed coupons showed the highest resistance to pitting corrosion. Interestingly, the material created by laser formation at both power levels still had similar characteristics to the base metal, indicating that the damage from laser forming was not severe. However, there was a notable variation in the observed data. That could

Process Step:	Data Summary Table				
	Study Group:	Rpit [mV]		Mass Loss [mg]	
		Average	Standard Deviation	Average	Standard Deviation
1.Base Material	RM-C	198,03	79,04	10,20	0,30
2.Laser Forming	LL-C	84,88	58,58	18,00	1,30
	HL-C	47,90	12,04	18,40	3,60
3-4.Remediation Method: Laser Ablation	LL-LA	237,17	136,46	122,10	3,80
	HL-LA	151,83	78,47	140,80	13,90
3-4.Remediation Method: Pickling	LL-P	152,42	100,87	164,80	67,00
	HL-P	197,69	88,29	149,10	9,90

Figure 64: Study Key Findings

be backed up via SEM, where the laser ablation coupons melted at both power levels. Also, the pickling coupons showed signs of edging. As a result, SEM observations indicated that the remediation coupons might have been less resistant to pitting and corrosion than both the base material and the laser-formed materials. The EDX analysis revealed that the oxygen concentration was lower in the base material, while the compositional percentages and ratios were similar across all other study groups. At the CPP test, each study group exhibited distinct behaviors with variations in the presence of metastable, stable pitting and uniform corrosion on their surfaces. The results led to improvements in pitting behavior following laser forming; however, due to statistical error, the results remained ambiguous with significant deviations. As an overall result, we cannot answer the research question of which, if any, remediation method was able to be the most pitting resistant enhancing after laser forming, especially when the same results from different characterization methods contradict, and with such a large error and uncertainty.

The obtained results from this study can be summarized as follows, with key finding values depicted in figure 64 :

- The base and laser-formed coupons showed up to be more resistant to mass loss corrosion deterioration during the ferric chloride immersion testing.
- Due to large deviation, no answer can be given whether any remediation methods were able to successfully mitigate pitting corrosion after laser formation and mark the most pitting-resistant study group. Remediated study groups showed higher pitting potential and pitting resistance than the laser formed, but lower open circuit corrosion potentials.
- Greater surface deterioration was observed on the coupons' surface that were either pickled or from laser ablation.

A key factor for the restoration of pitting corrosion resistance is the parameter of laser power intensity, which can play a vital role in whether SS remediation is indeed required. If we had reverse-engineered our studies with a much higher laser power, the energy deteriorating the

surface would have been greater. Thus, remediation could be successful or remove this oxide layer and enhance pitting resistance. We are making the laser power intensity choice the key factor in answering our research question. From this study, evidence showed that with a laser power range of 0,65-0,80 [kW], remediation causes more surface deterioration, so the most pitting-resistant process choice would be to omit remediations, such as the ones studied in this paper.

6.1 Perspectivation and Future Works

The results of this project clearly indicate that the metallurgical industry must actively pursue innovative methods for remediating the oxidation layer on stainless steel to significantly improve its pitting corrosion resistance. Additionally, it is crucial for researchers to delve into various laser processing remediation techniques to build upon the promising outcomes and insights presented in this study. The theoretical and practical limitations highlighted in this report will undeniably provide a solid foundation for advancing future research in this area.

Drawing from the existing literature, it is essential to conduct further characterization of the SS microstructure's corrosion behavior to gain a comprehensive understanding of how remediation treatments can enhance pitting resistance. It is strongly recommended to employ techniques such as AES, AFM, EIS, Interferometry, LPR, XPS, and XRD, along with modifications to the pickling solution formulation and adjustments to the parameters of the laser ablation remediation processes, as key methods for further investigation. Darker heat-tint staining would make more distinctive results.

Bibliography

[1] A. Adjorlolo, "Corrosion in commercial aviation," 2006.

[2] Z. Bai and J. L. Gilbert, "Corrosion performance of stainless steels, cobalt, and titanium alloys in biomedical applications," in *Corrosion: Environments and Industries*, pp. 837–852, ASM International, 2006.

[3] A. Standard *et al.*, "Standard test method for conducting cyclic potentiodynamic polarization measurements to determine the corrosion susceptibility of small implant devices," *ASTM International: West Conshohocken, PA, USA*, 2019.

[4] N. Ury, S. Firdosy, and V. Ravi, "Additive manufacturing of stainless steel biomedical devices," in *Additive Manufacturing in Biomedical Applications*, pp. 164–175, ASM International, 2022.

[5] A. Khan, "Pitting corrosion of copper pipes in a residential water delivery system," 2019.

[6] J. Cheng, Q. Yan, Z. Pan, and W. Wei, "On-line measurement and characterization of electrochemical corrosion of 304l stainless steel pipe wall in high-speed cl-containing solution," *Metals*, vol. 12, no. 8, p. 1324, 2022.

[7] H. P. Hack, *Designing cathodic protection systems for marine structures and vehicles*, vol. 1370. ASTM International, 1999.

[8] M. Schultz, T. McDonough, M. Eckart, and M. Bentkjaer, "Marine coatings," 2015.

[9] B. Mishra and J. Pak, "Corrosion in the mining and mineral industry," in *Corrosion: Environments and Industries*, pp. 1076–1082, ASM International, 2006.

[10] J. A. Beavers and N. G. Thompson, "External corrosion of oil and natural gas pipelines," 2006.

[11] B. Phull, "Evaluating pitting corrosion," 2003.

[12] A. D. SERIES, "Design guidelines for the selection and use of stainless steels,"

[13] S. Freeman, "Analysis and prevention of corrosion-related failures," in *Failure Analysis and Prevention*, pp. 749–760, ASM International, 2002.

[14] A. Wahid, D. Olson, D. Matlock, and C. Cross, "Corrosion of weldments," 1993.

[15] M. Cooney and R. Hoffman, "Forms of corrosion," in *Failure Analysis and Prevention*, pp. 479–517, ASM International, 2021.

[16] R. G. Kelly, "Pitting," *ASTM MANUAL SERIES MNL*, pp. 166–174, 1995.

[17] B. S. Yilbas, S. Akhtar, and S. Z. Shuja, *Laser forming and welding processes*. Springer, 2013.

[18] B. Podgornik, "Surface texturing," 2017.

[19] R. M. Hudson, "Pickling and descaling," 1994.

[20] P. Ghods, O. Isgor, G. McRae, J. Li, and G. Gu, "Microscopic investigation of mill scale and its proposed effect on the variability of chloride-induced depassivation of carbon steel rebar," *Corrosion Science*, vol. 53, no. 3, pp. 946–954, 2011.

[21] A. Bautista, G. Blanco, F. Velasco, M. Martı, *et al.*, "Corrosion performance of welded stainless steels reinforcements in simulated pore solutions," *Construction and Building Materials*, vol. 21, no. 6, pp. 1267–1276, 2007.

[22] T. Terasaki, T. Akiyama, and Y. Matsuo, "Effect of various factors produced by welding on the corrosion pit growth of high-tensile strength steel (ht 80) in artificial seawater," *CORROSION ENGINEERING*, vol. 37, no. 3, pp. 144–150, 1988.

[23] L. Vazquez-Santoyo, J. Perez-Bueno, A. Manzano-Ramírez, J. Gonzalez-Hernández, J. Perez-Robles, and Y. V. Vorobiev, "Origin of interference colors on austenitic stainless steel," *Inorganic materials*, vol. 41, pp. 955–960, 2005.

[24] M. Švantner, M. Kučera, and Š. Houdková, "Possibilities of stainless steel laser marking," in *METAL 2012—21st International Conference on Metallurgy and Materials*, pp. 980–986, 2012.

[25] J. Qi, K. Wang, and Y. Zhu, "A study on the laser marking process of stainless steel," *Journal of Materials Processing Technology*, vol. 139, no. 1-3, pp. 273–276, 2003.

[26] H. Liu, Y. Wei, C. K. I. Tan, S. H. Lim, and L. Zhang, "Laser-treatment-induced morphology and structure modifications of stainless steel: element segregations and phase evolutions," *Materials Chemistry and Physics*, vol. 266, p. 124570, 2021.

[27] M. Kučera, J. Martan, and A. Franc, "Time-resolved temperature measurement during laser marking of stainless steel," *International Journal of Heat and Mass Transfer*, vol. 125, pp. 1061–1068, 2018.

[28] P. Psyllaki and R. Oltra, "Preliminary study on the laser cleaning of stainless steels after high temperature oxidation," *Materials Science and Engineering: A*, vol. 282, no. 1-2, pp. 145–152, 2000.

[29] J. Xiong, S. Agarwala, M. Y. Tan, and M. Forsyth, "The restoration of the passivity of stainless steel weldments in pickling solutions observed using electrochemical and surface analytical methods," *Corrosion*, vol. 71, no. 10, pp. 1248–1256, 2015.

[30] Y. Zhang, H. Luo, Q. Zhong, H. Yu, and J. Lv, "Characterization of passive films formed on as-received and sensitized aisi 304 stainless steel," *Chinese Journal of Mechanical Engineering*, vol. 32, pp. 1–12, 2019.

[31] S. Hägg Mameng, A. Bergquist, and E. Johansson, "Corrosion of stainless steel in sodium chloride brine solutions," in *Nace Corrosion Conference*, NACE International, 2014.

[32] V. Zatkalíková and L. Markovičová, "Corrosion resistance of electropolished aisi 304 stainless steel in dependence of temperature," in *IOP Conference Series: Materials Science and Engineering*, vol. 465, p. 012011, IOP Publishing, 2019.

[33] K. Pradeep, "Influence of artificially produced tinting colors on the corrosion resistance of aisi 304 stainless steel," Master's thesis, Graz University of Technology, 2017.

[34] I. Esih, V. Alar, and I. Juraga, "Influence of thermal oxides on pitting corrosion of stainless steel in chloride solutions," *Corrosion engineering, science and technology*, vol. 40, no. 2, pp. 110–120, 2005.

[35] "Using pitting and protection potentials to predict pitting behavior: New insights," *Electric Power Research Institute*, 1991.

[36] G. Burstein and G. Ilevbare, "The effect of specimen size on the measured pitting potential of stainless steel," *Corrosion Science*, vol. 38, no. 12, pp. 2257–2265, 1996.

[37] P. Pistorius and G. Burstein, "Metastable pitting corrosion of stainless steel and the transition to stability," *Philosophical transactions of the royal society of London. Series A: Physical and Engineering Sciences*, vol. 341, no. 1662, pp. 531–559, 1992.

[38] W. Tian, N. Du, S. Li, S. Chen, and Q. Wu, "Metastable pitting corrosion of 304 stainless steel in 3.5% nacl solution," *Corrosion Science*, vol. 85, pp. 372–379, 2014.

[39] T. Von Moltke, P. Pitsorius, and R. Sandenbergh, "The influence of heat-tinted surface layers on the corrosion resistance of stainless steels," *INFACON 6.*, vol. 2, pp. 185–195, 1992.

[40] F. Elshawesh and A. Elhoud, "Role of heat tint on pitting corrosion of 304 austenitic stainless steel in chloride environment," 2004.

[41] A. Kaplan and H. Engström, *14th NOLAMP Conference: The 14th Nordic Laser Materials Processing Conference, August 26th–28th 2013, Gothenburg, Sweden.* Luleå tekniska universitet, 2013.

[42] G. Lu, J. Li, Z. Ji, H. Li, C. Yao, J. Li, K. Sugioka, and G. Zhao, "How does the pulsed laser turn into 'force'?," *Measurement*, vol. 185, p. 110016, 2021.

[43] R. Granata, "Surface modification using energy beams," 2003.

[44] C. Sørensen, A. Nissen, C. Brynning, J. Nielsen, R. Schøn, R. Malefijt, and M. Kristiansen, "Double-sided hybrid laser-arc welding of 25 mm s690ql high strength steel," in *IOP Conference Series: Materials Science and Engineering*, vol. 1135, p. 012004, IOP Publishing, 2021.

[45] P. Roberge, "Modeling corrosion processes," in *Corrosion: Fundamentals, Testing, and Protection*, pp. 430–445, ASM International, 2003.

[46] K. Hansen, M. Kristiansen, and F. Olsen, "Beam shaping to control of weldpool size in width and depth," *Physics Procedia*, vol. 56, pp. 467–476, 2014.

[47] T. Gooch, "Corrosion behavior of welded stainless steel," *Welding Journal-Including Welding Research Supplement*, vol. 75, no. 5, p. 135s, 1996.

[48] A. N. Thomsen, B. Endelt, and M. Kristiansen, "A new method for calculating the error term used in 2d feedback control of laser forming," *Physics Procedia*, vol. 89, pp. 148–155, 2017.

[49] A. F. Mikkelstrup, A. N. Thomsen, and M. Kristiansen, "A novel method for approximating local changes in the surface absorption for laser marking using 3d laser scanning," in *IOP Conference Series: Materials Science and Engineering*, vol. 1135, p. 012002, IOP Publishing, 2021.

[50] M. Epler, "Structures by precipitation from solid solution," in *Metallography and Microstructures*, pp. 134–139, ASM International, 2004.

[51] D. Engelberg, *Grain boundary engineering for intergranular stress corrosion resistance in austenitic stainless steel*. The University of Manchester (United Kingdom), 2006.

[52] J. F. Grubb, T. DeBold, and J. D. Fritz, "Corrosion of wrought stainless steels," in *Corrosion: materials*, pp. 54–77, ASM International, 2005.

[53] A. N. Thomsen, B. Endelt, and M. Kristiansen, "Feedback control of laser forming using flattening simulations for error determination," in *IOP Conference Series: Materials Science and Engineering*, vol. 651, p. 012093, IOP Publishing, 2019.

[54] A. N. Thomsen, E. Kristiansen, M. Kristiansen, and B. Endelt, "Influence of cooling on edge effects in laser forming," *Procedia CIRP*, vol. 74, pp. 394–397, 2018.

[55] M. V. Pantawane, S. S. Joshi, and N. B. Dahotre, "Laser beam machining of aluminum and aluminum alloys," in *Aluminum Science and Technology*, pp. 519–541, ASM International, 2018.

[56] W. Hung, "Postprocessing of additively manufactured metal parts," 2021.

[57] K. B. Tator, "Coating deterioration," in *Protective organic coatings*, pp. 462–473, ASM International, 2015.

[58] M. Maniruzzaman, X. Wang, and R. D. Sisson Jr, "Cleaning of steel for heat treatment," in *Steel Heat Treating Fundamentals and Processes*, pp. 265–274, ASM International, 2013.

[59] S. Sen-Britain, S. Cho, S. Kang, Z. Qi, S. Khairallah, D. Rosas, V. Som, T. T. Li, S. Roger Qiu, Y. Morris Wang, *et al.*, "Critical role of slags in pitting corrosion of additively manufactured stainless steel in simulated seawater," *Nature Communications*, vol. 15, no. 1, p. 867, 2024.

[60] R. W. Revie, "Uhlig's corrosion handbook, john wiley & sons," *Inc., New York, USA*, pp. 1227–1238, 2000.

[61] J. Kruger, "Passivity," *Corrosion: Fundamentals, Testing, and Protection*, pp. 61–67, 2003.

[62] T. A. S. of Mechanical Engineers, "Bioprocessing equipment," *ASME Setting the Standard*, 2009.

[63] C. Cotell, J. Sprague, and F. Smidt Jr, "Asm handbook volume 5: Surface engineering," *ASM International, Ohio*, 1994.

[64] R. Chai, "Rouge formation and remediation," 2019.

[65] M. A. Kappes, "Localized corrosion and stress corrosion cracking of stainless steels in halides other than chlorides solutions: a review," *Corrosion Reviews*, vol. 38, no. 1, pp. 1–24, 2020.

[66] V. Alar, I. Žmak, B. Runje, and A. Horvatić, "Development of models for prediction of corrosion and pitting potential on aisi 304 stainless steel in different environmental conditions," *International Journal of electrochemical science*, vol. 11, no. 9, pp. 7674–7689, 2016.

[67] P. Roberge, "Statistical interpretation of corrosion test results," in *Corrosion: fundamentals, testing, and protection*, pp. 425–429, ASM International, 2003.

[68] H. Böhni, T. Suter, and A. Schreyer, "Micro-and nanotechniques to study localized corrosion," *Electrochimica Acta*, vol. 40, no. 10, pp. 1361–1368, 1995.

[69] T. Bellezze, G. Giuliani, and G. Roventi, "Study of stainless steels corrosion in a strong acid mixture. part 1: cyclic potentiodynamic polarization curves examined by means of an analytical method," *Corrosion Science*, vol. 130, pp. 113–125, 2018.

[70] G. Frankel and N. Sridhar, "Understanding localized corrosion," *Materials today*, vol. 11, no. 10, pp. 38–44, 2008.

[71] N. Laycock, J. Noh, S. White, and D. Krouse, "Computer simulation of pitting potential measurements," *Corrosion Science*, vol. 47, no. 12, pp. 3140–3177, 2005.

[72] C.-O. Olsson and D. Landolt, "Passive films on stainless steels—chemistry, structure and growth," *Electrochimica acta*, vol. 48, no. 9, pp. 1093–1104, 2003.

[73] A. M. Anderko, N. Sridhar, C. S. Brossia, and D. S. Dunn, "A computational approach to predicting the occurrence of localized corrosion in multicomponent aqueous solutions," in *NACE CORROSION*, pp. NACE–04061, NACE, 2004.

[74] Y. H. Lee, Z. Takehara, and S. Yoshizawa, "Propagation and repassivation of pits on stainless steel in aqueous solutions containing chloride ions," *CORROSION ENGINEERING*, vol. 29, no. 8, pp. 379–384, 1980.

[75] K. Osozawa, N. Okato, Y. Fukase, and K. Yokota, "Effects of alloying elements on the pitting corrosion of stainless steels," *CORROSION ENGINEERING*, vol. 24, no. 1, pp. 1–7, 1975.

[76] Y. Lu, M. Ives, and C. Clayton, "Synergism of alloying elements and pitting corrosion resistance of stainless steels," *Corrosion Science*, vol. 35, no. 1-4, pp. 89–96, 1993.

[77] A. Gl, "Standard practice for preparing, cleaning, and evaluation corrosion test specimens," *ASTM international. lggg*, pp. 1–8, 2003.

[78] A. Designation, "Standard test methods for pitting and crevice corrosion resistance of stainless steels and related alloys by use of ferric chloride solution," *ASTM International*, 2009.

[79] A. G61-86, "Standard test method for conducting cyclic potentiodynamic polarization measurements for localized corrosion susceptibility of iron-, nickel-, or cobalt-based alloys," 2009.

[80] G. ASTM, "Standard reference test method for making potentiostatic and potentiodynamic anodic polarization measurements," in *American Society for Testing and Materials*, 2004.

[81] R. G. Kelly, "Crevice corrosion," in *Corrosion: Fundamentals, Testing, and Protection*, pp. 242–247, ASM International, 2003.

[82] R. Kain, "Evaluating crevice corrosion," 2003.

[83] S. Esmailzadeh, M. Aliofkhazraei, and H. Sarlak, "Interpretation of cyclic potentiodynamic polarization test results for study of corrosion behavior of metals: a review," *Protection of metals and physical chemistry of surfaces*, vol. 54, pp. 976–989, 2018.

[84] M. Stefanoni, U. Angst, and B. Elsener, "Local electrochemistry of reinforcement steel–distribution of open circuit and pitting potentials on steels with different surface condition," *Corrosion Science*, vol. 98, pp. 610–618, 2015.

[85] C. S.D. and J. B.S., Covino, "Asm handbook volume 13a: Potential measurements with reference electrodes," *ASM International, Ohio*, 2003.

[86] T. Okada, "Breakdown of passivity and pitting corrosion-kinetic processes," *CORROSION ENGINEERING*, vol. 36, no. 6, pp. 383–392, 1987.

[87] T. Suzuki and Y. Kitamura, "Testing method for localized corrosion of stainless steel considering the corrosion potential in its environment," *CORROSION ENGINEERING*, vol. 23, no. 7, pp. 331–334, 1974.

[88] X. G. Zhang, *Corrosion and electrochemistry of zinc*. Springer Science & Business Media, 1996.

[89] F. Mansfeld, "Electrochemical methods of corrosion testing," *Corrosion: Fundamentals, Testing, and Protection*, pp. 446–462, 2003.

[90] J. R. S. Kelly and G. Robert, "Methods for determining aqueous corrosion reaction rates, corrosion: Fundamentals, testing, and protection, asm handbook," *USA: ASM International*, vol. 13, 2003.

[91] L. Yang and N. Sridhar, "Monitoring of localized corrosion," 2003.

[92] S. Frangini and N. De Cristofaro, "Analysis of the galvanostatic polarization method for determining reliable pitting potentials on stainless steels in crevice-free conditions," *Corrosion science*, vol. 45, no. 12, pp. 2769–2786, 2003.

[93] K. Sasaki and G. Burstein, "The generation of surface roughness during slurry erosion-corrosion and its effect on the pitting potential," *Corrosion Science*, vol. 38, no. 12, pp. 2111–2120, 1996.

[94] M. Vanegas, K. Wang, and M. Iannuzzi, "Understanding the effect of applied current and potential on pitting in 316l stainless steels," *Journal of The Electrochemical Society*, vol. 170, no. 12, p. 121501, 2023.

[95] D. Shoesmith, "Kinetics of aqueous corrosion," in *Corrosion: Fundamentals, Testing, and Protection*, pp. 42–51, ASM International, 2003.

[96] A. G3-89, "Standard practice for conventions applicable to electrochemical measurements in corrosion testing," *Annual Book of ASTM Standards*, 2010.

[97] S. E. Microscopy, "He exner, eds," *ASM International*, vol. 9, 1992.

[98] G. F. Vander Voort, "Asm handbook volume 10: Light optical metallography," *ASM International, Ohio*, 2019.

[99] M. Abramowitz, "Electron excitation and emission," 2016.

[100] Z. Horita, T. Sano, and M. Nemoto, "Energy dispersive x-ray microanalysis in the analytical electron microscope," *isij international*, vol. 29, no. 3, pp. 179–190, 1989.

[101] M. Jokari-Sheshdeh, Y. Ali, S. C. Gallo, W. Lin, and J. Gates, "Effect of cr: Fe ratio on the mechanical properties of (cr, fe) 7c3 ternary carbides in abrasion-resistant white cast irons," *Journal of Materials Science*, vol. 58, no. 17, pp. 7504–7521, 2023.

[102] S. Hiromoto, "Corrosion of metallic biomaterials," in *Metals for biomedical devices*, pp. 131–152, Elsevier, 2019.

[103] K. F. Hounisen, "Microstructure and corrosion characterisation of selective laser melted 316l," Master's thesis, Aalborg University, 2021.

[104] D. C. Silverman, "Aqueous corrosion," 2003.

[105] P. Marcus, "Introduction to fundamentals of corrosion thermodynamics," 2003.

Appendix

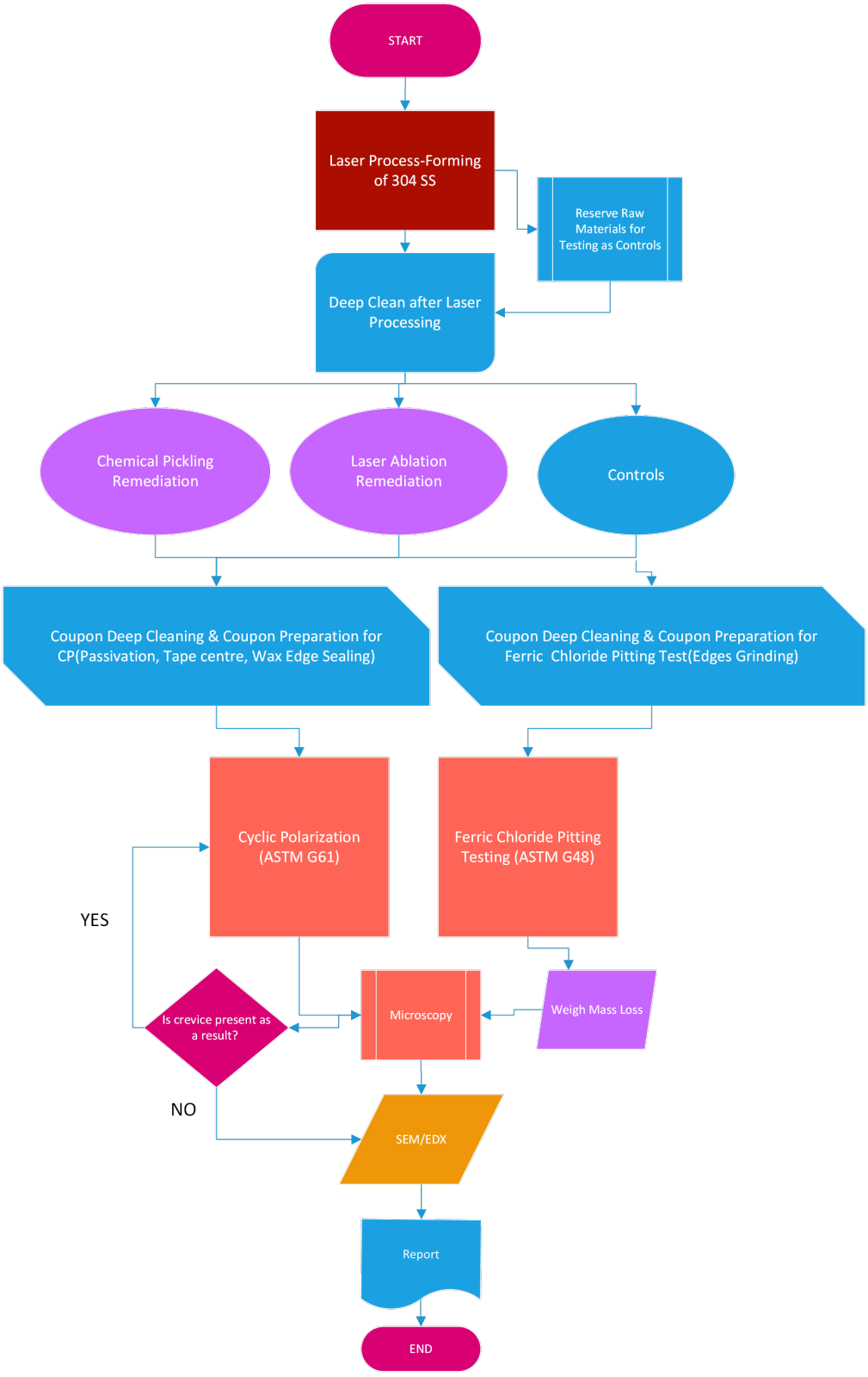

Figure 65: Thesis Project Flow Chart

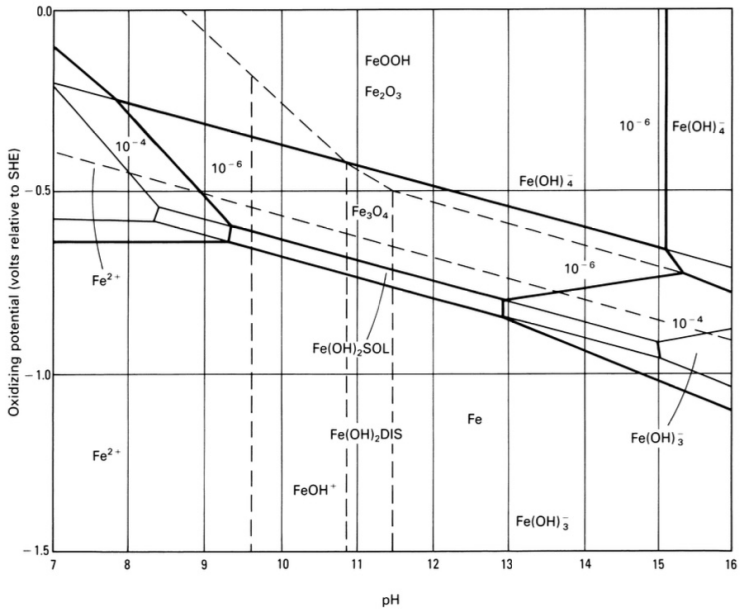

Figure 66: Potential-pH (Pourbaix) diagram for iron at 25 ^{o}C in water vs. SHE[104][105]

	Initial Mass(g) per Balance			After immersion testing			Statistical Analysis				t is 4,303 for 95%						
Coupons:	Initial Mass(g) +/-0,0001	Date	Balance used	Mass after FeCl3 Immersion(g)	Date	Balance used	Mass Loss(g)	Avg(x_)	Range	Deviation from the mean	Avg Deviation of the mean	RAD%	Standard Deviation	RSD%	Confidence Range of 95%	True Value(+)	True Value(-)
RM-C-PT1	30.2150	25-Sep	AND	30.2047	29-Sep	AND	0.0103			0.0001							
RM-C-PT2	30.2604	25-Sep	AND	30.2505	29-Sep	AND	0.0099			0.0099							
RM-C-PT3	30.2644	25-Sep	AND	30.2539	29-Sep	AND	0.0105	0.0102	0.0006	0.0105	0.0068	0.67	0.0003	0.03	0.0008	0.0110	0.0095
LL-C-PT1	30.2831	25-Sep	AND	30.2640	27-Sep	AND	0.0191			0.0011							
LL-C-PT2	30.2303	25-Sep	AND	30.2138	27-Sep	AND	0.0165			0.0165							
LL-C-PT3	30.2559	25-Sep	AND	30.2375	27-Sep	AND	0.0184	0.0180	0.0026	0.0184	0.0120	0.67	0.0013	0.07	0.0033	0.0213	0.0147
HL-C-PT1	30.2102	25-Sep	AND	30.1937	27-Sep	AND	0.0165			-0.0019							
HL-C-PT2	30.2620	25-Sep	AND	30.2394	27-Sep	AND	0.0226			0.0226							
HL-C-PT3	30.1808	25-Sep	AND	30.1646	27-Sep	AND	0.0162	0.0184	0.0064	0.0162	0.0136	0.74	0.0036	0.20	0.0090	0.0274	0.0095

Figure 67: Ferric Chloride Pit Testing Mass Loss Data Calculations and Statistical Analysis Table for RM-C, LL-C and HL-C Coupons

	Initial Mass(g)			After immersion testing			Statistical Analysis				t is 4,303 for 95%						
Coupons:	Initial Mass(g) +/- 0,0001	Date	Balance used	Mass after FeCl3 Immersion (g)	Date	Balance used	Mass Loss(g)	Avg(x_)	Range	Deviation from the mean	Avg Deviation of the mean	RAD%	Standard Deviation	RSD%	Confidence Range of 95%	True Value(+)	True Value(-)
LL-LA-PT1	30.2158	27-Sep	AND	30.0976	02 oct	AND	0.1182			-0.0039							
LL-LA-PT2	30.0866	27-Sep	AND	29.9609	02 oct	AND	0.1257			0.1257							
LL-LA-PT3	30.1690	27-Sep	AND	30.0466	02 oct	AND	0.1224	0.1221	0.0075	0.1224	0.0840	0.69	0.0038	0.03	0.0093	0.1314	0.1128
HL-LA-PT1	30.2554	27-Sep	AND	30.1085	02 oct	AND	0.1469			0.0061							
HL-LA-PT2	30.2623	27-Sep	AND	30.1116	02 oct	AND	0.1507			0.1507							
HL-LA-PT3	30.1566	27-Sep	AND	30.0317	02 oct	AND	0.1249	0.1408	0.0258	0.1249	0.0939	0.67	0.0139	0.10	0.0346	0.1754	0.1062

Figure 68: Ferric Chloride Pit Testing Mass Loss Data Calculations and Statistical Analysis Table for LL-LA and HL-LA Coupons

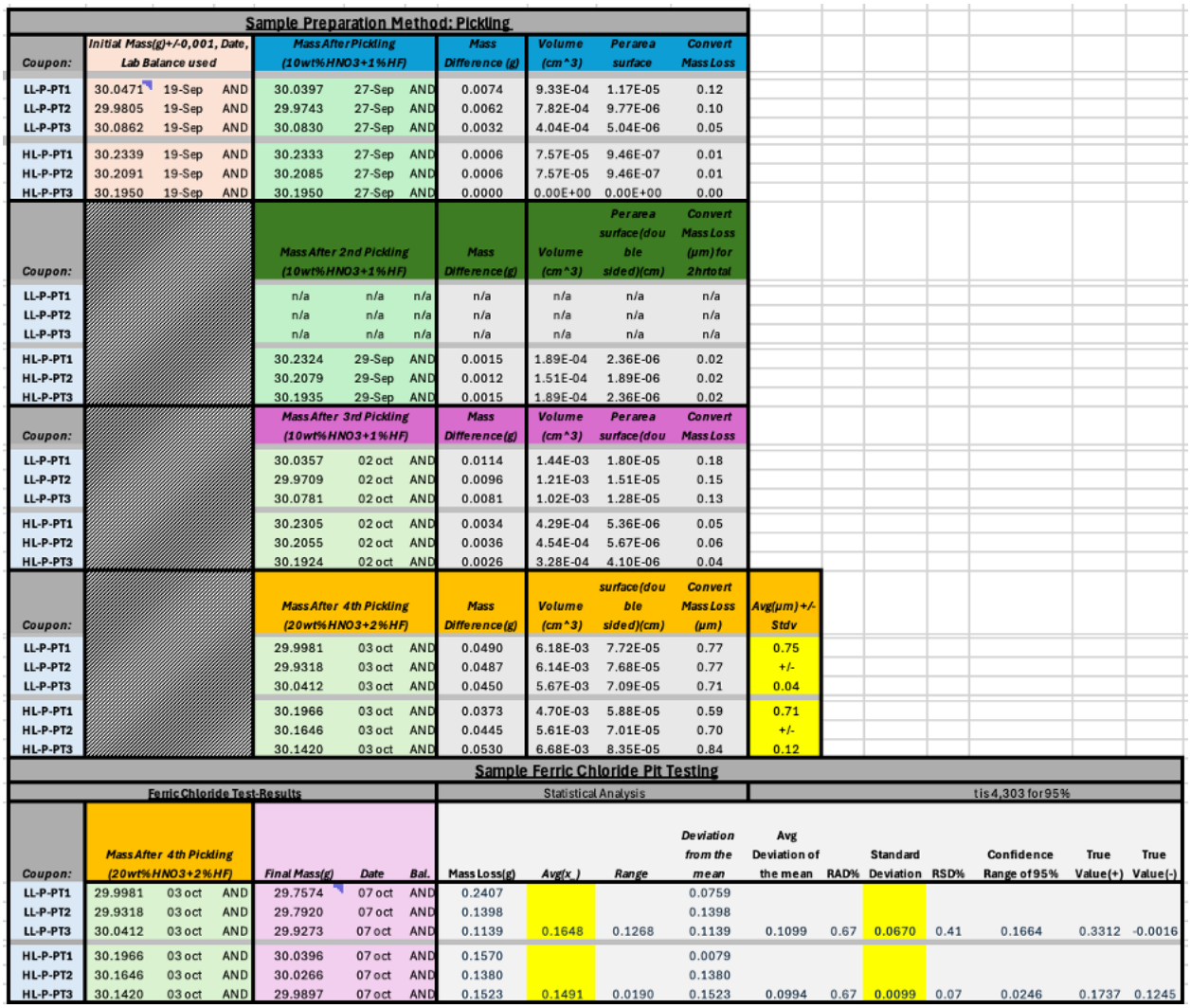

Sample Preparation Method: Pickling

Coupon:	Initial Mass(g)+/-0,001, Date, Lab Balance used			Mass After Pickling (10wt%HNO3+1%HF)			Mass Difference (g)	Volume (cm^3)	Per area surface	Convert Mass Loss
LL-P-PT1	30.0471	19-Sep	AND	30.0397	27-Sep	AND	0.0074	9.33E-04	1.17E-05	0.12
LL-P-PT2	29.9805	19-Sep	AND	29.9743	27-Sep	AND	0.0062	7.82E-04	9.77E-06	0.10
LL-P-PT3	30.0862	19-Sep	AND	30.0830	27-Sep	AND	0.0032	4.04E-04	5.04E-06	0.05
HL-P-PT1	30.2339	19-Sep	AND	30.2333	27-Sep	AND	0.0006	7.57E-05	9.46E-07	0.01
HL-P-PT2	30.2091	19-Sep	AND	30.2085	27-Sep	AND	0.0006	7.57E-05	9.46E-07	0.01
HL-P-PT3	30.1950	19-Sep	AND	30.1950	27-Sep	AND	0.0000	0.00E+00	0.00E+00	0.00

Coupon:	Mass After 2nd Pickling (10wt%HNO3+1%HF)			Mass Difference (g)	Volume (cm^3)	Per area surface (double sided)(cm)	Convert Mass Loss (μm) for 2hr total
LL-P-PT1	n/a	n/a	n/a	n/a	n/a	n/a	n/a
LL-P-PT2	n/a	n/a	n/a	n/a	n/a	n/a	n/a
LL-P-PT3	n/a	n/a	n/a	n/a	n/a	n/a	n/a
HL-P-PT1	30.2324	29-Sep	AND	0.0015	1.89E-04	2.36E-06	0.02
HL-P-PT2	30.2079	29-Sep	AND	0.0012	1.51E-04	1.89E-06	0.02
HL-P-PT3	30.1935	29-Sep	AND	0.0015	1.89E-04	2.36E-06	0.02

Coupon:	Mass After 3rd Pickling (10wt%HNO3+1%HF)			Mass Difference (g)	Volume (cm^3)	Per area surface (dou	Convert Mass Loss
LL-P-PT1	30.0357	02 oct	AND	0.0114	1.44E-03	1.80E-05	0.18
LL-P-PT2	29.9709	02 oct	AND	0.0096	1.21E-03	1.51E-05	0.15
LL-P-PT3	30.0781	02 oct	AND	0.0081	1.02E-03	1.28E-05	0.13
HL-P-PT1	30.2305	02 oct	AND	0.0034	4.29E-04	5.36E-06	0.05
HL-P-PT2	30.2055	02 oct	AND	0.0036	4.54E-04	5.67E-06	0.06
HL-P-PT3	30.1924	02 oct	AND	0.0026	3.28E-04	4.10E-06	0.04

Coupon:	Mass After 4th Pickling (20wt%HNO3+2%HF)			Mass Difference (g)	Volume (cm^3)	surface (double sided)(cm)	Convert Mass Loss (μm)	Avg(μm) +/- Stdv
LL-P-PT1	29.9981	03 oct	AND	0.0490	6.18E-03	7.72E-05	0.77	0.75
LL-P-PT2	29.9318	03 oct	AND	0.0487	6.14E-03	7.68E-05	0.77	+/-
LL-P-PT3	30.0412	03 oct	AND	0.0450	5.67E-03	7.09E-05	0.71	0.04
HL-P-PT1	30.1966	03 oct	AND	0.0373	4.70E-03	5.88E-05	0.59	0.71
HL-P-PT2	30.1646	03 oct	AND	0.0445	5.61E-03	7.01E-05	0.70	+/-
HL-P-PT3	30.1420	03 oct	AND	0.0530	6.68E-03	8.35E-05	0.84	0.12

Sample Ferric Chloride Pit Testing

Ferric Chloride Test-Results | Statistical Analysis | t is 4,303 for 95%

Coupon:	Mass After 4th Pickling (20wt%HNO3+2%HF)			Final Mass(g)	Date	Bal.	Mass Loss(g)	Avg(x_)	Range	Deviation from the mean	Avg Deviation of the mean	RAD%	Standard Deviation	RSD%	Confidence Range of 95%	True Value(+)	True Value(-)
LL-P-PT1	29.9981	03 oct	AND	29.7574	07 oct	AND	0.2407			0.0759							
LL-P-PT2	29.9318	03 oct	AND	29.7920	07 oct	AND	0.1398			0.1398							
LL-P-PT3	30.0412	03 oct	AND	29.9273	07 oct	AND	0.1139	0.1648	0.1268	0.1139	0.1099	0.67	0.0670	0.41	0.1664	0.3312	-0.0016
HL-P-PT1	30.1966	03 oct	AND	30.0396	07 oct	AND	0.1570			0.0079							
HL-P-PT2	30.1646	03 oct	AND	30.0266	07 oct	AND	0.1380			0.1380							
HL-P-PT3	30.1420	03 oct	AND	29.9897	07 oct	AND	0.1523	0.1491	0.0190	0.1523	0.0994	0.67	0.0099	0.07	0.0246	0.1737	0.1245

Figure 69: Pickling and Ferric Chloride Pit Testing Mass Loss Data Calculations and Statistical Analysis Table for LL-P and HL-P Coupons

Validation/Preliminary Data

Date	Sample	Beta a(V/decade)	Beta c(V/decade)	Icorr Current density (A/cm^2	Ecorr (mV)	Corrosion Rate(mpy)	X^2	Crevice	Notes
03-sep	burn1	1,49E-01	9,55E-02	1,00E-08	156	4,57E-03	12,39	Y	Apex:5mA/cm^2,7.5 surface area, sample period:2s, note that sample has been altered b/c of high diff on Eoc and Ecorr
04-sep	burn2	1,99E-01	1,29E-01	2,76E-08	215	1,26E-02	31,55	N	Apex I:0.1mA/cm^2,Samples period:2s
05-sep	burn 3	2,76E-02	2,32E-01	2,44E-08	144	1,12E-02	86,39	N	Apex I: 1mA/cm^2,sample period:1 s
06-sep	burn 4.2	2,98E-01	1,17E-01	9,64E-09	154	4,41E-03	36,37	N	Apex I: 1mA/cm^2,sample period:2 s,note that sample has been altered b/c of high diff on Eoc and Ecorr
06-sep	burn 5	1,16E-01	4,41E-02	4,43E-09	206	2,03E-03	6,669	N	Non-passivated(surface area 7.5cm^2), same parameters as above
06-sep	burn 6	1,53E-01	1,23E-01	6,38E-09	91,6	2,92E-03	8,557	N	All-passivated (surface area:9cm^2), note that sample has been altered b/c of high diff on Eoc and Ecorr
07-sep	burn 7	8,55E-02	1,07E-01	4,47E-07	208	2,04E-01	3,569	N	Bended+passivated , but sealed only on top of staining, surface area(10cm^2)
17-sep	burn 8	1,03E-01	1,34E-01	1,37E-08	168	6,24E-03	8,824	Y	Do not use, just checking b/c equipment was disassembled

Figure 70: CPP Data Acquisition of 304 SS Coupons for Method Development

			Raw Data							
Date	Sample	Crevice/Pitting	Beta a(V/decade)	eta c(V/decade	Icorr Current desnity(A/cm^2)	Ecorr(mV)	Corrosion Rate(mpy)	X^2	Epit (mV)	Rpit(mV)
18-Sep	RM-C-CP1	Y/Y	n/a	n/a	n/a	n/a	n/a	n/a	326.20	#VALUE!
19-Sep	RM-C-CP2	Y/Y	n/a	n/a	n/a	n/a	n/a	n/a	n/a	#VALUE!
23-Sep	RM-C-CP3	N/Y	1.50E-01	1.40E-01	1.70E-08	163	7.78E-03	21.26	356.8	193.80
24-Sep	RM-C-CP4	N/Y	1.75E-01	3.44E-01	3.67E-08	177	1.68E-02	22.44	220.3	43.30
24-Sep	RM-C-CP5	N/Y	4.05E-01	2.46E-01	4.06E-08	212.0	1.86E-02	4.863	459.2	247.20
24-Sep	RM-C-CP6	N/Y	1.93E-01	2.01E-01	1.780E-08	150.0	8.14E-03	9.244	407.8	257.80
25-Sep	RM-C-CP7	N/Y	2.23E-01	2.41E-01	2.010E-08	170.0	9.17E-03	4.761	388.8	218.80
24-Sep	RM-C-CP8	Y/Y	1.90E-01	9.32E-02	9.260E-09	175.0	4.23E-03	3.529	454.4	279.40
27-Sep	RM-C-CP9	N/Y	1.92E-01	1.01E-01	9.040E-09	181.0	4.13E-03	6.005	408.3	227.30
					Statistical Analysis					
		Average	2.23E-01	2.12E-01	2.35E-08	1.76E+02	1.08E-02	1.14E+01	3.74E+02	1.98E+02
		Range	2.55E-01	2.43E-01	3.16E-08	6.20E+01	1.44E-02	1.77E+01	2.39E+02	2.15E+02
		Avg Deviation of the mean	6.08E-02	6.48E-02	1.01E-08	1.45E+01	4.61E-03	6.95E+00	5.67E+01	5.30E+01
		RAD%	27.27%	30.53%	42.79%	8.26%	42.82%	60.79%	15.17%	26.76%
		Standard Deviation	9.24E-02	8.60E-02	1.23E-08	2.10E+01	5.65E-03	8.24E+00	8.21E+01	7.90E+01
		RSD%	41.45%	40.55%	52.44%	11.96%	52.46%	72.12%	21.98%	39.91%
t is 2.571 for 95%(N=6)		**Confidence Range of 95%**	9.70E-02	9.03E-02	1.30E-08	2.20E+01	5.93E-03	8.65E+00	8.62E+01	8.30E+01
		True Value(+)	3.20E-01	3.02E-01	3.65E-08	1.98E+02	1.67E-02	2.01E+01	4.60E+02	2.81E+02
		True Value(-)	1.26E-01	1.22E-01	1.06E-08	1.53E+02	4.84E-03	2.78E+00	2.87E+02	1.15E+02
	RM-C-CP3		-7.27E-02	-7.17E-02	-6.54E-09	-1.25E+01	-2.98E-03	9.83E+00	-1.67E+01	-4.23E+00
	RM-C-CP4		-4.84E-02	1.32E-01	1.32E-08	1.50E+00	6.03E-03	1.10E+01	-1.53E+02	-1.55E+02
Deviation from the mean	RM-C-CP5		1.82E-01	3.41E-02	1.71E-08	3.65E+01	7.80E-03	-6.57E+00	8.57E+01	4.92E+01
	RM-C-CP6		-3.04E-02	-1.11E-02	-5.74E-09	-2.55E+01	-2.62E-03	-2.18E+00	3.43E+01	5.98E+01
	RM-C-CP7		1.83E-04	2.86E-02	-3.44E-09	-5.50E+00	-1.59E-03	-6.67E+00	1.53E+01	2.08E+01
	RM-C-CP9		-3.08E-02	-1.11E-01	-1.45E-08	5.50E+00	-6.63E-03	-5.42E+00	3.48E+01	2.93E+01

Figure 71: CPP Data Calculations and Statistical Analysis Table for RM-C Coupons

			Raw Data							
Date	Sample	Crevice/Pitting	Beta a(V/decade)	Beta c(V/decade)	Icorr Current density(A/cm^2)	Ecorr(mV)	Corrosion Rate(mpy)	X^2	Epit(mV)	Rpit(mV)
25-Sep	LL-C-CP1	N/Y	2.56E-01	2.03E-01	1.77E-08	193	8.07E-03	48.49	225.2	32.2
25-Sep	LL-C-CP2	N/Y	7.46E-02	5.98E-02	2.34E-09	84.3	1.07E-03	11.99	212.6	128.3
25-Sep	LL-C-CP3	Y/Y	1.91E-01	2.44E-01	1.65E-08	191	7.52E-03	3.706	242.7	51.7
25-Sep	LL-C-CP4	N/Y	5.90E-03	1.29E-01	9.79E-09	187	4.48E-03	40.95	198.1	11.1
02 oct	LL-C-CP5	N/N	9.41E-02	1.21E-01	6.84E-09	129	3.13E-03	7.744	246.1	117.1
02 oct	LL-C-CP6	N/N	3.01E+05	1.42E-01	2.30E-08	109	1.05E-02	1.484	244.7	135.7
					Statistical Analysis					
		Average	6.03E+04	1.31E-01	1.19E-08	1.40E+02	5.45E-03	2.21E+01	2.25E+02	8.49E+01
		Range	3.01E+05	1.44E-01	2.07E-08	1.09E+02	9.42E-03	4.70E+01	4.80E+01	1.25E+02
		Avg Deviation of the mean	9.64E+04	3.33E-02	6.73E-09	3.96E+01	3.07E-03	1.81E+01	1.60E+01	5.06E+01
		RAD%	160.00%	25.44%	56.42%	28.22%	56.32%	81.65%	7.12%	59.59%
		Standard Deviation	1.35E+05	5.13E-02	8.34E-09	4.80E+01	3.80E-03	2.11E+01	2.07E+01	5.86E+01
		RSD%	223.61%	39.15%	69.89%	34.15%	69.81%	95.45%	9.18%	69.01%
t is 2.776 for 95%(N=5)		**Confidence Range of 95%**	1.67E+05	6.37E-02	1.04E-08	5.95E+01	4.72E-03	2.62E+01	2.57E+01	7.27E+01
		True Value(+)	2.28E+05	1.95E-01	2.23E-08	2.00E+02	1.02E-02	4.84E+01	2.51E+02	1.58E+02
		True Value(-)	-1.07E+05	6.73E-02	1.58E-09	8.09E+01	7.26E-04	-4.09E+00	2.00E+02	1.22E+01
	LL-C-CP1		-6.03E+04	7.23E-02	5.77E-09	5.25E+01	2.62E-03	2.64E+01	-1.40E-01	-5.27E+01
	LL-C-CP2		-6.03E+04	-7.12E-02	-9.59E-09	-5.62E+01	-4.38E-03	-1.01E+01	-1.27E+01	4.34E+01
Deviation from the mean	LL-C-CP4		-6.03E+04	-2.30E-03	-2.14E-09	4.65E+01	-9.70E-04	1.88E+01	-2.72E+01	-7.38E+01
	LL-C-CP5		-6.03E+04	-9.80E-03	-5.09E-09	-1.15E+01	-2.32E-03	-1.44E+01	2.08E+01	3.22E+01
	LL-C-CP6		2.41E+05	1.10E-02	1.11E-08	-3.15E+01	5.04E-03	-2.06E+01	1.94E+01	5.08E+01

Figure 72: CPP Data Calculations and Statistical Analysis Table for LL-C Coupons

			Raw Data							
Date	Sample	Crevice/Pitting	Beta a(V/decade)	Beta c(V/decade)	Icorr Current desnity	Ecorr(mV)	Corrosion Rate(mpy)	X^2	Epit(mV)	Rpit(mV)
26-Sep	HL-C-CP1	N/Y	2.11E-02	1.28E-01	4.14E-09	126	1.89E-03	253.7	160.2	34.2
27-Sep	HL-C-CP2	N/Y	2.34E-02	5.67E-01	1.35E-08	156	6.182E-03	296.8	208.7	52.7
26-Sep	HL-C-CP3	Y/Y	1.50E-02	2.72E-01	1.12E-08	138	5.11E-03	216.6	149.5	11.5
26-Sep	HL-C-CP4	N/Y	1.71E-02	9.06E-02	3.23E-10	217	1.48E-04	243.3	160.2	56.8
			Statistical Analysis							
	Average		2.05E-02	2.62E-01	5.99E-09	1.66E+02	2.74E-03	2.65E+02	1.76E+02	4.79E+01
	Range		6.30E-03	4.76E-01	1.32E-08	9.10E+01	6.03E-03	5.35E+01	4.85E+01	2.26E+01
	Avg Deviation of the mean		2.29E-03	2.03E-01	5.01E-09	3.38E+01	2.29E-03	2.15E+01	2.16E+01	9.13E+00
	RAD%		11.15%	77.60%	83.64%	20.31%	83.68%	8.11%	12.22%	19.07%
	Standard Deviation		3.19E-03	2.65E-01	6.78E-09	4.64E+01	3.11E-03	2.84E+01	2.80E+01	1.20E+01
	RSD%		15.53%	101.06%	113.23%	27.88%	113.27%	10.72%	15.88%	25.14%
t is 4.303 for 95%(N=3)	Confidence Range of 95%		7.92E-03	6.58E-01	1.68E-08	1.15E+02	7.71E-03	7.05E+01	6.96E+01	2.99E+01
	True Value(+)		2.85E-02	9.20E-01	2.28E-08	2.82E+02	1.05E-02	3.35E+02	2.46E+02	7.78E+01
	True Value(-)		1.26E-02	-3.96E-01	-1.09E-08	5.11E+01	-4.97E-03	1.94E+02	1.07E+02	1.80E+01
Deviation from the mean		HL-C-CP1	5.67E-04	-1.34E-01	-1.85E-09	-4.03E+01	-8.47E-04	-1.09E+01	-1.62E+01	-1.37E+01
		HL-C-CP2	2.87E-03	3.05E-01	7.51E-09	-1.03E+01	3.44E-03	3.22E+01	3.23E+01	4.80E+00
		HL-C-CP4	-3.43E-03	-1.71E-01	-5.66E-09	5.07E+01	-2.59E-03	-2.13E+01	-1.62E+01	8.90E+00

Figure 73: CPP Data Calculations and Statistical Analysis Table for HL-C Coupons

			Raw Data							
Date	Sample	revice/Pittin	Beta a(V/decade)	Beta c(V/decade)	Icorr Current desnity(A/cm^2)	Ecorr(mV)	osion Rate(	X^2	Epit(mV)	Rpit(mV)
27-Sep	LL-LA-CP1	Y/N	8.31E-02	1.53E-01	9.72E-08	-91.4	4.44E-02	0.5268	-11.65	79.75
29-Sep	LL-LA-CP2	Y/Y	2.11E-01	9.07E-02	4.70E-09	197	2.15E-03	32.66	361.2	164.2
29-Sep	LL-LA-CP3	N/Y	1.39E-01	7.97E-02	2.44E-09	178	1.12E-03	0.502	258.0	80
01 oct	LL-LA-CP4	N/N	2.17E-01	7.55E-02	3.07E-09	39.6	1.40E-03	16.54	365.1	325.5
02 oct	LL-LA-CP5	Y/N	1.02E-01	1.21E-01	5.04E-09	88.7	2.31E-05	17.32	161.2	72.5
10 oct	LL-LA-CP6	N/Y	2.19E-01	7.55E-02	1.62E-08	-10.9	7.41E-03	8.649	295.1	306
			Statistical Analysis							
	Average		1.92E-01	7.69E-02	7.24E-09	6.89E+01	3.31E-03	8.56E+00	3.06E+02	2.37E+02
	Range		7.97E-02	4.20E-03	1.38E-08	1.89E+02	6.30E-03	1.60E+01	1.07E+02	2.46E+02
	Avg Deviation of the mean		3.52E-02	1.87E-03	5.98E-09	7.27E+01	2.73E-03	5.37E+00	8.40E+01	1.05E+02
	RAD%		18.35%	2.43%	82.57%	105.56%	82.59%	62.76%	27.44%	44.18%
	Standard Deviation		4.57E-02	2.42E-03	7.77E-09	9.78E+01	3.55E-03	8.02E+00	5.44E+01	1.36E+02
	RSD%		23.85%	3.15%	107.35%	141.94%	107.38%	93.64%	17.77%	57.54%
t is 4.303 for 95%(N=3)	Confidence Range of 95%		1.13E-01	6.02E-03	1.93E-08	2.43E+02	8.83E-03	1.99E+01	1.35E+02	3.39E+02
	True Value(+)		3.05E-01	8.29E-02	2.65E-08	3.12E+02	1.21E-02	2.85E+01	4.41E+02	5.76E+02
	True Value(-)		7.81E-02	7.09E-02	-1.21E-08	-1.74E+02	-5.52E-03	-1.14E+01	1.71E+02	-1.02E+02
Deviation from the mean		LL-LA-CP3	-5.27E-02	2.80E-03	-4.80E-09	1.09E+02	-2.19E-03	-8.06E+00	-4.81E+01	-1.57E+02
		LL-LA-CP4	2.58E-02	-1.40E-03	-4.17E-09	-2.93E+01	-1.91E-03	7.98E+00	5.90E+01	8.83E+01
		LL-LA-CP6	2.70E-02	-1.40E-03	8.96E-09	-7.98E+01	4.10E-03	8.53E-02	-1.45E+02	6.88E+01

Figure 74: CPP Data Calculations and Statistical Analysis Table for LL-LA Coupons

					Raw Data					
Date	Sample	Crevice/Pitting	Beta a(V/decade)	Beta c(V/decade)	Icorr Current density(A/cm^2)	Ecorr(mV)	Corrosion Rate(mpy)	X^2	Epit(mV)	Rpit(mV)
30-Sep	HL-LA-CP1	Y/Y	1.31E-01	8.58E-02	2.19E-09	156	1.00E-03	48.62	261.2	105.2
30-Sep	HL-LA-CP2	Y/Y	4.209	3.77E-01	2.64E-08	199	1.21E-02	7.441	402.9	203.9
30-Sep	HL-LA-CP3	N/Y	9.86E-02	6.11E-02	1.30E-09	118	5.93E-04	5.968	360.4	242.4
30-Sep	HL-LA-CP4	Y/Y	3.56E-02	7.70E-02	1.32E-09	160.0	6.03E-04	14.89	193.2	33.2
02 oct	HL-LA-CP5	N/N	1.46E-01	1.58E-01	3.89E-09	134.0	1.779E-03	9.910	238.1	104.1
10 oct	HL-LA-CP6	N/N	7.01E-02	1.11E-01	4.46E-08	-28.5	2.04E-02	7.809	80.49	108.99
					Statistical Analysis					
		Average	1.05E-01	1.10E-01	1.66E-08	7.45E+01	7.58E-03	7.90E+00	2.26E+02	1.52E+02
		Range	7.60E-02	9.66E-02	4.33E-08	1.63E+02	1.98E-02	3.94E+00	2.80E+02	1.38E+02
		Avg Deviation of the mean	2.74E-02	3.25E-02	1.87E-08	6.87E+01	8.52E-03	1.34E+00	9.72E+01	6.04E+01
		RAD%	26.15%	29.57%	112.49%	92.17%	112.47%	17.01%	42.96%	39.77%
		Standard Deviation	3.84E-02	4.83E-02	2.43E-08	8.96E+01	1.11E-02	1.97E+00	1.40E+02	7.85E+01
		RSD%	36.59%	43.99%	146.33%	120.21%	146.31%	24.98%	62.00%	51.69%
t is 4.303 for 95%(N=3)		Confidence Range of 95%	9.54E-02	1.20E-01	6.03E-08	2.22E+02	2.75E-02	4.90E+00	3.49E+02	1.95E+02
		True Value(+)	2.00E-01	2.30E-01	7.69E-08	2.97E+02	3.51E-02	1.28E+01	5.75E+02	3.47E+02
		True Value(-)	9.55E-03	-1.02E-02	-4.37E-08	-1.48E+02	-2.00E-02	3.00E+00	-1.22E+02	-4.31E+01
	Deviation from the mean	HL-LA-CP3	-6.33E-03	-4.87E-02	-1.53E-08	4.35E+01	-6.98E-03	-1.93E+00	1.34E+02	9.06E+01
		HL-LA-CP5	4.12E-02	4.79E-02	-1.27E-08	5.95E+01	-5.80E-03	2.01E+00	1.18E+01	-4.77E+01
		HL-LA-CP6	-3.48E-02	8.00E-04	2.80E-08	-1.03E+02	1.28E-02	-8.67E-02	-1.46E+02	-4.28E+01

Figure 75: CPP Data Calculations and Statistical Analysis Table for HL-LA Coupons

					Raw Data					
Date	Sample	revice/Pitti	Beta a(V/decade)	Beta c(V/decade)	Icorr Current desnity(A/cm^2)	Ecorr(mV)	Corrosion Rate(mpy)	X^2	Epit(mV)	Rpit(mV)
05 oct	LL-P-CP1	N/N	1.35E-01	7.79E-02	7.04E-09	31.8	3.22E-03	6.018	241	209.2
06 oct	LL-P-CP2	N/N	1.28E-01	5.22E+04	4.77E-09	109	2.18E-03	1.531	382.3	273.3
09 oct	LL-P-CP3	N/N	1.69E-01	3.64E-02	3.62E-09	34.2	1.66E-03	0.8248	167.0	132.8
07 oct	LL-P-CP4	N/N	1.91E-02	1.13E-01	9.22E-09	86.9	4.21E-03	47.24	113.6	26.7
07 oct	LL-P-CP5	N/N	1.20E-01	8.78E-02	5.69E-09	98.6	2.60E-03	3.083	325.2	226.6
07 oct	LL-P-CP6	N/N	1.82E-02	5.73E-02	2.11E-09	75.00	9.64E-04	48.04	120.9	45.9
					Statistical Analysis					
		Average	9.83E-02	8.70E+03	5.41E-09	7.26E+01	2.47E-03	1.78E+01	2.25E+02	1.52E+02
		Range	1.51E-01	5.22E+04	7.11E-09	7.72E+01	3.25E-03	4.72E+01	2.69E+02	2.47E+02
		Avg Deviation of the mean	5.31E-02	1.45E+04	1.91E-09	2.64E+01	8.73E-04	1.99E+01	9.12E+01	8.40E+01
		RAD%	54.02%	166.67%	35.29%	36.36%	35.30%	111.87%	40.52%	55.08%
		Standard Deviation	6.39E-02	2.13E+04	2.52E-09	3.27E+01	1.15E-03	2.32E+01	1.11E+02	1.01E+02
		RSD%	64.99%	244.95%	46.60%	45.07%	46.61%	130.37%	49.35%	66.18%
t is 2.571 for 95%(N=6)		Confidence Range of 95%	6.71E-02	2.24E+04	2.65E-09	3.43E+01	1.21E-03	2.43E+01	1.17E+02	1.06E+02
		True Value(+)	1.65E-01	3.11E+04	8.05E-09	1.07E+02	3.68E-03	4.21E+01	3.42E+02	2.58E+02
		True Value(-)	3.13E-02	-1.37E+04	2.76E-09	3.82E+01	1.26E-03	-6.55E+00	1.08E+02	4.65E+01
	Deviation from the mean	LL-P-CP1	3.71E-02	-8.70E+03	1.63E-09	-4.08E+01	7.47E-04	-1.18E+01	1.60E+01	5.68E+01
		LL-P-CP2	3.00E-02	4.35E+04	-6.38E-10	3.64E+01	-2.93E-04	-1.63E+01	1.57E+02	1.21E+02
		LL-P-CP3	7.05E-02	-8.70E+03	-1.79E-09	-3.84E+01	-8.16E-04	-1.70E+01	-5.80E+01	-1.96E+01
		LL-P-CP4	-7.92E-02	-8.70E+03	3.81E-09	1.43E+01	1.74E-03	2.95E+01	-1.11E+02	-1.26E+02
		LL-P-CP5	2.18E-02	-8.70E+03	2.82E-10	2.60E+01	1.29E-04	-1.47E+01	1.00E+02	7.42E+01
		LL-P-CP6	-8.01E-02	-8.70E+03	-3.30E-09	2.42E+00	-1.51E-03	3.03E+01	-1.04E+02	-1.07E+02

Figure 76: CPP Data Calculations and Statistical Analysis Table for LL-P Coupons

Sample	Rpit(mV)	Sample	Rpit(mV)	Sample	Rpit(mV)	Sample	Rpit(mV)	Sample	Rpit(mV)	Sample	Rpit(mV)	Sample	Rpit(mV)
RM-C-CP1	N/a	LL-C-CP1	32.2	HL-C-CP1	34.2	LL-LA-CP1	79.75	HL-LA-CP1	105.2	LL-P-CP1	209.2	HL-P-CP1	149.69
RM-C-CP2	N/a	LL-C-CP2	128.3	HL-C-CP2	52.7	LL-LA-CP2	164.2	HL-LA-CP2	203.9	LL-P-CP2	273.3	HL-P-CP2	329.9
RM-C-CP3	193.80	LL-C-CP3	51.7	HL-C-CP3	11.5	LL-LA-CP3	80	HL-LA-CP3	242.4	LL-P-CP3	132.8	HL-P-CP3	160.9
RM-C-CP4	43.30	LL-C-CP4	11.1	HL-C-CP4	56.8	LL-LA-CP4	325.5	HL-LA-CP4	33.2	LL-P-CP4	26.7	HL-P-CP4	150.25
RM-C-CP5	247.20	LL-C-CP5	117.1			LL-LA-CP5	72.5	HL-LA-CP5	104.1	LL-P-CP5	226.6		
RM-C-CP6	257.80	LL-C-CP6	135.7			LL-LA-CP6	306	HL-LA-CP6	108.99	LL-P-CP6	45.9		
RM-C-CP7	218.80												
RM-C-CP8	279.40												
RM-C-CP9	227.30												
Statistical Analysis													
Average	**1.98E+02**		**8.49E+01**		**4.79E+01**		**2.37E+02**		**1.52E+02**		**1.52E+02**		**1.98E+02**
Range	2.15E+02		1.25E+02		2.26E+01		2.46E+02		1.38E+02		2.47E+02		1.80E+02
Avg Deviation of the mean	5.30E+01		5.06E+01		9.13E+00		1.05E+02		6.04E+01		8.40E+01		6.61E+01
RAD%	26.76%		59.59%		19.07%		44.18%		39.77%		55.08%		33.44%
Standard Deviation	**7.90E+01**		**5.86E+01**		**1.20E+01**		**1.36E+02**		**7.85E+01**		**1.01E+02**		**8.83E+01**
RSD%	39.91%		69.01%		25.14%		57.54%		51.69%		66.18%		44.66%
Confidence Range of 95%	8.30E+01		7.27E+01		2.99E+01		3.39E+02		1.95E+02		1.06E+02		1.40E+02
True Value(+)	***2.81E+02***		***1.58E+02***		***7.78E+01***		***5.76E+02***		***3.47E+02***		***2.58E+02***		***3.38E+02***
True Value(-)	***1.15E+02***		***1.22E+01***		***1.80E+01***		***-1.02E+02***		***-4.31E+01***		***4.65E+01***		***5.72E+01***
Deviation from the mean													
RM-C-CP3	-4.23E+00	LL-C-CP1	-5.27E+01	HL-C-CP1	-1.37E+01	LL-LA-CP3	-1.57E+02	HL-LA-CP3	9.06E+01	LL-P-CP1	5.68E+01	HL-P-CP1	-4.80E+01
RM-C-CP4	-1.55E+02	LL-C-CP2	4.34E+01	HL-C-CP2	4.80E+00	LL-LA-CP4	8.83E+01	HL-LA-CP5	-4.77E+01	LL-P-CP2	1.21E+02	HL-P-CP2	1.32E+02
RM-C-CP5	4.92E+01	LL-C-CP4	-7.38E+01	HL-C-CP4	8.90E+00	LL-LA-CP6	6.88E+01	HL-LA-CP6	-4.28E+01	LL-P-CP3	-1.96E+01	HL-P-CP3	-3.68E+01
RM-C-CP6	5.98E+01	LL-C-CP5	3.22E+01							LL-P-CP4	-1.26E+02	HL-P-CP4	-4.74E+01
RM-C-CP7	2.08E+01	LL-C-CP6	5.08E+01							LL-P-CP5	7.42E+01		
RM-C-CP9	2.93E+01									LL-P-CP6	-1.07E+02		

Figure 78: CPP Data Calculations and Statistical Analysis Table for Rpit of all Study Groups

Raw Data										
Date	Sample	Crevice/Pitting	Beta a (V/decade)	Beta c (V/decade)	Icorr Current density(A/cm^2)	Ecorr(mV)	Corrosion Rate(mpy)	X^2	Epit (mV)	Rpit(mV)
05 oct	HL-P-CP1	N/N	1.35E-01	5.27E-02	8.93E-09	-5.79	4.08E-03	5.779	143.9	149.69
06 oct	HL-P-CP2	N/N	4.19E-02	1.14E-01	7.85E-09	73	3.59E-03	16.23	402.9	329.9
06 oct	HL-P-CP3	N/N	1.11E-01	6.97E-02	6.94E-09	141	3.17E-03	4.594	301.9	160.9
09 oct	HL-P-CP4	N/N	6.195	8.13E-02	1.25E-08	5.05	5.72E-03	57.14	155.3	150.25
Statistical Analysis										
Average			1.62E+00	7.94E-02	9.06E-09	5.33E+01	4.14E-03	2.09E+01	2.51E+02	1.98E+02
Range			6.15E+00	6.11E-02	5.56E-09	1.47E+02	2.54E-03	5.25E+01	2.59E+02	1.80E+02
Avg Deviation of the mean			2.29E+00	1.82E-02	1.72E-09	5.37E+01	7.88E-04	1.81E+01	1.01E+02	6.61E+01
RAD%			141.14%	22.90%	19.02%	100.69%	19.05%	86.47%	40.40%	33.44%
Standard Deviation			3.05E+00	2.58E-02	2.44E-09	6.81E+01	1.12E-03	2.47E+01	1.24E+02	8.83E+01
RSD%			188.20%	32.48%	26.91%	127.67%	26.94%	117.96%	49.49%	44.66%
t is 3.182 for 95%(N=4)	Confidence Range of 95%		4.85E+00	4.10E-02	3.88E-09	1.08E+02	1.77E-03	3.93E+01	1.98E+02	1.40E+02
True Value(+)			6.47E+00	1.20E-01	1.29E-08	1.62E+02	5.91E-03	6.02E+01	4.49E+02	3.38E+02
True Value(-)			-3.23E+00	3.84E-02	5.18E-09	-5.50E+01	2.37E-03	-1.84E+01	5.34E+01	5.72E+01
Deviation from the mean		HL-P-CP1	-1.49E+00	-2.67E-02	-1.25E-10	-5.91E+01	-5.62E-05	-1.52E+01	-1.07E+02	-4.80E+01
		HL-P-CP2	-1.58E+00	3.44E-02	-1.21E-09	1.97E+01	-5.54E-04	-4.71E+00	1.52E+02	1.32E+02
		HL-P-CP3	-1.51E+00	-9.67E-03	-2.12E-09	8.77E+01	-9.66E-04	-1.63E+01	5.09E+01	-3.68E+01
		HL-P-CP4	4.57E+00	1.93E-03	3.45E-09	-4.83E+01	1.58E-03	3.62E+01	-9.57E+01	-4.74E+01

Figure 77: CPP Data Calculations and Statistical Analysis Table for HL-P Coupons

Coupon Tested	Elements(Surface + Partial Bulk) Conc. in [%] per EDX						Elem. Ratios	
	O	Si	Cr	Mn	Fe	Ni	Fe:O	Cr:Fe
RM-C	0.83	0.33	18.44	1.75	71.13	7.52	85.70	0.259
LL-C	1.86	0.40	17.74	1.61	70.22	8.17	37.75	0.253
LL-LA	1.75	0.47	18.30	1.91	69.83	7.74	39.90	0.262
HL-LA	3.18	0.37	17.77	1.73	69.35	7.60	21.81	0.256
LL-P	1.53	0.46	18.74	1.94	69.87	7.46	45.67	0.268
HL-P	1.57	0.39	18.54	1.90	69.60	8.00	44.33	0.266

Figure 80: EDX Data Results Summary Table

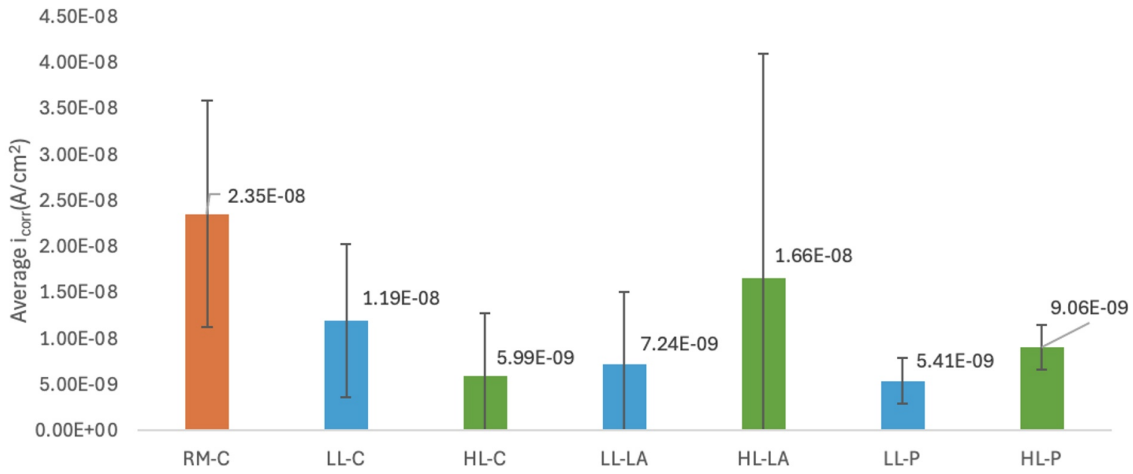

Figure 79: Average Current Density(log) per Study Group

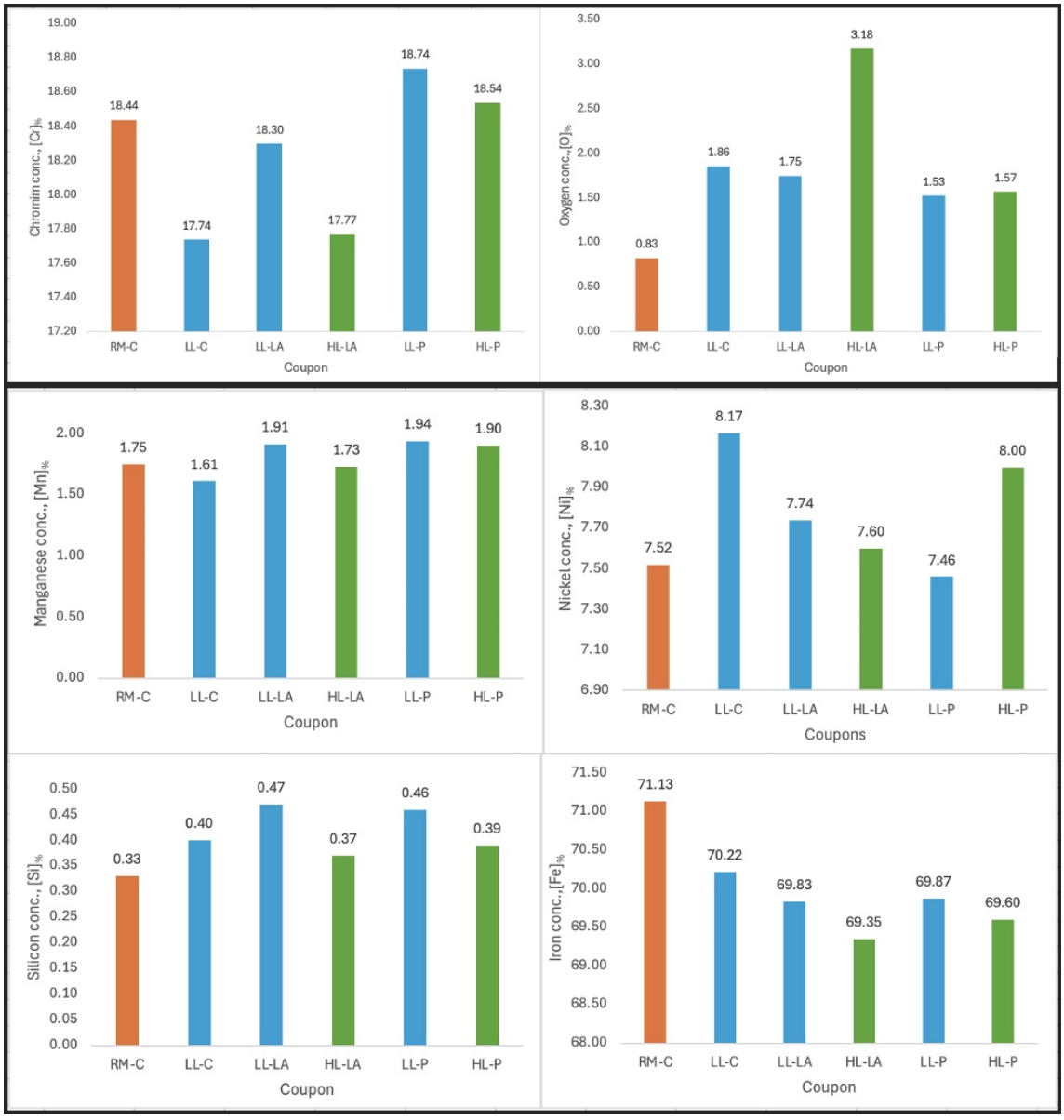

Figure 81: EDX Chemical Composition Percentages of 304 SS Sample per Study Group

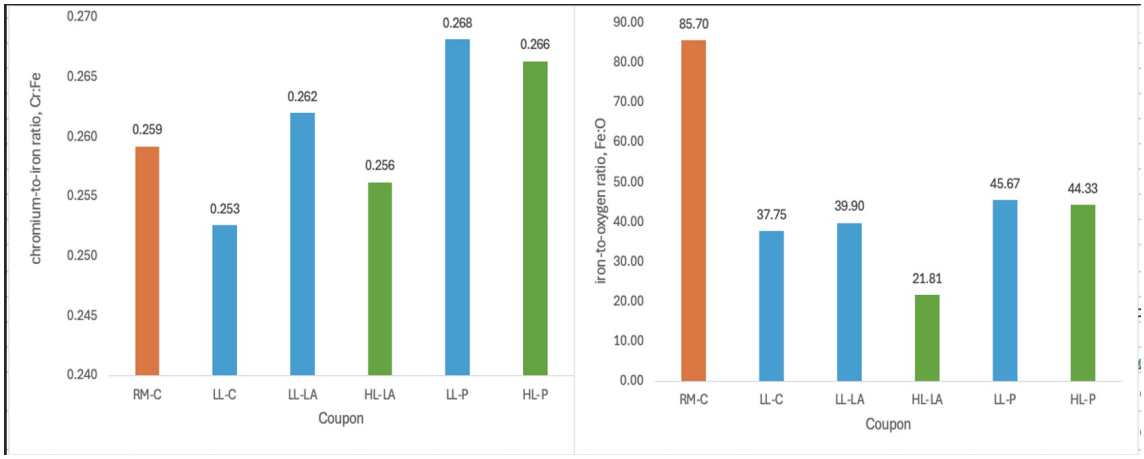

Figure 82: EDX Data Result Ratios of Cr:Fe and Fe:O per Study Group